THE OBSERVED DISRUPTION OF INTENSE RUNAWAY ELECTRON STREAMS IN A PLASMA BETATRON

A Thesis

Submitted to the Faculty of Graduate Studies

in Partial Fulfilment of the Requirements

for the Degree of

Doctor of Philosophy

in the Department of Physics

University of Saskatchewan

by

Lloyd Thomas Shepherd

Saskatoon, Saskatchewan

April, 1962

UNIVERSITY OF SASKATCHEWAN

College of Graduate Studies

SUMMARY OF THE DISSERTATION

Submitted in Partial Satisfaction

of the Requirements for the

DEGREE OF DOCTOR OF PHILOSOPHY

by

LLOYD THOMAS SHEPHERD

B.Sc. (Elect. Eng.) 1956 (University of Alberta)

M.Sc. (Physics) 1960 (University of Saskatchewan)

DEPARTMENT OF PHYSICS

April 1963

Committee in Charge:

Prof. R.N.H. Haslam (Chairman)
Prof. H.M. Skarsgard (Supervisor)
Prof. L. Katz
Prof. O.R. Skinner
Prof. R.W.C. Cobbold
Dean B.W. Currie

External Examiner:

Prof. F.L. Curzon, Department of Physics, University of British Columbia, Vancouver.

BIOGRAPHICAL

1935 Born at Medicine Hat, Alberta.

1952 Senior matriculation, Lethbridge Collegiate Institute, Lethbridge, Alberta.

1956 B.Sc. in Electrical Engineering, University of Alberta, Edmonton, Alberta.

1956-57 Engineer, Defence Research Board, Valcartier, Quebec.

1957-58 Engineer, Alberta Government Telephones, Edmonton, Alberta.

1960 M.Sc. in Physics, University of Saskatchewan, Saskatoon, Saskatchewan.

THESIS

THE OBSERVED DISRUPTION OF INTENSE RUNAWAY ELECTRON STREAMS IN A PLASMA BETATRON

An experiment has been conducted in an attempt to produce and study the behaviour of an intense stream of energetic electrons. A betatron electric field was used to accelerate electrons within a plasma contained in a doughnut vacuum chamber. The plasma was formed initially by striking a radio-frequency discharge in argon gas at a pressure of about 3×10^{-4} mm Hg. Accelerating electric fields up to 8.8×10^{3} volts/m were used. In addition to the betatron field, a steady azimuthal magnetic filed of 0.1 w/m^2 was employed. During the betatron acceleration the current flowing around the doughnut was observed; x-rays emitted from the walls of the vacuum chamber were also studied -- by means of techniques especially developed for this work.

Intense streams of accelerated electrons were observed. However, the streams were disrupted soon after their formation. X-rays produced during the disruption showed that the electrons striking the walls of the chamber had considerably less energy than that corresponding to normally accelerated electrons.

This behaviour cannot be explained in terms of interactions between the streaming particles and known electromagnetic fields associated with the stream itself or provided by the experimental system. Furthermore, ordinary binary collisions between the streaming electrons and other charged or neutral particles cannot account for the results observed. It is concluded that the disruption of the electron stream is due to an unidentified collective interaction or instability. Some consideration has been given to some types of collective interaction which may be involved.

PUBLICATIONS

Shepherd, L.T. and Skarsgard, H.M. Radio-Frequency Breakdown Controlled by Drift of Electrons in an Inhomogeneous Magnetic Field. Can. J. Phys. 39, 983, 1961.

Shepherd, L.T. and Skarsgard, H.M. Observed Disruption of Intense Runaway Electron Streams. Phys. Rev. Letters 10, 121, 1963.

ACKNOWLEDGEMENTS

The author wishes to gratefully acknowledge the assistance and supervision of Dr. H. M. Skarsgard over the past four years. The author is also indebted to the students, especially Mr. J. V. Gore and Mr. O. D. Olson, who have been associated with plasma physics during this time.

Financial aid from the Atomic Energy Control Board of Canada is gratefully acknowledged.

ABSTRACT

This thesis describes an investigation of the problem of producing an intense stream of runaway electrons. With an argon plasma (density from 4×10^{10} to 4×10^{11} cm^{-3}) in an azimuthal magnetic field of 0.1 webers/m^2, accelerating fields from 8.8×10^2 to 8.8×10^3 volts/m were used. Refined Rogowski-coil and scintillation-detector diagnostic techniques were used to study the behavior of the system. Intense runaway electron streams were observed. Disruption of the stream occurred approximately 0.4 μsec after its formation. X radiation was observed during the disruption. The energy of the electrons producing the x rays (approximately 100 kev), is less than would have been observed if they were accelerated freely from the moment of application of the accelerating field. It is concluded that the disruption of the streaming motion is due to an instability.

CONTENTS

LIST OF TABLES

LIST OF FIGURES

CHAPTER 1
INTRODUCTION

1.1 The Problem

This thesis concerns a plasma betatron experiment in progress in the Physics Department, University of Saskatchewan. The experiment was conducted for the purpose of studying the production and disruption of an intense stream of runaway electrons, electrons which are accelerated rapidly to high energies without suffering significant momentum transfer due to collisions with the positive ions or neutral gas molecules.

Interest in producing such a beam of electrons was stimulated by Budker (1) in 1956 with the suggestion that in a relativistic pinched beam of electrons an equilibrium condition should exist in which the energy gained from an accelerating field is dissipated by radiation. In 1957-58, a group at CERN, Geneva (2) constructed two plasma betatrons in an attempt to reach the so-called 'Budker condition'. They used the plasma betatron in order to overcome the space-charge limitation on the current in conventional betatrons.

The experiment reported in this thesis is similar to the ones carried out by the CERN group - a betatron accelerating field is applied to a plasma in the presence of a steady azimuthal magnetic field. The major differences between the two experiments are that in the experiment reported in this thesis, the accelerating fields are higher, and the diagnostic techniques are more refined. Furthermore, the theory of the plasma betatron has been extended. It will be seen that due to these factors a clearer understanding emerges of the

processes involved in the plasma betatron.

1.2 An outline of the thesis.

In addition to the experimental work, some theoretical analyses were carried out. These comprise an investigation of the problem of the acceleration of electrons in a plasma betatron with an azimuthal magnetic field (Chapter 2), and an analysis of some instabilities (Chapter 3).

In Chapter 2 it is found that:

(1) Under a wide range of conditions encountered in this experiment, the forces on the electrons due to the self-field of the beam current (the pinch forces) are the dominant focusing forces. There is, however, no constriction of the beam because of the azimuthal magnetic field.

(2) The self-field of the electron beam produces a distortion in the betatron field, as do errors in the current distribution in the betatron winding. It is found, however, that almost normal acceleration should be possible for the first half microsecond of the acceleration period.

(3) Small plasma inhomogeneities may inhibit many electrons from being accelerated.

In the investigation of instabilities (Chapter 3) most attention was given to the two-stream instability due to longitudinal electrostatic oscillations. Under idealized conditions it is found that the two-stream instability could possibly cause the disruption of the electron beam in the plasma betatron.

The experimental investigation of the behaviour of the plasma betatron was carried out as follows. For a range of

plasma densities and accelerating fields, the beam current was observed using a Rogowski coil which provided information on the number of electrons being accelerated and the time at which disruption of the beam occurs. The x rays produced when some of the electrons strike the walls of the torus are observed with a pair of scintillation detectors. A technique has been developed whereby information may readily be obtained on the number and energy of the electrons producing the x rays. A description of the Rogowski coil and the scintillation detectors is the subject of Chapter 4.

The results of the experimental investigation are given in Chapter 5. The important results are as follows:

(1) An intense beam of electrons is produced in the plasma betatron. The beam is disrupted because of an instability and subsequently x-rays are produced in the walls of the torus.

(2) Of the available electrons, not more than half are accelerated as runaway electrons and not more than a few per-cent are involved in the production of x-rays.

(3) The upper limit on the average energy of the electrons producing the x rays is approximately one quarter to two thirds of the energy of normally-accelerated runaway electrons.

(4) The time of disruption of the beam is found to vary inversely as the square root of the accelerating field but to be independent of the plasma density over a wide range of values.

1.3 An historical sketch

1.3.1 Plasma physics.- While the activity in the field of plasma physics has been most intense in the last decade, its

beginnings were much earlier. W. Crookes in 1879 realized that the phenomenon in discharge tubes may represent a fourth state of matter. It is interesting to note that several Greek philosophers, including Aristotle, held that the material universe was built of the four 'roots'; earth, water, air and fire. This could be compared to the modern terminology of solid, liquid, gas, and plasma.

At the beginning of this century the importance of ionized matter in the processes of outer space was realized by astrophysicists. From their ranks came much of the early contributions to plasma physics.

It was Langmuir, however, about forty years ago, who developed the basic theory of ionized gases and first named the ionized gas a plasma. It was the tendency of the ionized gas to oscillate as a jelly-like substance which suggested the name plasma. The term protoplasma had been used by biologists to describe the jelly-like component of cells.

At the time when the thermonuclear reaction was being exploited in the production of the hydrogen bomb, there was increased interest in the possibility of setting up a controlled thermonuclear reaction. The interest in controlled thermonuclear research and space exploration are mainly responsible for the intense activity in plasma physics at this time.

Most of the effort in controlled thermonuclear research has been directed through three basic approaches toward the problem of confinement and heating of a plasma. These approaches are: (1) The pinch devices in which the confinement is to be achieved through the self-magnetic field of the current.

(2) The mirror-like devices in which charged particles are confined by suitably shaped magnetic fields. (3) The Stellarator which is topologically a torus with a special magnetic field designed to minimize particle losses peculiar to systems with nonending geometry.

1.3.2 Relativistic plasma devices.- Devices which involve relativistic electrons in a plasma have received relatively little attention. Proposals have been made which concern both the field of controlled thermonuclear research and that of high-energy accelerators.

One proposal for the use of relativistic electrons in controlled thermonuclear research has come from Christofilos (3) with his proposal for the Astron. The Astron is related to the magnetic mirror machines. It is suggested that a cylindrical sheet of relativistic electrons circulating in a magnetic mirror geometry can both confine and heat a plasma.

Another proposal, due to Linhart and Schoch (4), involves the confinement and heating of a plasma by the use of a beam of relativistic electrons. It is proposed that the formation of a pinched beam of relativistic electrons should produce a potential well in which ions are both confined and heated.

In 1956 Budker proposed the use of a pinched beam of relativistic electrons to provide strong focusing in a particle accelerator. For highly relativistic beams a steady state could be expected to be set up in which the dissipative processes in the electron beam were compensated for by the application of a steady field. Budker's analysis showed that radiation would be an important dissipative mechanism in a highly-pinched

beam. The 'Budker condition' describing the steady state of a relativistic beam of electrons is expressed as

$$\begin{matrix}\text{(Electron energy)} \\ \text{in Mev}\end{matrix} \times \begin{matrix}\text{(Current)} \\ \text{in amps}\end{matrix} = 17{,}000. \qquad 1.1$$

If a stable, intense beam of relativistic electrons could be produced in a betatron, for example, there are many possible applications. The beam could be used as a guide field for a thermonuclear reactor or for a high-energy accelerator of small dimensions. The beam could also be used for producing a very intense photon flux from bremsstrahlung. Generation of electromagnetic radiation in the millimeter and sub-millimeter range is also a possibility.

There are several experiments in various stages of completion in which the object is the formation and study of relativistic electron beams.

(1) Budker and Naumov (5) reported experiments carried out at the USSR Academy of Sciences, Moscow. Using a conventional betatron a 10-amp beam current of 3-Mev electrons was obtained.

(2) Reynolds and Skarsgard (2) reported on the results obtained from two plasma betatrons constructed at CERN, Geneva, in 1957-58. Runaway electrons were observed corresponding to a stable current of 1 ampere at the full energy of the machine (2 Mev). Larger currents of runaway electrons could be produced (up to 20 amps) but the electrons struck the chamber walls after they had gained relatively little energy (about 100 kev).

(3) Finkelstein (6) proposed the construction of the megatron (short for MEGAgauss betaTRON) which is a small-

diameter (10 cm) accelerator designed to produce particularly strong accelerating fields (up to about 10^5 volts/m). Experiments on this device are now underway at the Stevens Institute of Technology, Hoboken, New Jersey.

(4) de Packh (7) predicted theoretically that the 'Budker condition' may not be required for useful applications of relativistic electrons in the particle-accelerator field. Experimental work to investigate these ideas was proposed.

(5) Miyamoto and colleagues (8) have stated their intention of carrying out some plasma betatron experiments at the University of Tokyo, Japan.

(6) The plasma betatron experiment, currently underway at the University of Saskatchewan has yielded preliminary results. These have been reported briefly by Shepherd and Skarsgard (9). A more complete discussion of the results of this work is the subject of this thesis.

(7) Stephanovski (10) recently reported results of some experiments on the acceleration of electrons in a plasma carried out at the Institute of Nuclear Physics, Moscow. Under similar conditions to those of the experiment reported in this thesis the electron beam was found to be unstable.

The results of the experiments of Reynolds and Skarsgard and those of Stephanovski will be discussed at greater

length in conjunction with the results of the investigation forming the subject of this thesis.

1.4 A description of the experiment

Photographs of the plasma betatron used in this experiment are shown in Figures 1 and 2. The main features are shown diagramatically in Figure 3. In the presence of a steady azimuthal magnetic field, B_φ, an rf field ionizes argon gas in the vacuum chamber. At the end of the rf pulse an aximuthal (betatron) accelerating field, E_φ, is applied to the plasma. The sequence of events is shown in Figure 3(b) and the waveform of the accelerating field is shown in Figure 3(c).

The betatron is operated on a pulsed basis. Each pulse is initiated by an operator after several initial conditions are satisfied. A flow of gas is set up through the torus. The gas pressure in the torus (about 10^{-4}mm Hg) is adjusted by means of a needle valve. Storage capacitors for betatron, rf, and B_φ circuits are charged to predetermined values. The sequence of events in each pulse is controlled by conventional trigger and delay circuits. A block diagram of the system is shown in Figure 4.

The major components of the apparatus are described below:

(1) The betatron winding.- The design and construction of the betatron winding have been reported by Gore (11). The winding consists of four turns of Litz wire connected in parallel and imbedded in two micarta discs. The betatron

Figure 1. Photograph of the plasma betatron.

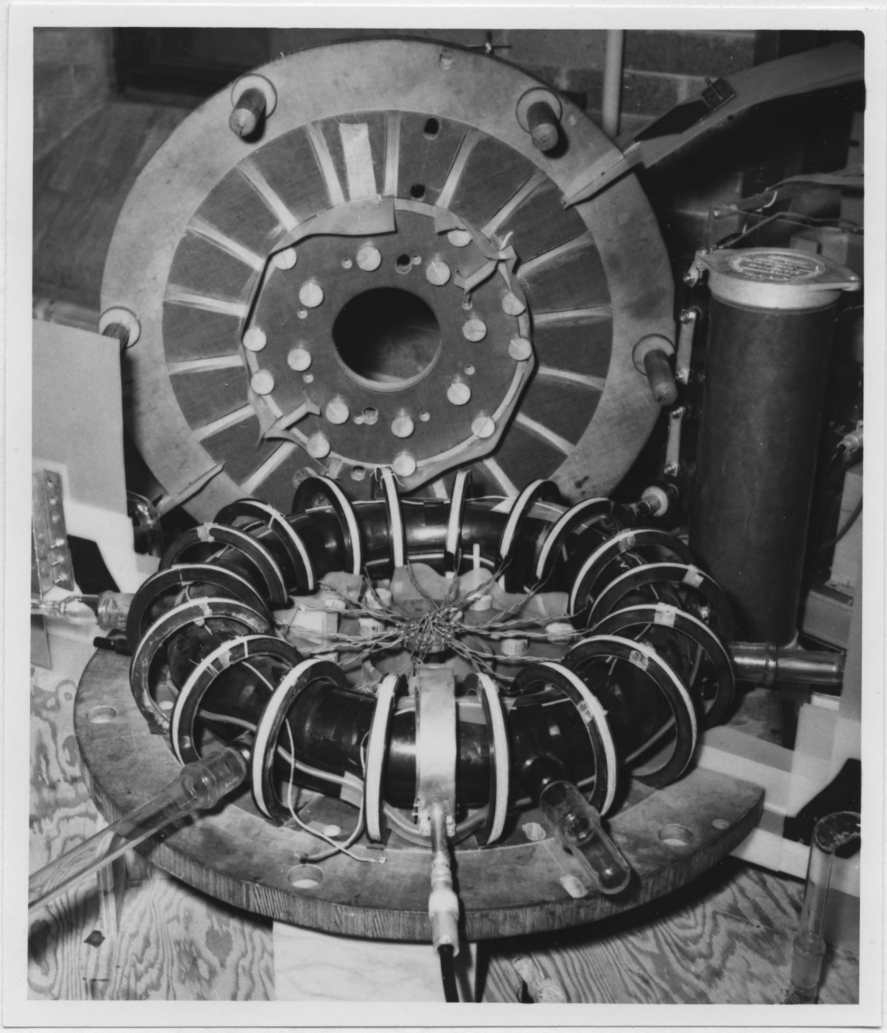

Figure 2. Photograph of the plasma betatron with the upper micarta disc removed.

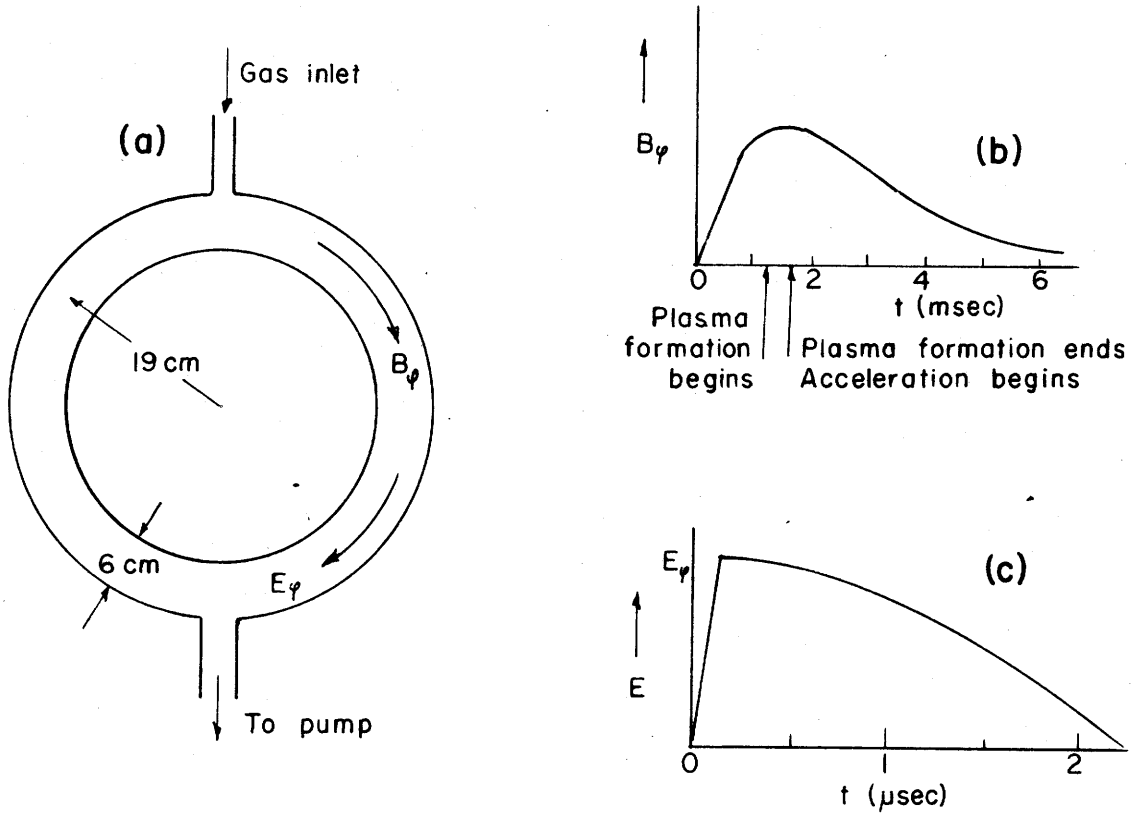

Figure 3. Diagramatic representation of the important features of the plasma betatron experiment.

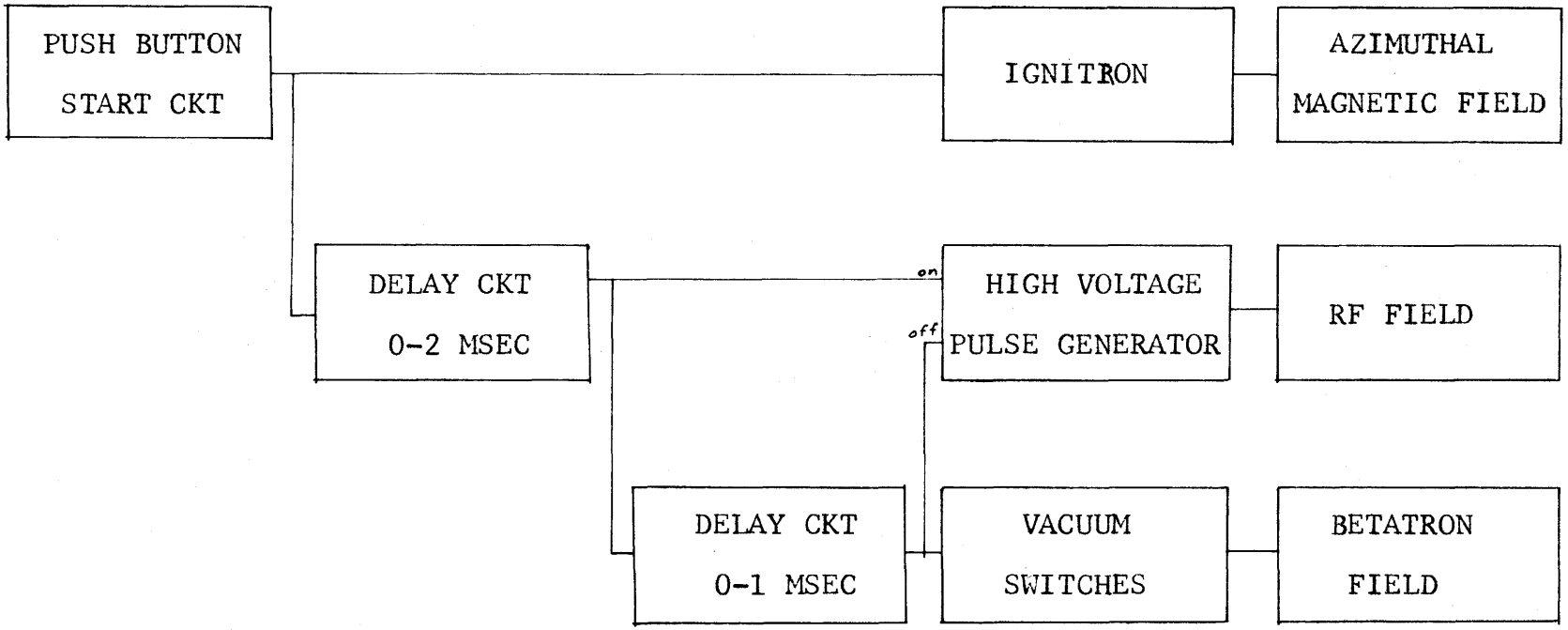

Figure 4. A block diagram of electronics for the plasma betatron system.

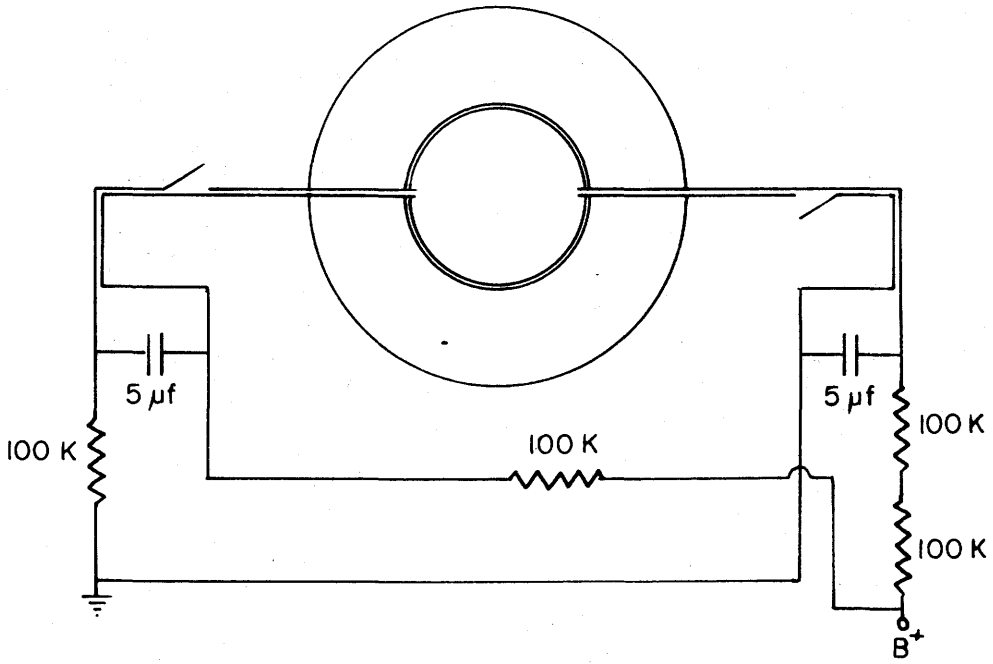

Figure 5. The betatron circuit diagram.

winding is connected through vacuum switches to two 5- μf capacitor banks. As indicated in the circuit diagram in Figure 5, the capacitors are charged in parallel and discharged in series. The betatron circuit rings at 116 kc. Only the first quarter cycle is of interest in this experiment. The design peak accelerating field is 1.77×10^4 volt/m. Accelerating fields up to half this value have so far been used.

(2) The switches.- The vacuum switches used to close the betatron circuit were developed in this laboratory and have been described by Gore and also Eikel and Skarsgard (12). The switches were triggered simultaneously by a Bostick plasma gun located in each switch.

(3) The torus.- The torus was custom made of pyrex glass. The major diameter is approximately 0.38 meters, the minor diameter approximately 0.06 meters. There are six ports located on the torus for the purpose of making gas inlet and outlet connections and for inserting probes and gauges etc.

The interior of the torus is coated with a layer of graphite. This was achieved by momentarily filling the torus with Aquadag--a colloidal graphite solution and pouring off the residue. The metal rings - forming electrodes used in the production of the plasma- were placed in contact with the graphite coating at diametrically opposite points in the torus. Provision was made for the electrical connection to these rings from outside the torus.

The resistance between the two metallic rings is approximately 100K.

The torus is connected to a mercury diffusion pump with a liquid-nitrogen vapor trap. The ultimate vacuum is in the neighborhood of 10^{-5}mm Hg.

(4) The azimuthal magnetic field.- Encircling the body of the torus and recessed into the micarta discs are eighteen coils which provide the azimuthal magnetic field, B_φ . These eighty-turn coils are connected in parallel through an ignitron switch to an electrolytic condenser bank. Storage capacity under normal operating conditions is 400 joules. Peak magnetic fields from 0.01 to 0.15 webers/m^2 were generated.

(5) The rf rack.- The plasma is formed in the torus mainly by means of an rf pulse inductively coupled into the torus. Weak preionization is achieved by connecting the rf pulse directly across the two ring electrodes in contact with the graphite coating. Construction of this apparatus and an investigation of the problem of plasma formation was reported previously (13) (14).

The rf was either 8 or 15 Mc in this experiment. The amplitude of the rf field decreases with time during the pulse. It is found that the density of the plasma depends on the amplitude of the rf. Control of the duration of the rf pulse therefore provides a convenient control on the plasma density.

(6) The control circuits.- The control circuits were constructed by the author and described in his M.Sc. thesis

(13). They consist of pulse and variable delay circuits so that the sequence and timing of B_φ , rf, and betatron acceleration can be controlled.

(7) Diagnostic apparatus.- The apparatus used to determine the behaviour of the plasma consists of a pair of scintillation detectors and a Rogowski coil. The signals from the scintillation detectors and the Rogowski coil are displayed and photographed using a double-beam Tektronix 551 oscilloscope. The diagnostic techniques are described in detail in Chapter 4.

CHAPTER 2

THEORY OF THE PLASMA BETATRON WITH AN AZIMUTHAL MAGNETIC FIELD

I. BASIC THEORY

2.1 Introduction

The theoretical treatment of a plasma can take many forms. The approximations which can be made depend on quantities like the density and temperature of the plasma, time and length scales, and the magnitude of the electromagnetic fields. For the case in which the interaction between particles can be neglected in comparison to the particle interaction with the electromagnetic fields, a single-particle model may be used. Using this model it is assumed that each particle is acted on individually by the electromagnetic field. The single-particle model, when applicable, has the advantage of being simple and the processes are more readily visualized.

It will be shown that in this experiment the interaction between particles of the plasma is small compared to the interaction with the electromagnetic fields so that the single-particle model is expected to be appropriate. It should be pointed out however that if this model is to be used the electromagnetic fields considered should include the fields produced within the plasma due to collective particle motions as well as the externally-applied fields.

In the plasma betatron experiment the plasma experiences many electromagnetic fields - accelerating and focusing fields of the betatron, self-fields due to the circulating electron current, electrostatic fields due to charge separation and the applied azimuthal magnetic field. A description of the resultant behaviour of the plasma is the object of this chapter. The question of stability will be considered in the next chapter.

After the coordinates, symbols, and units are defined some elementary plasma theory is presented as a foundation for the analysis which follows. This elementary theory includes the equations of motion and the equations for particle drifts which form the basis of single-particle theory. Two aspects of a plasma are then discussed briefly; the tendency for a plasma to maintain charge neutrality and collision phenomena in a plasma. The elementary plasma theory is given in many texts - for example those by Spitzer (15), Chandrasekhar (16), Rose and Clark (17), and Glasstone and Loveberg (18) - and therefore the derivation of the equations is not included in this thesis.

The production of runaway electrons in a plasma is the first question of interest in this experiment. A simple description of the runaway process for a uniform plasma is given in Section 2.4.1. This is followed by a crude description - original to this thesis - of the effect on runaway of inhomogeneities in the plasma density.

The expected behaviour of the system during the early stages of the betatron acceleration is given in Section 2.5. A description and comparison is given of the forces on the electrons due to the betatron field, the forces due to be self-fields of the circulating current, and possible electrostatic forces. A discrepency in the literature regarding the beam current limitation of plasma betatrons is pointed out and resolved. Time-dependent equations are presented describing the drifts of electrons in the azimuthal magnetic field. These include time-dependent solutions of the radial motion of the plasma due to the disturbing effects of large beam currents and possible defects in the betatron field. These time-dependent solutions are original to this thesis.

2.2 Coordinates, symbols, and units

The coordinate system used in this thesis is a combination of cylindrical and toroidal coordinates. Normally cylindrical coordinates z, ρ, and φ are used for quantities which exist both inside and outside the beam and the toroidal coordinates r, θ, and φ for quantities inside the beam. Often it is convenient to neglect the finite curvature of the beam and picture the beam as a cylinder of infinite extent. The coordinate system is illustrated in Figure 6.

Unless noted otherwise in the text, the symbols used in this thesis are defined as follows:

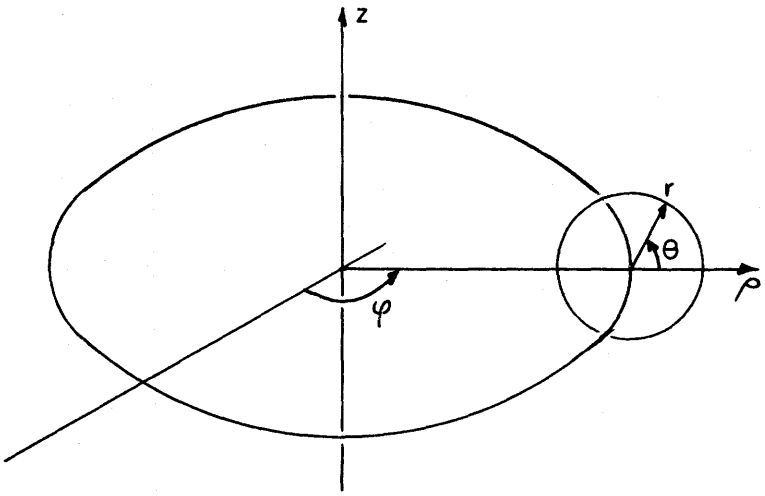

Figure 6. The coordinate system used in this thesis.

a acceleration

A magnetic vector potential

b electron beam minor radius

B magnetic field

c velocity of light

C arbitrary constant

d width or thickness

e charge on the proton

E electric or accelerating field

f $= m/M + f'$

f' ratio of the number of electrons at rest to the number of runaway electrons

F force

G geometrical factor (see Section 4.2.1)

h Debye shielding distance

i,I current

$\mathcal{I}$ luminous intensity

k wave number

K constant

ℓ mean free path

L inductance

m rest mass of electron

M mass of ion

n number density

N number of turns

P radiation energy

q charge

$r_o = e^2/4\pi\epsilon_o mc^2$; the classical radius of the electron

s distance

S angular distribution shape factor (see Section 4.2.2)

t transmission

T a factor related to transmission (see Sections 4.2.1 and 4.2.5)

U electron temperature in electron volts

v velocity

V voltage

w drift velocity

W energy

Z atomic number

α imaginary component of ω

β ratio of electron velocity to that of light

δ a small displacement

$\gamma = (1 - \beta^2)^{-\frac{1}{2}}$

ϵ_o Permittivity of free space

ϵ error in current ratio in betatron winding

η efficiency

H_c a factor related to efficiency (see Sections 4.2.1 and 4.2.5)

λ geometrical factor related to inductance (see Section 2.5.3)

Λ ratio of maximum to minimum impact parameter

μ_o permeability of free space

ν number of electrons in a slice of beam of thickness r_o.
(The slice is contained between two planes which are perpendicular to the beam axis)

ρ_o equilibrium orbit of the betatron

σ {cross section
attenuation coeffiecient for Compton effect

τ {exponent for plasma oscillation amplification
attenuation coefficient for photoelectric effect

ϕ magnetic flux

ω angular frequency

$\omega_{pe} = (ne^2/m\epsilon_o)^{\frac{1}{2}}$ the electron plasma frequency

$\omega_{pi} = (ne^2/M\epsilon_o)^{\frac{1}{2}}$ the ion plasma frequency

Rationalized MKS units are used in this thesis unless otherwise stated.

2.3 Elementary plasma theory

2.3.1 Equations of motion.- The basic equation of motion of a particle with electric charge q and mass m in an electric and magnetic field is

$$m\, d\vec{v}/dt = q(\vec{E} + \vec{v} \times \vec{B}). \qquad 2.1$$

If there is no electric field the particle will execute a helical motion with angular frequency

$$\omega_c = qB/m. \qquad 2.2$$

The angular frequency, ω_c , is called the cyclotron frequency or gyromagnetic frequency or sometimes the Larmor frequency.

2.3.2 Particle drifts.- The solution of equation 2.1 is best described in terms of a circular motion and the motion of the instantaneous center of gyration (called the guiding

center). The motion of the guiding center perpendicular to the magnetic field is called the drift of the particle in the magnetic field. For the case of a constant electric and magnetic field the steady-state drift velocity is $\vec{w}_d = \vec{E} \times \vec{B}/B^2$. 2.3

This equation is valid so long as $w_d < c$. The direction of drift is the same for particles with either positive or negative charge.

The cross-field drift described above will also result from other external forces. The equations will apply if the force is expressed in terms of an equivalent electric field,

$$\vec{E} = \vec{F}/q. \qquad 2.4$$

2.3.3 Electrical neutrality.- A basic property of a plasma is its strong tendency toward neutrality. If, over a large volume of plasma, the number of electrons differ appreciably from the corresponding number of ions large electrostatic forces tend to restore neutrality.

Under normal conditions the distance over which a plasma may not be neutral is given by the Debye shielding distance,

$$h = (2\ \epsilon_o\ U/3ne)^{\frac{1}{2}}. \qquad 2.5$$

The Debye length also represents the approximate distance over which the coulomb field of a particle is effective in a plasma and gives the approximate thickness of the sheath formed between a plasma and the walls of its con-

tainer.

In the plasma betatron experiment it is often convenient to express the plasma density in terms of the dimensionless quantity ν , the number of electrons in a slice of the beam one classical electron radius in thickness. (The slice is contained between two planes which are perpendicular to the beam axis). If all the electrons are in a uniform beam of minor radius b, then

$$\nu = ne^2b^2/4\epsilon_o mc^2. \qquad 2.6$$

From equations 2.5 and 2.6, for a charge-neutralized beam of radius 0.02 m in which the electrons have a random energy of 10 ev,

$$h = 3.6 \times 10^{-5} \nu^{-\frac{1}{2}}. \qquad 2.7$$

2.3.4 Collision phenomena in a plasma.- It is found that the coulomb field of the particles in a plasma are of such a long-range nature that each particle is influenced by many other particles simultaneously. As a particle moves through a plasma it will suffer many small deflections but there will be a net scattering effect similar to the classical large angle scattering. A collision cross section for scattering through 90^o can be determined (18).

$$\left.\begin{aligned} \sigma &= e^4 \ln \Lambda / 2\pi \epsilon_o{}^2 m^2 v^4 \\ &= e^2 \ln \Lambda / 8\pi \epsilon_o{}^2 U^2 \\ &= 8\pi r_o{}^2 \ln \Lambda \; c^4/v^4 \end{aligned}\right\} \quad m^2/\text{ ion} \qquad 2.8$$

where $\Lambda \equiv$ maximum impact parameter (taken to be h) divided by the minimum impact parameter. For plasmas of interest in this experiment, $\ln\Lambda$ is about 10. The cross

section decreases rapidly with increasing electron energy. For 10-ev electrons, the cross section is approximately 1.3×10^{-18} m^2/ion.

From these results a mean free path may be calculated. For 10-ev electrons

$$\left.\begin{aligned} \ell &= 1/n\sigma \\ &\approx 4/\nu \, . \end{aligned}\right\} \qquad 2.9$$

It is understood that this mean free path is the length of path an average electron would traverse while being scattered through 90°.

The time taken for a particle to traverse its mean free path is called the 'relaxation time', t_r. It is a measure of the time taken for appreciable change in momentum of the particles and so indicates the rate at which a nonequilibrium state returns through collisions to an equilibrium state.

$$t_r = 1/n\sigma v. \qquad 2.10$$

It is found that for electron-electron encounters and electron-ion encounters, t_r is approximately the same. For 10-ev electrons

$$t_r = 2.3 \times 10^{-6}/\nu \, . \qquad 2.11$$

Comparing t_r for 10-ev electrons with the cyclotron period it is evident that for magnetic fields (0.1 webers/m^2) and beam densities ($\nu = 10^{-3}$ to 1) of interest in this experiment, the electrons make many revolutions in the magnetic field between 'collisions'. The single-particle ap-

proach is then justified provided collective interactions are treated explicitly. Note that t_r increases as the energy of the electrons increases - through a betatron acceleration for example - but that even for the 10-ev electrons t_r is longer than the total acceleration period for ν values encountered in this experiment.

2.4 Runaway electrons in a plasma

2.4.1 The runaway effect in a uniform plasma.- When a particle moving in a plasma gains momentum continuously from an applied field it is said to be 'runaway'. Several workers, including Dreicer (19) and Harrison (20)(21), have investigated the conditions under which electrons in a plasma may be accelerated continuously and become decoupled from the positive ion background. Dreicer's treatment is the most rigorous one which has been carried out. Dreicer, neglecting collective effects, designates electrons with drift velocity several times the mean thermal velocity as runaway electrons. Harrison would call these 'suprathermal' while reserving the term runaway for those which gain energy continuously in spite of collective effects. In this thesis Dreicer's definition will be used as collective effects will be considered as part of the larger question of instabilities.

In the treatments of the workers referred to above, the dynamical friction force was evaluated using the Boltzmann equation. The electric field required to overcome

this friction force - and hence produce runaway - was then determined. While Dreicer's work should be referred to for the most accurate description of the runaway process, a simpler treatment due to Linhart (22) is adequate for the purposes of this thesis. This 'mean-free-path' approach is given below.

Under a constant accelerating field, E, the drift velocity of the electrons is

$$v = eEt/m \qquad 2.12$$

while the distance traversed by the electrons is

$$s = eEt^2/2m. \qquad 2.13$$

From equations 2.8, 2.9, and 2.13 the mean free path of an electron in the plasma is found to be

$$\ell = 2\pi\epsilon_o^2 E^4 t^4/nm^2 \ln\Lambda . \qquad 2.14$$

Since the mean free path varies as t^4 while the distance travelled varies only as t^2, if an average particle does not suffer a 'collision' before ℓ/s reaches unity it will not be involved in a collision thereafter. The critical electric field, E_c, for the free acceleration of all electrons may be found by setting ℓ/s equal to unity after a time equal to the average collision time, t_r.

$$\left.\begin{aligned} E_c &= ne^2 \ln\Lambda \,/(128)^{1/3}\pi\,\epsilon_o^2 U \\ &\approx 60\,\nu/U. \end{aligned}\right\} \qquad 2.15$$

The value of E_c calculated here is three times greater than that computed by Dreicer.

2.4.2 The runaway effect in an inhomogeneous plasma.- If an accelerating field is applied to an inhomogeneous plasma there will be electrostatic fields set up due to the separation of electrons and ions in an inhomogeneity. If the accelerating field is not sufficiently strong to separate completely the electrons and ions in the inhomogeneity a potential barrier is erected which may trap some of the electrons.

The potential, although possibly due to a small inhomogeneity, could trap many electrons if the electrons did not initially have sufficient energy or did not receive enough energy from the accelerating field to pass over the potential. The fate of the electrons would be determined in a time comparable to the time taken for an electron to move one wavelength. In an experiment of the kind described here the time involved would probably be less than 10^{-8} sec - shorter than the time taken for the accelerating field to reach its maximum value. It would appear that the initial velocity distribution of the electrons is more significant in determining how many electrons escape the inhomogeneity than the maximum value of the accelerating field or the magnitude of the inhomogeneity.

Of course under certain conditions all electrons could be accelerated in spite of a density inhomogeneity. The field required to decouple the electrons and ions from an

inhomogeneity of density Δn and wave number k is

$$\left.\begin{aligned} E^c &\simeq \Delta ne/\ \epsilon_o\ k \\ &\simeq 4\ \Delta\gamma\ mc^2/kb^2e. \end{aligned}\right\} \qquad 2.16$$

The field E^c can be regarded as a critical electric field for the acceleration of all electrons over an inhomogeneity. In the plasma betatron, if the inhomogeneity is associated with the spacing of the coils producing the azimuthal magnetic field, for a beam of radius 0.02 m

$$E^c = 5 \times 10^5 \gamma \quad \text{volts/m.} \qquad 2.17$$

The analysis given above is little more than qualitative. No estimate about the number of electrons which will be accelerated normally can be made at this point. The tendency for the fields to smooth out the inhomogeneity may release some of the electrons subsequent to the initial trapping.

2.5 Plasma betatron theory

2.5.1 Introduction.- The purpose of this section is to describe the forces acting on the electrons in the plasma betatron and determine if possible the effect of these forces. The betatron field provides the acceleration to the electrons as well as a focusing force. The magnetic fields due to the circulating beam current produce the well known pinch forces along with a radial force tending to move the beam to the axis of the betatron. The effect of the azimuthal magnetic field will be considered.

Several approximations will be made in the theory set down here. In addition all equations neglect relativistic effects. The equations therefore apply to the initial stages of the acceleration only. It will be seen that this is not a serious limitation.

2.5.2 The force equation.- The net unbalanced radial force on an electron in the plasma betatron may be written

$$F = -ev_\varphi B_z + mv_\varphi{}^2/\rho . \qquad 2.18$$

The velocity of the electron may be written in terms of the magnetic vector potential A_φ(23),

$$v_\varphi = eA_\varphi /m. \qquad 2.19$$

In the cylindrical geometry of the plasma betatron A_φ is a function of ρ and is given simply by

$$\left.\begin{aligned} A_\varphi &= \Phi /2\pi\rho \\ &= \left(\int B_z \rho \, d\rho \right)/\rho . \end{aligned}\right\} \qquad 2.20$$

It is assumed in calculating the various forces that the electrons are 'frozen' to the lines of azimuthal magnetic field and do not move in a radial direction. It will be shown in Section 2.5.5 that the electrons actually rotate about the equilibrium orbit so that the velocity given by equation 2.19 will be in error. However since the rotation near the beginning of the acceleration is slow and since in the plasma betatron the variation of A_φ with ρ is slight, the error introduced will be small.

The magnetic vector potential, A_φ , is made up of contributions from the betatron field, A^b, and the self-field

of the beam, A^s,—both functions of ρ .

$$A_\varphi = A^b + A^s. \qquad 2.21$$

The magnetic field B_z is made up of a z component, B^b, from the betatron field and two z components from the self-field, B_1^s and B_2^s.

$$B_z = B^b + B_1^s + B_2^s. \qquad 2.22$$

The component of self-field, B_1^s, is the magnetic field that would be produced if the beam were straight and B_2^s is the component of magnetic field due to the curvature of the beam.

Substitution in equation 2.18 shows the resultant radial force on an electron to be 2.23

$$F= -e^2A_\varphi (B^b-A^b/\rho)/m - e^2A_\varphi B_1^s/m - e^2A_\varphi (B_2^s-A^s/\rho)/m.$$

The first term in the above equation is the betatron focusing force and the second term is the self-focusing (pinch) force. The third term is a radial force due to the self-fields of the circulating current. The part involving B_2^s represents a force tending to expand the orbit. The part involving A^s/ρ represents a self-inductance effect whereby the electrons have a reduced energy which tends to reduce the orbit. It will be shown that for a betatron of the type described in this thesis the third term represents a net force directed radially inward.

2.5.3 Reduction of accelerating field due to the self-field.- It is convenient now to consider the effect of the self-field on the accelerating field and the energy of the accelerated

electrons. If ν represents the runaway electrons then the beam current will be

$$\left.\begin{aligned} I &= -\nu e \bar{v}_\varphi \, / n_o \\ &= -10^7 \, \nu \, \bar{A}_\varphi \end{aligned}\right\} \qquad 2.24$$

where $\bar{A}_\varphi$ is the average vector potential over the beam cross section. Since the electric field induced by the beam current is the time derivative of the vector potential (24), one may write

$$2 \pi \rho \, dA^s/dt = L \, dI/dt. \qquad 2.25$$

The inductance, L, of the beam is dependent on the geometry and is given by

$$L = 10^{-7} 2 \pi \rho \lambda \qquad 2.26$$

where (25)

$$\lambda = 0.66 + 2 \ln (\rho/b). \qquad 2.27$$

The magnetic vector potential due to the beam current is found from the above equations to be

$$A^s = - \lambda \nu \bar{A}_\varphi \, . \qquad 2.28$$

From equations 2.21 and 2.28 the resultant vector potential is $\bar{A}_\varphi = A^b/(1 + \lambda\nu)$. 2.29

The above equation shows that the accelerating field is reduced by a factor $(1 + \lambda\nu)$ in the nonrelativistic region. From the above equations and using the relation between vector potential and accelerating field.

$$dI/dt = 10^7 \, E^b \, \nu/(1 + \lambda\nu). \qquad 2.30$$

It is convenient in this experiment to refer to E^b as the

accelerating field rather than the actual accelerating field which is smaller by the factor $(1 + \lambda\nu)$. It is evident that for any given accelerating field there is an upper limit to the beam current.

2.5.4 The forces in the plasma betatron.- (1) The betatron focusing force.- In cylindrical geometry

$$B^b = A^b/\rho + \partial A^b/\partial\rho \qquad 2.31$$

hence the term for betatron focusing in Equation 2.23 becomes

$$F^b = -(e^2 A_\varphi/m)(\partial A^b/\partial\rho). \qquad 2.32$$

Data on the betatron in this experiment (11) indicates that in the region of interest

$$\partial A^b/\partial\rho \approx 15A^b(\rho_o - \rho). \qquad 2.33$$

This holds up to $r \approx 0.02$ m where $\partial A^b/\partial\rho$ reaches a maximum.* The betatron focusing force may now be written (assuming $A_\varphi \approx \bar{A}_\varphi$)

$$F^b = 15e^2\bar{A}_\varphi \bar{A}^b r/m. \qquad 2.34$$

The force is roughly independent of the coordinate θ and is directed toward the equilibrium orbit.

(2) The pinch force.- The self-magnetic field, B_1^s, depends on the beam current and the distribution of the current in the beam. For an electron beam with a uniform distribution over a circular cross section of radius b, the magnetic field B_1^s within the beam may be written

$$B_1^s = \mu_o i/2\pi r \qquad 2.35$$

* $\partial A^b/\partial\rho$ is connected with the field index, n, which varies from 0.3 to 0.9 over the region of interest. The index is independent of time.

where r is the distance from the center of the beam and i is the current within the circle of radius r. The current is given by

$$i = -10^7 \nu \bar{A}_\varphi \, (r/b)^2. \qquad 2.36$$

Using the equations 2.35 and 2.36 the term for the pinch force in equation 2.23 may be written (assuming $\bar{A}_\varphi \approx \bar{A}_\varphi$)

$$F^p = 2e^2 \bar{A}_\varphi^{\,2} \, \nu \, r/mb^2. \qquad 2.37$$

The pinch force is independent of θ and acts toward the center of the beam.

(3) The radial force due to the self-field.- An expression for the component of self-magnetic field, B_2^s, has been derived by Reynolds and Skarsgard (2).

$$B_2^s = -\bar{A}_\varphi \, \nu(2 + \lambda)/2\rho \qquad 2.38$$

where ρ is the coordinate of the center of the beam. Using equations 2.28 and 2.38 the radial force due to the self-magnetic field may be obtained from equation 2.23 (assuming $A_\varphi \approx \bar{A}_\varphi$)

$$F^s = -e^2 \bar{A}_\varphi^{\,2} \, \nu(\lambda - 2)/2m\rho. \qquad 2.39$$

For the electron beams encountered in this experiment $\lambda > 2$ so that F^s is a force directed toward the center of the betatron.

(4) Electrostatic forces.- It was noted in Section 2.3.3 that plasmas have a strong tendency to neutrality. There are at least two situations which may produce strong electrostatic forces in the plasma betatron experiment.

(a) Separation of the electron and ion streams.- The force on an electron in a beam due to a separation δ of the centers of the electron and ion beams is given by (26)

$$F^{\delta} = 4 \nu mc^2 \delta / 3b^2 \qquad 2.40$$

where b is again the radius of the beam.

(b) Excess loss of electrons.- Under some conditions electrons may be lost from the beam and strike the walls of the chamber. The electrostatic fields set up would tend to reduce further loss of electrons and to accelerate the ions toward the wall. The force on the electrons—a focusing force—is readily calculated from Gauss' Law. For the uniform loss of electrons from a beam of radius b,

$$F^{e} = 2 \nu_{\ell} mc^2 r/b^2 \qquad 2.41$$

where ν_{ℓ} corresponds to the electrons lost from the beam.

2.5.5 The Comparison of the Forces in the Plasma Betatron.-

(1) Comparison of the betatron and pinch focusing forces. From equations 2.29, 2.34, and 2.37 the relative magnitude of the betatron and pinch forces may be determined.

$$F^{p}/F^{b} = \nu/7.5\ b^2(1 + \lambda\nu) \qquad 2.42$$

For b = 0.02 m

$$F^{p}/F^{b} = 3.3 \times 10^2\ \nu/(1 + \lambda\nu). \qquad 2.43$$

It is evident that for $\nu > 3 \times 10^{-3}$ the pinch forces dominate over the betatron focusing forces.

(2) Comparison of the betatron focusing force and the radial force due to the self-field.- The self-field effect will tend to move the electron beam toward the center of the betatron. Such a movement would be opposed by the betatron focusing force. It is interesting to determine under what conditions the two forces balance. From Equations 2.29, 2.37, and 2.39, the two forces would be in equilibrium when

$$\frac{\nu(\lambda - 2)}{(1 + \lambda\nu)} = \frac{2\rho}{A^b} \left(\frac{\partial A^b}{\partial \rho}\right) . \qquad 2.44$$

The betatron field configuration and the value of λ are fixed; consequently there is a maximum value of ν for which an equilibrium orbit will exist within the betatron chamber. Taking b = 0.02 m for the betatron in this experiment, the value of λ is approximately 5. Calculating $(\partial A^b/\partial \rho)_{max}$ from data given by Gore then indicates that

$$\nu_{max} = 0.032. \qquad 2.45$$

The result (2.44) is essentially the same as that given by Maisonnier and Finkelstein (27) for $\lambda\nu \ll 1$. More recently Schmidt (23) has obtained a different result based on a self-consistent theory. However he has neglected the forces tending to expand the beam. His result for ν_{max} is therefore too low. The equation 2.44 is believed to be the correct self-consistent equation. The ν_{max} calculated in this way is larger than that calculated by the Maisonnier and Finkelstein equation.

(3) Comparison of electrostatic forces to other forces.- The electrostatic force due to the separation of the electron and ion beams may readily be compared to the radial force due to the self-field. With the two forces equal the separation of the axes of the electron and ion beams is found from equations 2.39 and 2.40. Expressed as a ratio of separation to beam radius,

$$\left.\begin{aligned} \delta/b &= (e\bar{A}_\varphi/mc)^2\, 3(\lambda - 2)\, b/8\rho \\ &= 3\beta^2(\lambda - 2)b/8\rho\ . \end{aligned}\right\} \qquad 2.46$$

For 100-kev electrons in a beam 0.02 meters in diameter

$$\delta/b = 0.035. \qquad 2.47$$

This indicates that the radial force due to the self-field discussed in Section 2.5.3 would not produce large movements in the electron beam without moving the ion beam as well.

The force on an electron due to the electrostatic field set up by the loss of electrons from the beam may usefully be compared to the pinch forces. By equations 2.37 and 2.41 one finds that for this electrostatic force to be larger than the pinch force,

$$\nu_e/\nu > \beta^2. \qquad 2.48$$

For example, this indicates that if 10% of the electrons were lost from the beam the electrostatic forces would be stronger than the pinch forces until the electrons reached an energy of about 28 kev.

2.5.6 Particle motions in the plasma betatron.- In addition to the motion of the electrons in the azimuthal direction, it is of interest to examine the motions in the ρ-z plane due to the various forces described in Section 2.5.4.

(1) Electron drifts due to the focusing forces.- The focusing forces will produce an equivalent E/B drift in the azimuthal magnetic field. The drift is in the θ direction and so produces a rotation of the beam about the beam axis. In most normal circumstances encountered in the plasma betatron of this experiment the pinch force is the dominant focusing force.

For the steady-state equations of crossed-field drifts to apply, two conditions must be satisfied. (1) The time scale for changes in the magnitude of the forces must be small compared with the cyclotron period of the particle in the magnetic field; and (2) the calculated drift velocity must be less than the velocity of light. In this experiment the focusing force increases with time according to t^2. For an azimuthal magnetic field of 0.1 webers/m^2 and after a time greater than 10^{-8} seconds, an electron completes one cyclotron orbit in the magnetic field while the focusing force increases by less than 10%. The calculated crossed-field drift is normally much smaller than c. The equations in Section 2.3.2 are therefore accurate enough for the purposes of this thesis.

The angular frequency of rotation is found from equations 2.3 and 2.37.

$$\omega_\theta = 2e\bar{A}_\varphi^2 \nu / mB_\varphi b^2. \qquad 2.49$$

The total angle through which the beam has rotated is given by

$$\theta = 2\nu E^b e t^3 / 3mB_\varphi b^2 (1 + \lambda\nu)^2. \qquad 2.50$$

For a beam with b = 0.02 m; B_φ = 0.1 weber/m^2; E^b = 4.4 x 10^3 volt/m, the maximum rate of rotation is for $\nu \approx$ 0.2. It is found that under these conditions the beam completes one radian of rotation by time t = 0.07 μsec at which time the energy of a normally accelerated electron is 2 kev. The rate of rotation increases rapidly after this however.

A comparison between the frequency of rotation in the θ direction and the frequency of circulation in the φ direction may readily be obtained.

$$\left.\begin{aligned} \omega_\theta/\omega_\varphi &= 2\nu \bar{A}_\varphi \rho / B_\varphi b^2 \\ &\approx 16 \beta \nu . \end{aligned}\right\} \qquad 2.51$$

For $\nu = 0.2$, $\omega_\theta/\omega_\varphi$ would be unity when the electrons had an energy of 27 kev.

In the above equations the centrifugal force due to the rotation in the θ direction has been neglected. For high values of ω_θ this becomes important and the equations no longer hold. It can be shown that the centrifugal force becomes important only when ω_θ is comparable to $\beta \omega_{pe}$. When the centrifugal force is taken into account

the angular frequency of rotation is limited to a maximum value given by

$$(\omega_\theta / \omega_\varphi)_{max} = \sqrt{2\nu}\ \rho_o/b. \qquad 2.52$$

Note that this value is independent of the azimuthal magnetic field - so long as the cyclotron radius is small compared to the beam radius.

The drifts which are produced in the beam have the result that no contraction of the beam can take place. The pinch forces are transformed away by the electron drifts in the azimuthal magnetic field.

(2) Motion of the beam due to the radial force from the self-field.- Often in the course of this experiment actual ν values are encountered which exceed the ν_{max} as given by equation 2.45. In these circumstances it is important to estimate the time required for the radial force due to the self-field to have a significant effect on the beam.

Chandrasekhar (16) has shown that if a plasma is surrounded by nonconducting walls and experiences a net force perpendicular to the magnetic field it is accelerated in the direction of the force. The acceleration is dependent only on the total force and the total mass and is given simply by Newton's Second Law. This somewhat idealized model will be employed here in calculating the expected motion of the beam in the plasma betatron experiment due to a force in the radial direction. In any case this accelera-

tion will be an upper limit to the correct value.

The upper limit on the acceleration of the beam due to the radial force associated with the self-field is

$$\left.\begin{aligned} a &= F^s/M \\ &= e^2\bar{A}_\varphi^2\,\nu\,(\lambda - 2)/2mM\rho. \end{aligned}\right\} \qquad 2.53$$

Substituting for $\bar{A}_\varphi$ and integrating, the displacement of the beam from its initial position is

$$s = e^2\nu\,(\lambda - 2)E^{b^2}t^4/24mM\rho\,(1 + \lambda\nu)^2. \qquad 2.54$$

For $\lambda = 5$; $E^b = 4.4 \times 10^3$ volt/m and singly ionized argon the time taken for a displacement of 0.02 m is given by

$$t' = 2.5 \times 10^{-7}\,(1 + \lambda\nu)^{\frac{1}{2}}\nu^{-\frac{1}{4}}. \qquad 2.55$$

The time required for this displacement therefore is a slowly varying function of ν. The minimum value of t' under the stated conditions occurs for about $\nu = 0.2$ and has the value of 0.54 μsec.

The value of t' is indicative of the time taken for the beam to reach the equilibrium position (in the sense of equation 2.44), or, if ν exceeds the value for which an equilibrium exists, t' is indicative of the time taken for the beam to reach the wall of the chamber.

(3) Motion of the beam due to errors in the betatron guide field.- An estimate of the magnitude of the radial force on an electron resulting from an incorrect current distribution in the betatron winding is given in Appendix A. The result is in terms of ϵ, the fractional error in the ratio of currents in the inner and outer turns. The

result is a net outward force if the current in the inner turns is too large and a net inward force if the current in the inner turns is too small. This radial force is given by

$$F^{\epsilon} = 0.6\epsilon e^2 \bar{A}_{\varphi} A^b/m\rho. \qquad 2.56$$

As was the case for the force due to the self-field, a force F^{ϵ} will tend to move the beam towards a wall of the chamber. The upper limit on the magnitude of the acceleration is given by Newton's Second Law. The displacement of the beam in the radial direction will be

$$s = 0.6\epsilon e^2 \dot{B} b^2 t^4/12mM\rho(1 + \lambda\nu). \qquad 2.57$$

With an accelerating field of 4.4×10^3 volt/m, an error in the current ratio of 10% will cause a beam of electrons of low ν value and singly ionized argon ions to move 0.02m in approximately 0.55 μsec. The time required would be somewhat longer for a beam of high ν value.

Incidentally one may estimate the maximum value of ϵ which will still yield an equilibrium orbit within the betatron chamber. By equating the radial force due to the error in the current distribution to the betatron focusing force at r = 0.02 m (where it is a maximum), one obtains from equations 2.34 and 2.56 that

$$\epsilon_{max} = 0.095. \qquad 2.58$$

The above results show that an error of 9% or more in the ratio of the currents in the inner and outer turns causes serious changes in the betatron guide field. Errors

of this magnitude however will not cause significant movement of the beam until approximately one half microsecond after the beginning of the acceleration.

2.6 Summary of important results

The theory presented in this chapter predicts the following:

(1) Only moderate accelerating fields are required to produce large numbers of runaway electrons. Accelerating fields in excess of 10 volts/m should, in the absence of inhomogeneities in the plasma, decouple the electrons from the ions under the conditions of this experiment. Small inhomogeneities in the plasma may however trap large numbers of electrons.

(2) One effect of the self-field of the circulating electrons is to reduce the accelerating field. The accelerating field - and hence the electron energy - is reduced by a factor $(1 + \lambda\nu)$. This becomes important in this experiment for $\nu > 0.05$ and leads to a current limitation in the plasma betatron.

(3) For $\nu > 3 \times 10^{-3}$ the pinch forces are stronger than the betatron focusing forces but no constriction of the beam occurs due to the presence of the azimuthal magnetic field.

(4) An error of about 9.5% in the ratio of the currents in the inner and outer turns of the betatron winding

will destroy the betatron condition.

(5) There is an upper limit to the number of electrons which may be accelerated in an equilibrium orbit in the plasma betatron. This limit - represented by $\nu_{max} = 0.032$ - is due to the self-fields of the beam current.

(6) Even if the betatron condition is not realized and the number of electrons exceeds the limit noted above, normal acceleration should result during the first half microsecond of the acceleration period. The disturbing effects noted in (4) and (5) above are most serious for $\lambda\nu$ equal to unity - that is for $\nu \approx 0.2$ in this experiment.

CHAPTER 3

THEORY OF THE PLASMA BETATRON WITH AN AZIMUTHAL MAGNETIC FIELD

II. STABILITY THEORY

3.1 Introduction

In the analysis of the operation of the plasma betatron given in the previous chapter the effects of instabilities were ignored. A short discussion of several potential instabilities is given in this chapter. Unfortunately the instability analysis is often quite complex and a great deal of theoretical work is still required on this problem. The contribution of this thesis in this regard is small - amounting to little more than an estimation of the time when disruption of the beam could occur through the two-stream instability.

The total energy content of a plasma is made up of four components:

(1) the thermal energy or energy of random motion,

(2) the kinetic energy of ordered motion,

(3) the stored energy of electric fields, and

(4) the stored energy of magnetic fields.

These four energy components are mutually coupled through the motion and distribution of the plasma particles and by their electromagnetic fields. This coupling can give rise to an oscillatory or unidirectional exchange of en-

ergy between the energy components. The runaway effect, sometimes classed as an instability, is an example of the unidirectional exchange of energy from an electric field to kinetic energy of ordered motion.

The usual method in stability analysis is to begin with an equilibrium plasma configuration and then test the stability of the configuration under different types of perturbation. If a perturbation is found to grow indefinitely the system is said to be unstable. If the perturbation does not grow or decays then the system is said to be stable with respect to that perturbation. All possible types of instabilities must be considered before a plasma configuration can be said to be stable.

If a system is found to be unstable with respect to some perturbation then the question of rate of growth of the instability is of practical importance. For systems which operate on a pulsed basis a slowly growing instability may be tolerable.

In this chapter the stability of one particular equilibrium configuration is investigated - that of a circulating beam of electrons frozen to an azimuthal magnetic field and in a background of positive ions.

Finkelstein and Sturrock (26) have shown that for magnetohydrodynamic theory to apply to a system like the betatron the following inequality must hold;

$$\nu/\gamma \gg 1. \qquad 3.1$$

This inequality does not hold for the conditions of interest in this experiment. For this reason the considerable work done on magnetohydrodynamic instabilities is of little help here.

Six proposed instability mechanisms will be considered. They are:

(1) The negative-mass instability

(2) The ion-wave instability

(3) The screw instability

(4) The transverse instabilities (two)

(5) The two-stream instability.

The first five will be considered briefly but the two-stream instability will be dealt with at somewhat greater length. It should be noted that the above list may be incomplete.

3.2 Five instabilities

3.2.1 The negative mass instability. This instability, first investigated by Nielson (28) should be considered where circulating currents of (energetic) electrons are involved. In a normal betatron, for example, with no azimuthal magnetic field a force on an electron tending to increase its energy will decrease its revolution frequency by moving it to a larger orbit where it will lag in phase. This results in a negative term involving the mass in the dispersion relation - hence the name negative mass instability. The effect of an azimuthal magnetic field on this mechanism

has not been investigated yet. However it seams clear that a strong azimuthal magnetic field will greatly reduce the coupling between longitudinal and transverse degrees of freedom necessary for the manifestation of this instability.

3.2.2 The ion-wave instability.- This instability (29), proposed to explain the anomalous diffusion in the stellarator, involves the energy exchange between the kinetic energy of the ions and the electromagnetic fields. Since the period of the ion oscillation is not short compared to the acceleration time this instability is not expected to be serious.

3.2.3 The screw instability.- Not to be confused with the kink instability, the screw instability was proposed by Kadomtsev and Nedospasov (30) and extended by Hoh (31) and others. The theory has had a measure of success in predicting the critical magnetic field for the onset of anomalous diffusion observed in some experimental systems.

The instability may occur where there is a longitudinal electric field applied to a plasma column in a longitudinal magnetic field. If there is a helical density perturbation the longitudinal electric field will produce a separation of the electron and ion 'screws' with the result that electric fields perpendicular to the magnetic fields are produced. Under some conditions the E/B drifts will increase the perturbation and the system is unstable. The un-

stable condition destroys the currents set up by the longitudinal electric field and increases the loss of the plasma across the magnetic field.

Major modifications must be made to the existing theory if it is to be applied to the plasma betatron. The high mobility of the electrons along the azimuthal magnetic field and the tendency of the electrons to move along the magnetic lines of force must be taken into account. In addition, predictions of growth rates - not included in existing theory - are necessary if verification is to be made using results of the plasma betatron experiment.

The required modifications to the theory have not yet been successfully carried out and therefore little can be said regarding the severity of this instability mechanism in the plasma betatron. It would appear however that if the system were susceptible to this instability the growth rate would not be strongly dependent on the plasma density.

3.2.4 The transverse instabilities.- While the system under study here is different from the simple magnetohydrodynamic pinch, the perturbations which lead to instability in the simple pinch should be investigated. The perturbation in question is of the form $\exp i(k\rho_o\varphi \pm m\theta + \omega t)$ where k is the wave number of the perturbation and m is an integer. The m = 0 mode is called the 'varicose' or 'sausage' type instability due to the form of the perturbed beam and the m = 1 mode is called the 'sinuous' or 'kink' insta-

bility due to the screw-like deformation of the beam. The two perturbations, including the azimuthal magnetic field, are shown in Figure 7.

(1) The varicose (m = 0) instability.- The addition of an azimuthal magnetic field to the plasma betatron should stabilize the beam against perturbations of this kind. The stability is achieved through the removal of the driving force tending to increase the perturbations. As was noted in Section 2.5.6 any force tending to change the radius of the beam would be transformed away by a rotation of the plasma in the azimuthal magnetic field.

(2) The kink (m = 1) instability.- Finkelstein and Sturrock have analysed a case in which the kinetic energy of the beam is larger than the magnetic energy - as in proposed relativistic beams. In the absence of an azimuthal magnetic field, a region of stability is found when the stabilizing effect of the electrostatic attraction between the electron and ion streams is taken into account. In terms of parameters for the experiment described in this thesis, stability is predicted for

$$\nu < 3b^2/\rho_o^2. \qquad 3.2$$

For a beam of radius 0.02 m the predicted maximum ν for stability for this model is then 0.03.

In this experiment the beam kinetic energy is expected to be larger than the magnetic energy except at the

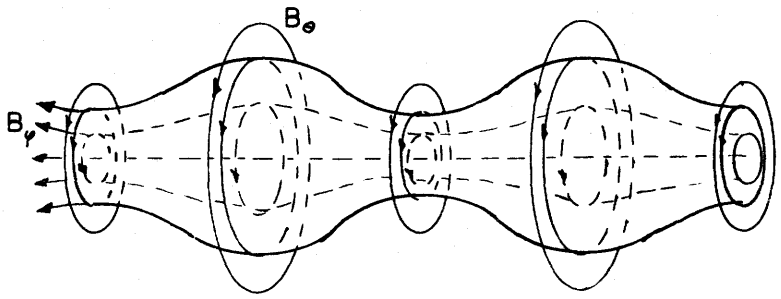

(a) The varicose instability

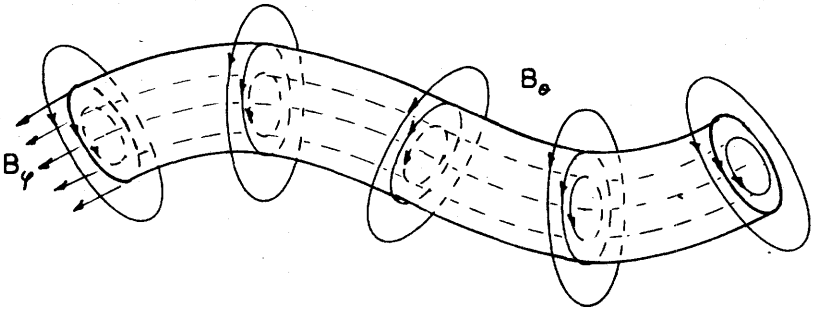

(b) The kink instability

Figure 7. Diagramatic representation of the perturbations of the transverse instabilities.

high ν values (>0.2). However the stabilizing effect of the azimuthal magnetic field is expected to extend the range of stability considerably. The azimuthal magnetic field is a stabilizing effect because a growth of the perturbation would involve a distortion of the azimuthal magnetic field which is frozen in the beam.

3.3 The two-stream instability

3.3.1 Introduction.- A collective effect of potential importance in the plasma betatron experiment is the two-stream instability. It is due to longitudinal plasma oscillations which can occur in a plasma. With contrastreaming charged particles longitudinal plasma oscillations can grow rapidly under certain conditions, transforming the directed energy of the particles into fluctuation energy of the oscillations.

Buneman (32) has calculated the initial energy of the thermodynamically 'free' plasma oscillations in an infinite plasma and described the amplification of this energy to levels where the electron drift energy is converted to turbulence. The growth mechanism is a velocity and density modulation of the particles as they pass over the potential waves. Certain wavelength groups are amplified strongly until disruption of the drift motion is complete. Skarsgard (33) has shown that for the plasma betatron growth of the oscillations is restricted in some cases. This results from the fact that in a finite plasma there is limited amplifica-

tion of a limited range of wave lengths.

The essentials of the two-stream instability are given here with certain predictions about the stability properties of the plasma betatron under somewhat idealized assumptions for the velocity distributions of the electrons and ions. The theory set down in this section is non-relativistic.

3.3.2 The dispersion relation.- The dispersion relation for the case of a two-component plasma with stationary ions and streaming electrons is (32)

$$\omega_{pi}^2/\omega^2 + \omega_{pe}^2/(Kv - \omega)^2 = 1. \qquad 3.3$$

In this equation k is the wave number of the perturbation, v the mean electron velocity and ω_{pe} and ω_{pi} are the electron and ion plasma frequencies. The dispersion relation for a special case of a three component plasma including a number of electrons at rest is (33)

$$(\omega_{pi}^2 + f'\omega_{pe}^2)/\omega^2 + \omega_{pe}^2/(Kv - \omega)^2 = 1. \qquad 3.4$$

In this equation ω_{pe} is the plasma frequency corresponding to the number of electrons at the mean streaming velocity, v, and f' is the ratio of the number of electrons at rest to the number in the stream.

The solution of the two preceding equations - published by Buneman - is reproduced in Figure 8 in terms of f, where f is given by

$$f = m/M + f'. \qquad 3.5$$

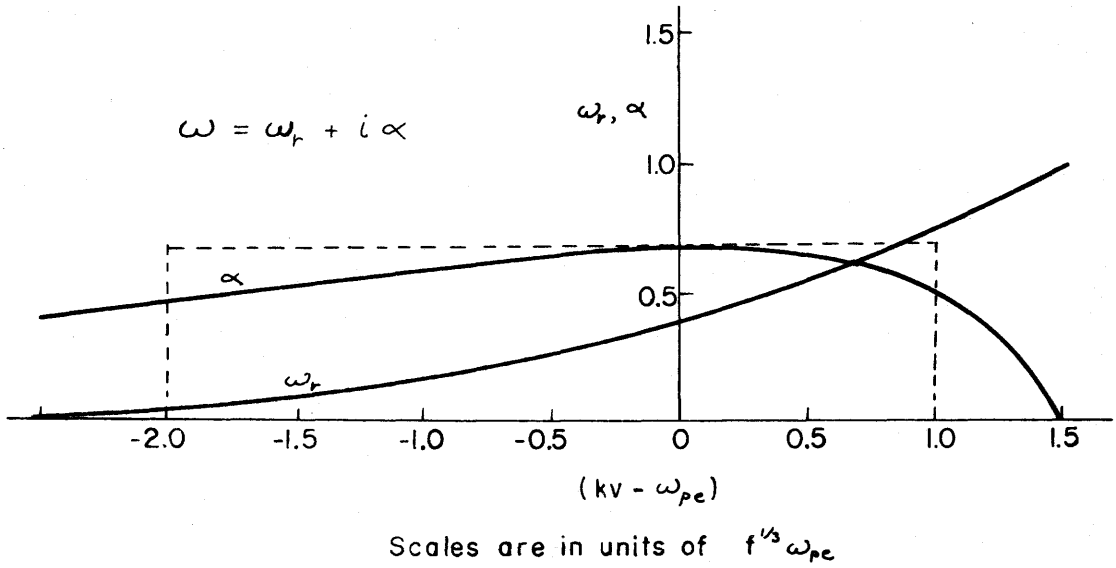

Figure 8. The solution of the dispersion relation for the two-stream instability.

The curves show the real part and the imaginary part of ω. A positive imaginary component, α, leads to an exponentially growing wave, - hence an unstable condition.

3.3.3 Growth of the plasma oscillations.- Buneman has shown that in a uniform plasma there are 'free' (undamped) plasma oscillations. The free plasma oscillations are those which have phase velocities too great to be affected by Landau damping. The growth of these oscillations in the presence of a constant accelerating field is of interest here.

With the electron beam being accelerated from rest, at first oscillations with very short wavelengths will be amplified. As the drift velocity increases longer wavelengths will be 'in resonance' and amplified strongly. The growth of the plasma oscillations is at the expense of the drift energy of the electrons.

The solution of the dispersion relation is approximated by a square topped function as indicated in Figure 8. Amplification of a given wave number k lasts only as long as v is within a band of width $3f^{1/3}\,\omega_{pe}/k$ around the value ω_{pe}/k. Since the acceleration under a constant electric field is eE/m the duration of amplification is therefore

$$\left.\begin{aligned} \text{'duration'} &= m\,\Delta v/eE \\ &= 3f^{1/3}\, m\, \omega_{pe}/eEk. \end{aligned}\right\} \qquad 3.6$$

The energy amplification of the oscillation of wave number k is then given by $\exp\tau$ where

$$\left.\begin{aligned}\tau &= 2\,\alpha_m \times \text{'duration'} \\ &= 4.12\ f^{2/3}\ m\ \omega_{pe}{}^2/eEk.\end{aligned}\right\} \qquad 3.7$$

3.3.4 Disruption of the beam.- The total amplified fluctuation energy is found by integrating over the range of wave numbers which have passed through 'resonance'. Alternatively the integration can be performed over the corresponding range of τ values. Equation 3.7 shows that the amplification of the smallest wavenumbers (longest wavelengths) are the most serious. It is found that beam disruption can be expected to occur if the range of values extends up to a critical value τ_1. For a wide range of conditions $\tau_1 \simeq 40$ for this experiment (33).

If k_1 is the wavenumber undergoing amplification at the time of disruption t_1 then for the case of a constant electric field (see Figure 8)

$$eEt_1/m = \omega_{pe}/k_1 \qquad 3.8$$

and equation 3.7 becomes

$$\tau_1 = 4.12\ f^{2/3}\ \omega_{pe}\ t_1. \qquad 3.9$$

Setting $\tau_1 = 40$ and expressing ω_{pe} in terms of the beam parameters, for a beam of radius 0.02 m,

$$t_1 = 3.24 \times 10^{-10}\ f^{-2/3}\ \gamma^{-\frac{1}{2}}. \qquad 3.10$$

This equation is plotted as solid lines in Figure 9. The portion where relativistic effects are significant is

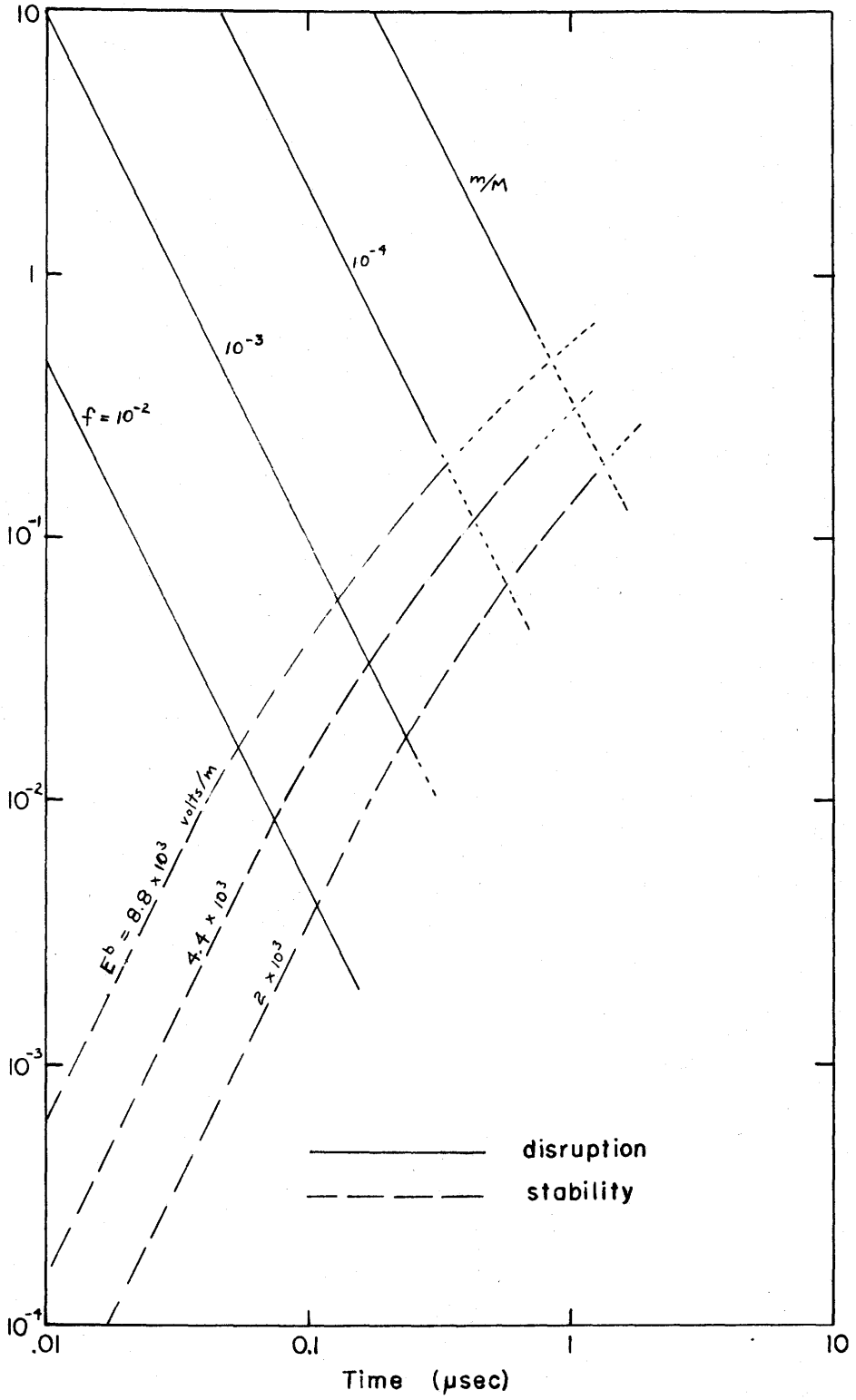

Figure 9. Curves showing the time of beam disruption due to, or the time that stability is secured against the two-stream instability in the plasma betatron.

shown dotted.

3.3.5 Persistence of the beam.- Skarsgard has taken into consideration the fact that the longest wavelength which could be involved in any instability of this kind in the plasma betatron is limited by the geometry of the system. the minimum wave number which can undergo significant amplification in this system is approximately 1/b.

Clearly from the solution of the dispersion relation (Figure 8) if an electron drift velocity can be established such that

$$v > (1 + 1.5\ f^{1/3})\ \omega_{pe}\ /k_{min} \qquad 3.11$$

there will be no further amplification of longitudinal oscillations.

Using equation 3.8, a critical time t_c may be found when the smallest (and most dangerous) wave number ceases to be amplified. If the fraction of electrons at rest is small

$$t_c = \omega_{pe} m/eEk_{min}. \qquad 3.12$$

In the plasma betatron $E = E^b/\ (1 + \lambda v)$ and k_{min} is taken to be b^{-1}. The critical time is then given by

$$t_c = 2mc\sqrt{v}\ (1 + \lambda v)\ //\ eE. \qquad 3.13$$

If the beam has not been destroyed by this time its stability with respect to the electrostatic oscillations is secured. Equation 3.13 is plotted for three values of accelerating field as dashed lines in Figure 9. Again the part of the curves where relativistic effects may be sig-

nificant are shown dotted.

3.3.6 Discussion.- The stability characteristics of the plasma betatron with respect to the two-stream instability may be inferred from Figure 9. Under specified conditions of ν, f, and E, if the dashed line crosses the given ν value at an earlier time than the solid line, the system should be stable. If the solid line crosses first the system is predicted to be unstable. Figure 9 also indicates the time during the acceleration period at which disruption of the beam should occur or the time at which stability is secured.

The curves in Figure 9 indicate the strong dependence of the growth of the instability on the beam density and the fraction of electrons at rest; only a small change in the number of electrons at rest changes the stability situation considerably. The assumptions made about the electron velocity distribution are probably unrealistic and it is not known how the results are affected by these assumptions.

The situation with regard to an inhomogeneous plasma (as discussed in Section 2.4.2) may be somewhat different. The initial plasma oscillations may be of much higher amplitude but would be expected to have a characteristic wave number k' - associated with the spacing of the coils producing the azimuthal magnetic field for example. In this case if disruption of the beam were due to amplification

of these oscillations it should occur when the drift velocity had the value ω_{pe}/k'.

CHAPTER 4

DIAGNOSTIC TECHNIQUES

4.1 The Rogowski coil

4.1.1 Description of the coil.- The Rogowski coil is a device for measuring current. It consists of a toroidal winding which encircles the current to be measured. A signal is produced in the coil which is proportional to dI/dt. For an N-turn coil on a toroidal former of rectangular cross section it is easily shown that the voltage induced in the coil is given by

$$V = -2 \times 10^{-7} Nd \ln(r_2/r_1) \frac{dI}{dt} \qquad 4.1$$

where d is the width of the coil and r_1 and r_2 are the inside and outside radii of the coil. This voltage may be integrated electronically with respect to time and the integrated signal, which is proportional to the current being measured, displayed on an oscilloscope.

The sensitivity of the coil depends on the dimensions of the coil and the number of turns. If a large number of turns is used a ringing circuit is formed by the inductance and distributed capacitance of the winding unless special measures are taken. In the Rogowski coil used in this experiment a satisfactory sensitivity (3.6×10^{-7} volt-sec/amp) was achieved without ringing being produced by winding the coil with resistance wire. The 1.3K resistance of the winding was sufficient to damp any oscillations and still

had negligible effect on the integration of the signal.

The integration is performed by a simple RC circuit with C consisting of the capacitance of a coaxial cable plus the input capacitance of the oscilloscope. The time constant of the RC circuit is approximately 20 μsec.

In order to place the coil around the torus the coil was constructed in two sections. It was found necessary to enclose the coil in a brass shield because noise from the vacuum switches was excessive. A photograph of the coil and shield is shown in Figure 10. The coil is shown in its place in the plasma betatron in Figures 1 and 2.

4.1.2 Rogowski coil calibration.- The integrated signal from the Rogowski coil is proportional to the current being measured. A calibration of the system was made using a transient current of duration approximately the same as is observed in the plasma betatron experiment. Thus it was possible to check the frequency response of the Rogowski coil. The circuit used is shown in Figure 11. The calibration in terms of voltage deflection on the oscilloscope is

$$I = 110\ V. \qquad 4.2$$

This calibration is estimated to be correct to within 20%.

4.1.3 Calculation of ν.- It will be shown in Chapter 5 that the oscilloscope traces from the Rogowski coil indicate that there is a period near the beginning of the betatron acceleration during which the current rises lin-

Figure 10. Photograph of the Rogowski coil removed from its shield.

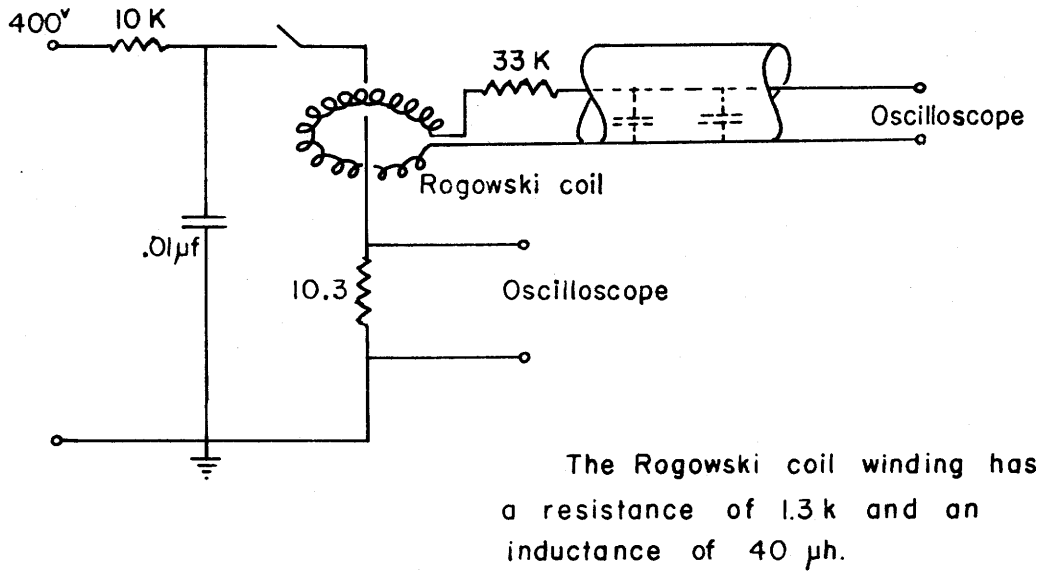

Figure 11. The circuit diagram for the calibration of the Rogowski coil.

early. If it is assumed that this current is due to runaway electrons, a calculation of ν can be made if the accelerating field is known. The validity of this assumption is discussed in Section 5.5.1 in the light of the results of the experiment.

From equation 2.30 the rate of change of current is given by

$$dI/dt = 10^{7}E^{b}\,\nu/(1 + \lambda\nu). \qquad 4.3$$

Using equation 4.2 one obtains

$$\frac{\nu}{1 + \lambda\nu} = \frac{1.1 \times 10^{-5}}{E^{b}}\,\frac{dV}{dt} \qquad 4.4$$

where dV/dt is the slope of the linear portion of the Rogowski coil trace in volts/second.

For $\lambda\nu \ll 1$ the right side of equation 4.4 yields ν directly. For large ν the curves in Figure 12 may be used to estimate ν. The value of λ is not known accurately but is approximately 5 for this experiment. Note that the accuracy of this method of determining ν decreases at high values of ν.

4.2 Scintillation detectors

4.2.1 Introduction.- Evidence of runaway electrons can be obtained by detecting x rays emitted from the apparatus. Knowledge of the intensity and quality of the x rays can lead to information about the number and energy of the electrons producing the x rays.

In this experiment bremsstrahlung radiation is produced

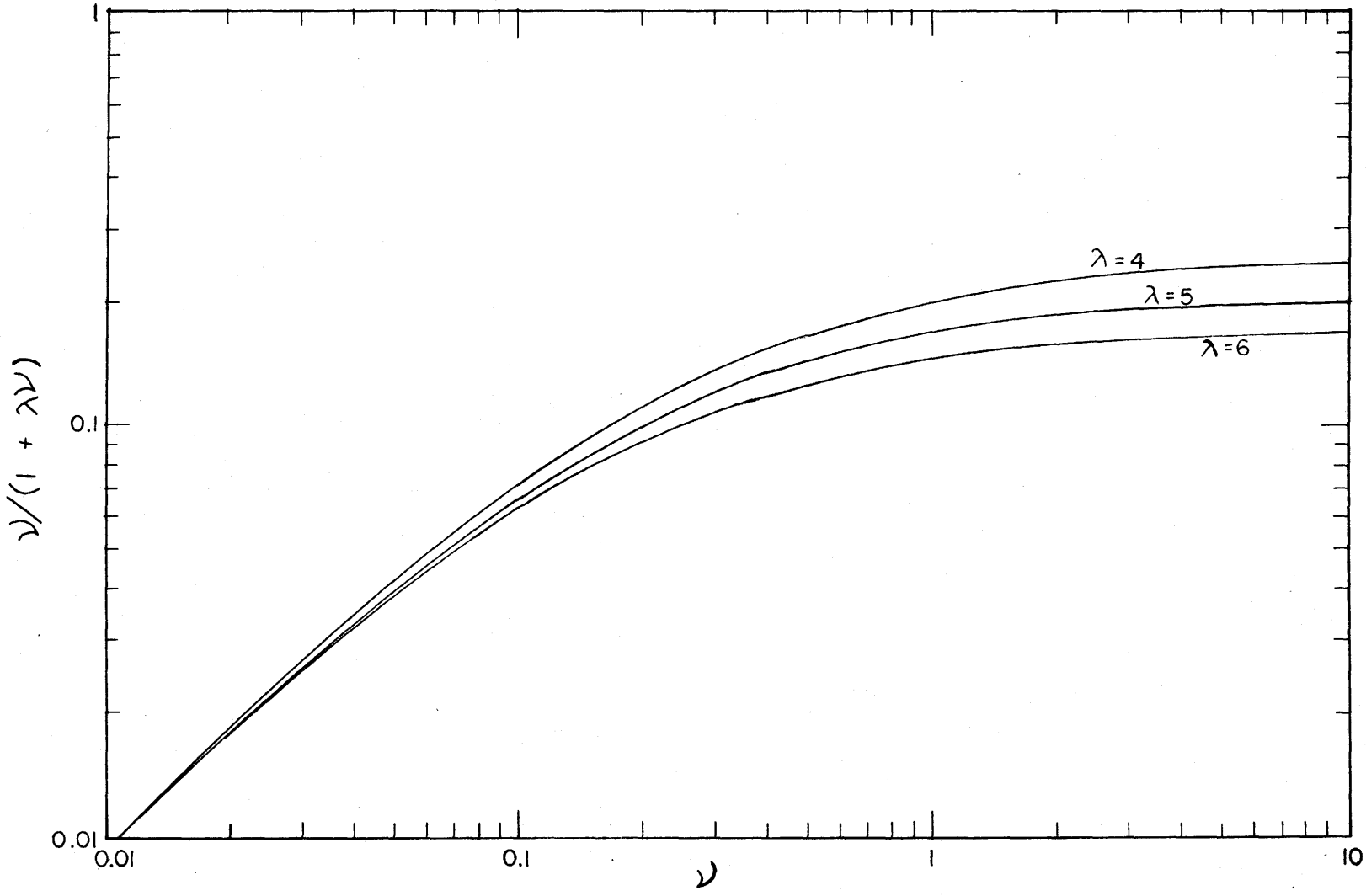

Figure 12. Curves of $\nu/(1 + \lambda\nu)$ vs ν used in the determination of ν by the Rogowski-coil technique.

by electrons striking the walls of the chamber. A pair of photomultipliers with plastic phosphor crystals provide simultaneous detection of the x rays. One unit detects radiation coming directly from the apparatus while the other detects radiation which has been filtered by a thin sheet of lead.

A photograph of the x ray detecting system is shown in Figure 13. A part of the energy of the x radiation reaching the crystal is converted to fluorescent radiation which is detected by the photomultiplier tube. As indicated in the circuit diagram of Figure 14, the signal from the photomultiplier goes to a cathode follower and through a coaxial cable to a double beam oscilloscope.

Electrons of energy W striking the wall of the torus will produce bremsstrahlung radiation with total energy

$$P_t = 2\pi\rho\,\nu_\ell\,\eta_t\,W/n_0 \qquad 4.5$$

where ν_ℓ is the number of electrons lost from a slice of beam one classical electron radius thick and η_t is the efficiency of bremsstrahlung production. The energy deposited in the crystal will be

$$P_d = P_t G T \mathcal{H}_c \qquad 4.6$$

where G is a geometrical factor equal to the fractional solid angle subtended by the scintillation crystal at the center of the betatron donut ($G = 1.77 \times 10^{-5}$ for the measurements reported in this thesis), T accounts for the

Figure 13. Photograph of the scintillation detectors with power supplies.

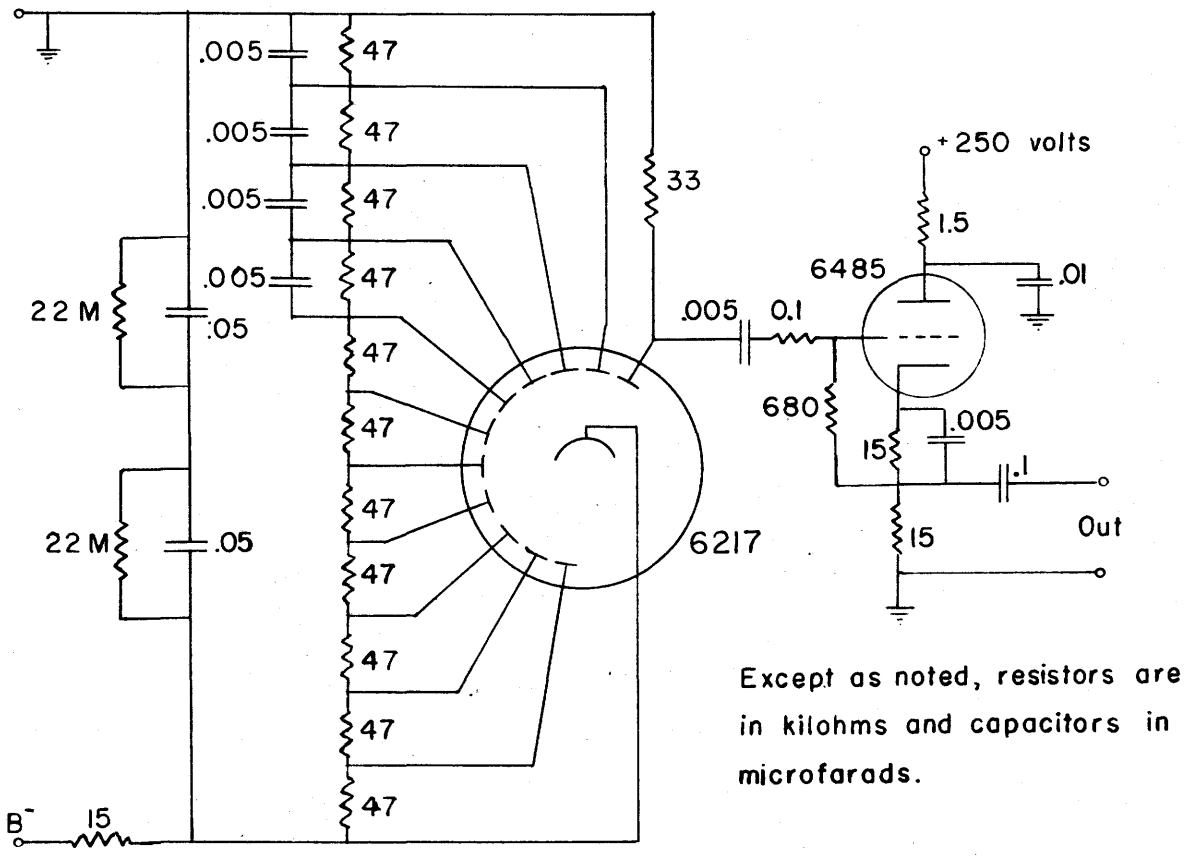

Figure 14. Circuit diagram for the scintillation detectors.

transmission through the apparatus and η_c accounts for the crystal efficiency.

The evaluation of some of the terms in these equations depend on the spectrum of the bremsstrahlung radiation and the absorbing properties of several materials. Since the electrons striking the walls of the torus may not be monoenergetic the x-ray spectrum may not be known. The procedure followed is to assume that the electrons striking the wall of the chamber have one of three types of energy distribution. For each type the resulting x-ray spectra is approximated and calculations are made for the amount of the x-ray energy which would be deposited in a crystal. Calculations are also made of the x-ray energy which would be deposited in a crystal after it had passed a thin lead filter. The calculations are repeated over a range of electron energies and curves are produced which reveal that the ratio of unfiltered to filtered energy deposited in the crystal is indicative of the energy of the electrons. The amounts of radiation energy deposited in the crystals of course would be indicative of the number of electrons producing the radiation.

In the next section a discussion of the bremsstrahlung radiation from a thick target is given. Following this, consideration is given to the interaction of x rays with various materials for the purpose of evaluating crys-

tal efficiency and the transmission of radiation through the apparatus as a function of photon energy. The three types of x-ray spectra used in the calculations are given in Section 4.2.4. Curves for the calculation of W and ν_ℓ are then produced from appropriate calculations. A Section on the calibration of the system is followed by a discussion of probable errors. A summary of the information which can be obtained from this diagnostic technique concludes this chapter.

Many assumptions and simplifications are made in the course of the calculations. The results are, however, accurate enough to yield useful information on the events taking place in the plasma betatron.

4.2.2 Bremsstrahlung radiation from a thick target.- The three pertinent features of the bremsstrahlung radiation from thick targets are the target efficiency, the spectral distribution and the angular distribution. Reviews of data for thick targets have been presented by Stephenson (34) and by Koch and Motz (35).

(1) Target efficiency.-When electrons with energy of interest in this work penetrate matter, most of the kinetic energy is given up in the production of heat but a small amount goes into the production of bremmstrahlung radiation.

The efficiency, η_t , of x ray production depends on the atomic number, Z, of the target nucleus and the energy, W, of the electrons.

$$\eta_t = KZW \qquad 4.7$$

where K is a proportionality constant. Compton and Allison (36) in a review of measurements of the constant K estimate that to within 20% the value of K is 1.1 x 10^{-6} if the electron energy is in kev. The effective atomic number of pyrex glass was calculated in Appendix B to be 9.59.

(2) Spectral distribution.- Kramer (37), in a theoretical treatment of x rays, concluded that for thick targets, the continuous spectrum integrated over all angles should have the simple form

$$\mathcal{I}_w = C(W_{max} - W) \qquad 4.8$$

where $\mathcal{I}_w$ is the intensity of photons at energy W, and W_{max} is the photon energy corresponding to the energy of the bombarding electrons.

It is assumed for the purposes of these calculations that the spectral distribution is of the form indicated by equation 4.8 and is independent of the direction of the emitted radiation. Early measurements of the spectrum made by Kulenkampff (38) as well as several more recent measurements (39) (40), are in reasonable agreement with the theoretical spectrum of equation 4.8 for electron energies up to several hundred kev at least.

Superimposed on the continuous spectrum is a character-

istic spectrum. For the relatively light elements of the target used in this experiment the characteristic radiation is in the region of a few kev. It will be shown that essentially all radiation produced in this region is absorbed in the target material and therefore the characteristic radiation from the target may be neglected.

(3) Angular distribution.- Information on the angular distribution of bremsstrahlung radiation from thick targets is scarce. One would expect however that in a thick target, since most electrons suffer several collisions in the process of giving up the kinetic energy, the bremsstrahlung radiation would tend to be isotropic. The effect of different angular distributions can, to a certain extent, be taken into account.

For the calculations in this chapter it is assumed that the angular distribution of bremsstrahlung radiation may be represented by the intensities J_0, J_{90} and J_{180} in four quadrants as illustrated in Figure 15. The average intensity is defined by

$$4\pi J_{av} = 2\pi (0.293 J_0 + 1.414 J_{90} + 0.293 J_{180}). \qquad 4.9$$

The calculations are made in terms of a shape factor, S, defined by

$$S = (J_0 + J_{180})/2J_{90}. \qquad 4.10$$

The average intensity may be written in terms of the intensity at 90° to the incident electron beam and the shape factor.

$$J_{av} = J_{90}(0.707 + 0.293S). \qquad 4.11$$

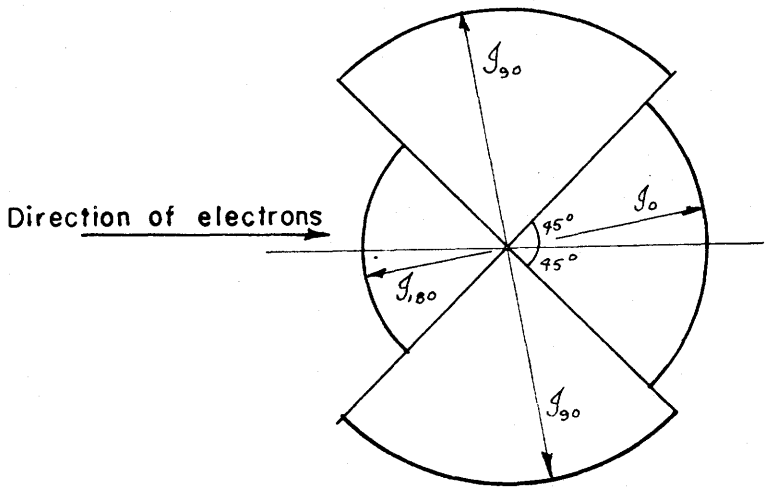

Figure 15. Diagramatical representation of the angular distribution of bremsstrahlung radiation from thick targets.

For an isotropic distribution S = 1. If the distribution has a maximum in the forward direction S may be greater than 1. The few measurements available (41) indicate that for electron energies of interest in this experiment the intensity may be greatest in the quadrant at right angles to the bombarding electron beam making S less than 1.

4.2.3 The interaction of x rays with the apparatus.-

(1) Efficiency of the crystal.- By crystal efficiency is meant the percentage of energy incident on the crystal which is deposited in the crystal. Most of the energy deposited appears as electron kinetic energy which is partially converted to fluorescent radiation through excitation and ionization of atoms of the crystal. A description of the crystal and the calculation of the photoelectric and Compton attenuation coefficients appear in Appendix B.

The intensity of radiation which is absorbed directly by the crystal is given by

$$\mathcal{I}_a = \left(\frac{\tau+\sigma_a}{\tau+\sigma}\right)\mathcal{I}\left[1 - \exp-(\tau+\sigma)d\right] \qquad 4.12$$

where $\mathcal{I}$ is the incident intensity, d is the depth of the crystal, τ (cm^{-1}) the attenuation coefficient for the photoelectric effect and σ (cm^{-1}) is the total Compton attenuation coefficient. The Compton attenuation coefficient has two components

$$\sigma = \sigma_a + \sigma_s \qquad 4.13$$

where σ_a corresponds to absorbed energy and σ_s corresponds to scattered energy. Note that the symbols used to denote attenuation coefficients here are normally used to denote cross sections.

The radiation which is scattered through the Compton effect -

$$\mathcal{I}_s = \left(\frac{\sigma_s}{\tau+\sigma}\right)\mathcal{I}\left[1 - \exp-(\tau+\sigma)d\right] \qquad 4.14$$

must also pass through the crystal material in order to escape. If the effective absorbing thickness for the scattered radiation is taken as d/2 then there is an additional amount of energy absorbed.*

$$\left.\begin{aligned}\mathcal{I}_a' &= \left(\frac{\tau+\sigma_a}{\tau+\sigma}\right)\mathcal{I}_s\left[1 - \exp-(\tau+\sigma)d/2\right] \\ &= \left(\frac{\sigma_s}{\tau+\sigma}\right)\mathcal{I}_a\left[1 - \exp-(\tau+\sigma)d/2\right].\end{aligned}\right\} \qquad 4.15$$

Neglecting additional small terms, the efficiency of the crystal at a given wavelength is approximately

$$\eta_c = (\mathcal{I}_a + \mathcal{I}_a')/\mathcal{I}. \qquad 4.16$$

Using the attenuation coefficients determined in Appendix B, η_c was determined as a function of photon energy and is shown in Figure 16.

Ignored in this calculation is the possible escape from the crystal of the photoelectrons before their energy is transferred to the atoms. It is found however that the range of 100 kev electrons in the crystal is approximately 10^{-2} cm and therefore in this experiment the

* The attenuation coefficients for the scattered radiation have been taken to be the same as for the primary radiation. This does not introduce significant errors.

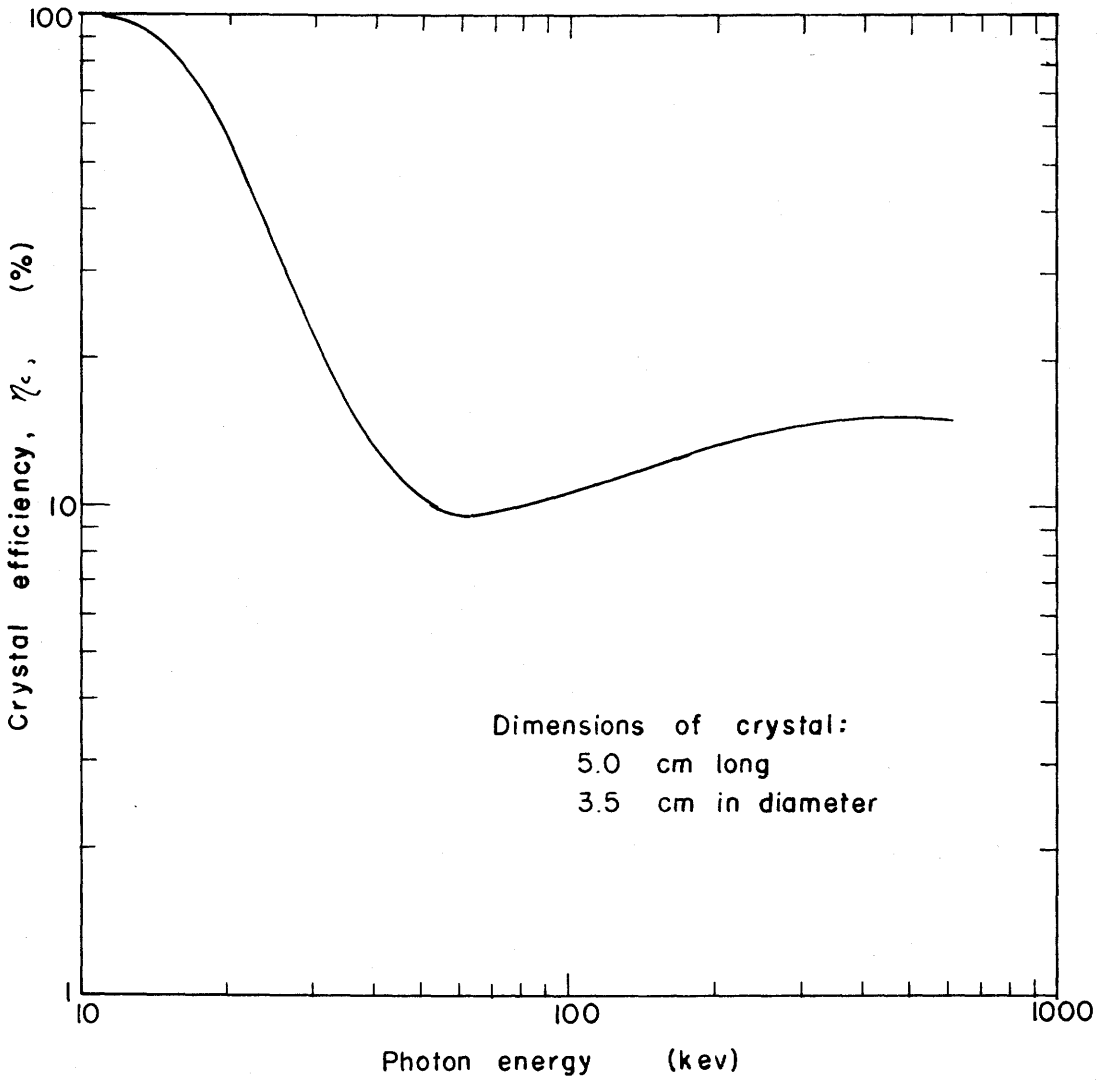

Figure 16. Curve of the efficiency of the NE 102 plastic phosphor as a function of photon energy.

loss of electrons from the crystal is negligible.

(2) Transmission coefficients.- The transmission of photons through several materials is required to evaluate the equations 4.5 and 4.6. Specifically, transmissions are required for 0.3 and 0.6 cm of pyrex glass, 0.38 cm copper (the effective thickness of the coils used to produce the azimuthal magnetic field or the Rogowski coil shield), and 0.05 cm lead.

Equations 4.12 and 4.15 may be used to calculate the transmission coefficients at a given wavelength;

$$t = 1 - (\mathcal{I}_a + \mathcal{I}_a') / \mathcal{I} . \qquad 4.17$$

The appropriate calculations were made using the attenuation coefficients in Appendix B and other published data (42) (43). The results are plotted in Figure 17.

(3) Transmission through the apparatus.- The radiation received at the detectors will have originated from many areas of the torus and will have passed various amounts of absorbing material. To estimate the overall transmission it is convenient to divide the torus into four quadrants as indicated in Figure 18.

In terms of Figure 15, the radiation directed at the detectors and originating in quadrants 1 and 3 will have intensity $\mathcal{I}_{90}$ while that from quadrant 2 will have intensity $\mathcal{I}_{180}$ and from quadrant 4 intensity $\mathcal{I}_0$. It is estimated that the radiation reaching the detectors from

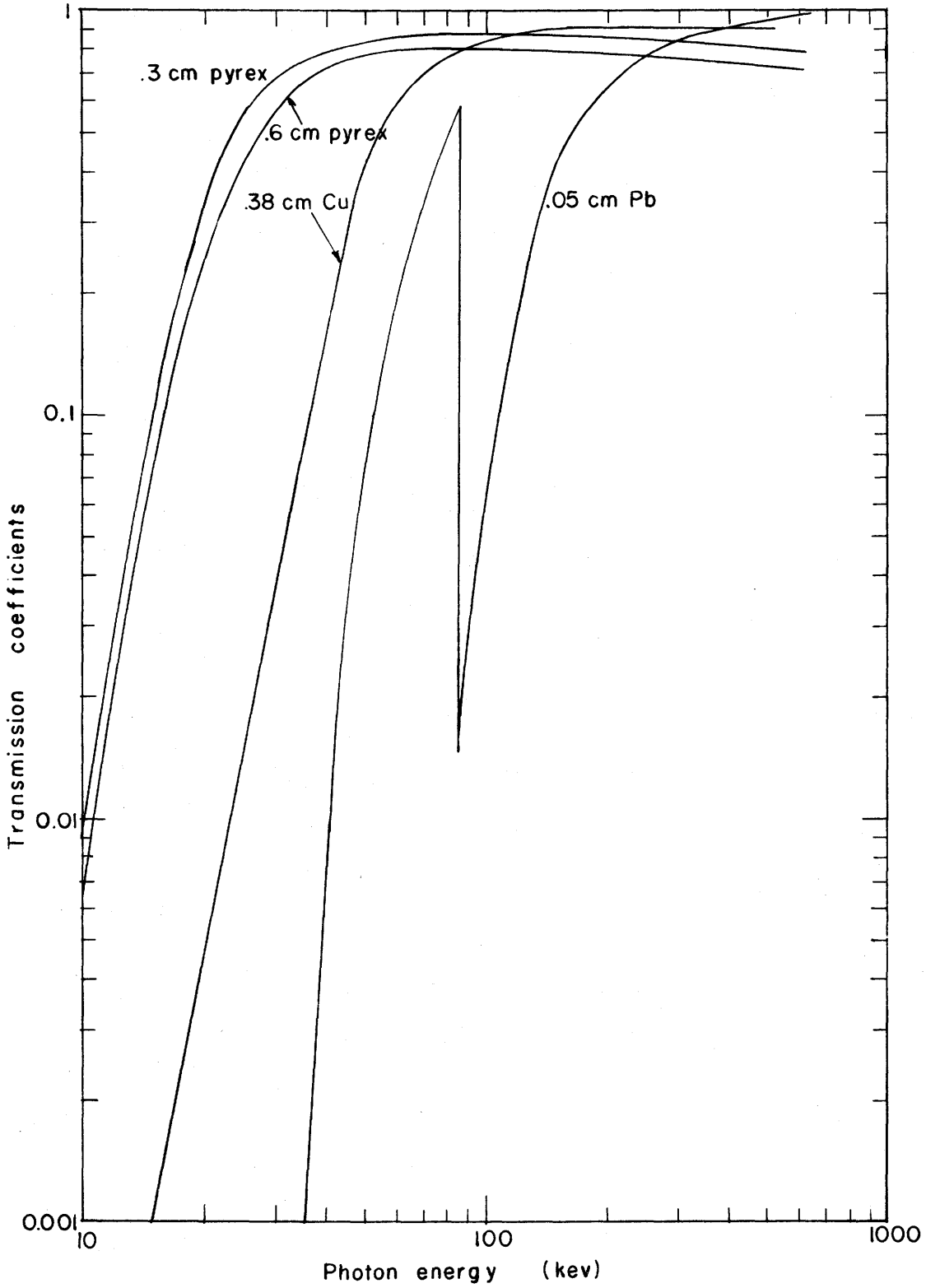

Figure 17. Curves of transmission coefficients as a function of photon energy for several materials in the plasma betatron experiment.

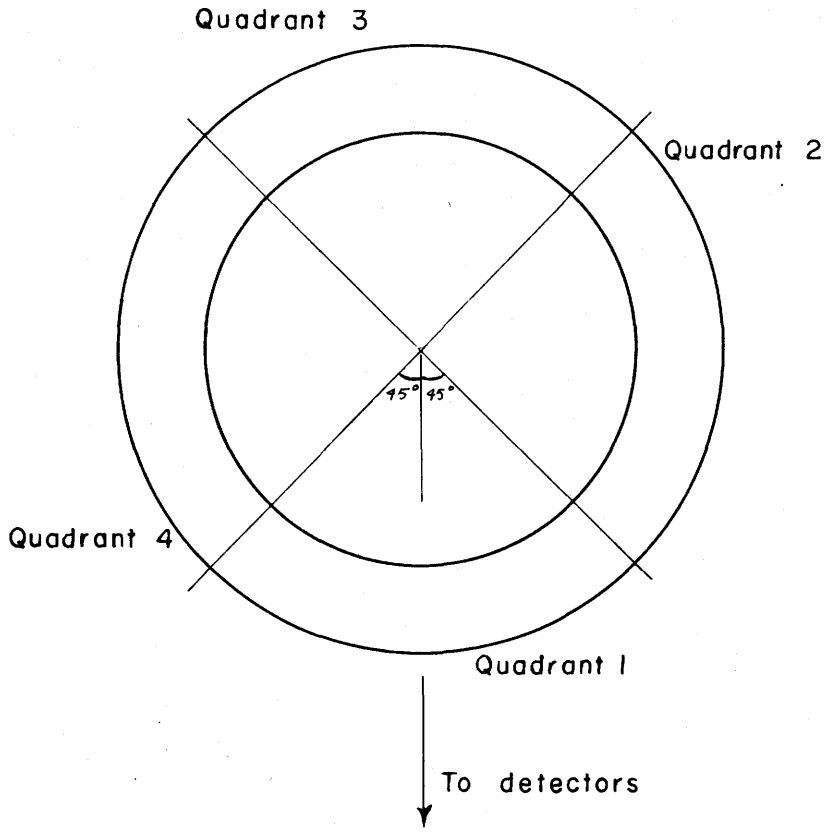

Figure 18. Diagram showing the division of the torus into quadrants for the purpose of calculating the resultant transmission coefficients.

quadrant 1 passes through 0.3 cm of glass, from quadrants 2 and 4 the thickness of glass is estimated at 0.6 cm while that from quadrant 3 is approximately 0.9 cm. It is estimated that 14% of the radiation from quadrant 1, 43% from quadrant 3 and 30% from quadrants 2 and 4 must also pass through 0.38 cm of copper. Defining t' by the equation

$$t' = (\text{Intensity transmitted to detectors})/\mathcal{J}_{av} \quad , \qquad 4.18$$

equations 4.10 and 4.11 may be used to obtain

$$t' = 0.25(X + 2SY)/(0.707 + 0.293S) \qquad 4.19$$

where

$$X = .86t_1 + .14t_1t_c + .57t_1t_2 + .43t_1t_2t_c$$
$$Y = .70t_2 + .30t_2t_c \qquad 4.20$$

and t_1 is the transmission of 0.3 cm glass, t_2 is the transmission of 0.6 cm of glass and t_c is the transmission of 0.38 cm of copper.

The calculations were made for three values of S representing a wide variation in angular distribution. The results are plotted in Figure 19. The indication is that an assumption of an isotropic angular distribution would not introduce an error in t' in excess of 30%.

4.2.4 The assumed x ray spectra.- Since the electrons striking the wall of the torus may not be monoenergetic it was decided that calculations would be made for several different cases. The x-ray spectrum resulting from a bombardment by electrons with a distribution of electron en-

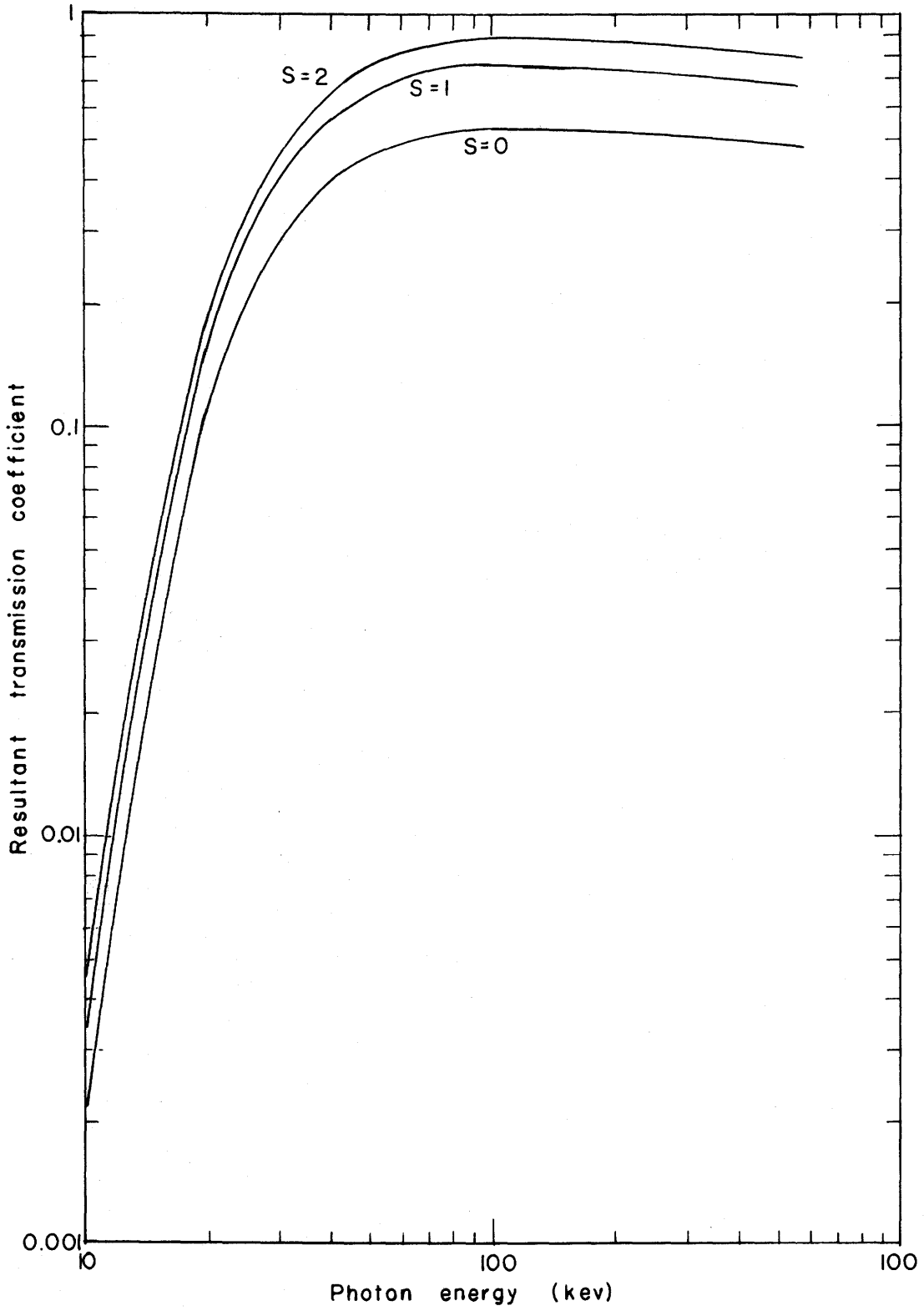

Figure 19. Curves showing the resultant transmission coefficients for the apparatus as a function of photon energy.

ergy may be approximated by superimposing appropriate Kramer distributions. Figure 20 illustrates the three cases chosen.

The quantity of interest here is ν_e , representing the number of electrons producing the x rays. If the electron stream in question is expressed as a sum of monoenergetic electron streams with electron energies W_i, then from equations 4.5 and 4.7

$$\nu_e = \sum_i \nu_i = C \sum_i P_i/W_i^2. \qquad 4.21$$

An 'effective' electron energy W_{eff} for any electron energy distribution may be defined by the equation

$$\nu_e = CP_t/W_{eff}^2; \qquad 4.22$$

From equations 4.21 and 4.22

$$W_{eff}^2 = P_t/\sum_i P_i/W_i^2 \ . \qquad 4.23$$

Calculations for W_{eff} for the three cases considered here are tabulated in Appendix C and summarized in Table I.

TABLE I

SUMMARY OF CALCULATIONS ON THREE ASSUMED X RAY SPECTRA

Spectrum type	W_{eff}	W_{av}
A	$1.000W_{max}$	$1.000W_{max}$
B	$0.612W_{max}$	$0.560W_{max}$
C	$0.428W_{max}$	$0.387W_{max}$

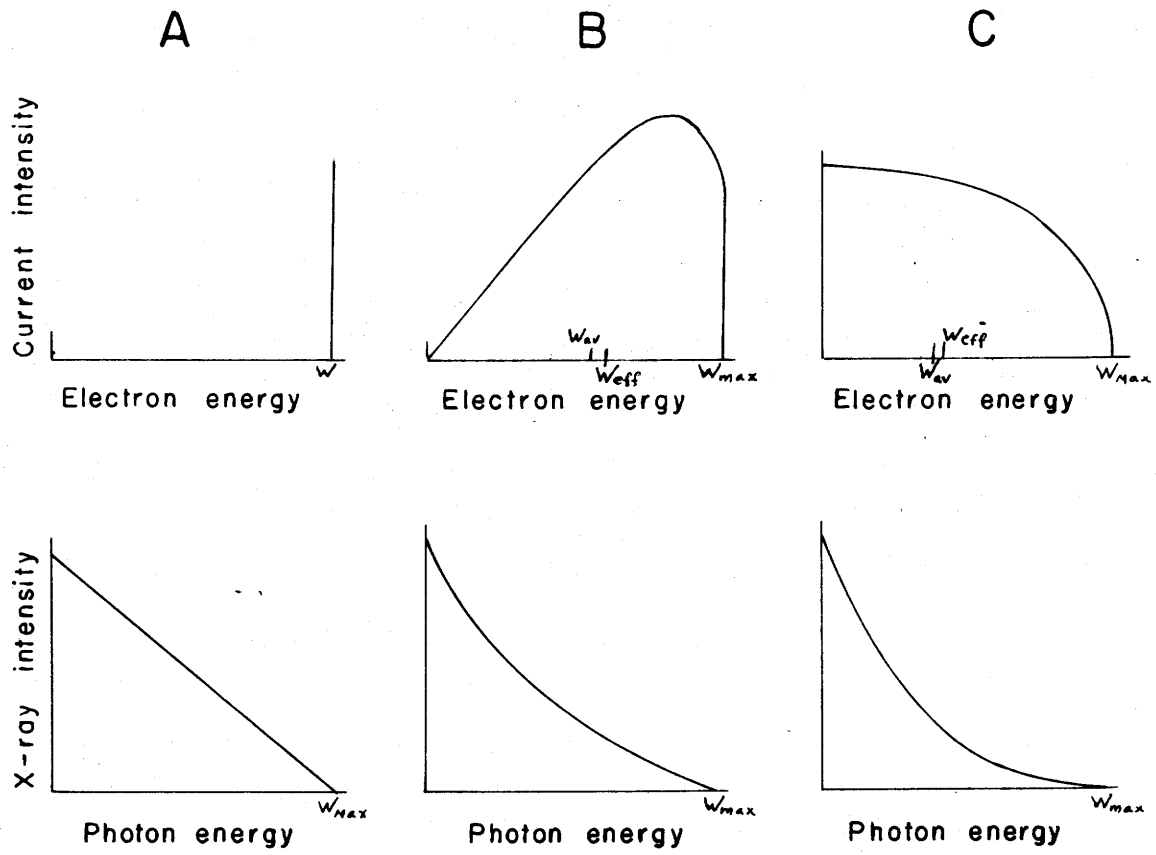

Figure 20. The three assumed x-ray spectra with the corresponding electron energy distributions.

An average electron energy W_{av} may also be calculated for the various electron energy distributions by the equation

$$\left.\begin{aligned} W_{av} &= \sum_i \nu_i W_i / \nu_\ell \\ &= \left(\sum_i P_i / W_i\right) / \left(\sum_i P_i / W_i^2\right). \end{aligned}\right\} \qquad 4.24$$

The calculations for W_{av} are also tabulated in Appendix C and summarized in Table I.

4.2.5 The calculation of the final curves.- Calculations may now be made to find the ratio of unfiltered to filtered energy deposited in the crystal. At the same time the factor $(T \mathcal{H}_c)$ may be evaluated. The calculations are made for each spectrum type for maximum photon energies of 60, 90, 120, 240 and 480 kev. Each spectrum is operated on by the appropriate values of transmission, t', and crystal efficiency, η_c, to determine the fraction of radiation produced at each energy which is deposited in the crystal. The case of the 120-kev 'A' spectrum is illustrated in Figure 21.

The area under the intensity curves is proportional to the total energy. The ratio of area II to area III is the ratio of unfiltered to filtered energy deposited in the crystal. The ratio of area II to area I is $(T \mathcal{H}_c)$. Using equations 4.5 and 4.6, ν_ℓ / P_d may be evaluated. The areas were measured with a planimeter and the calculations summarized in Table II.

The results in Table II are plotted in Figures 22 and 23.

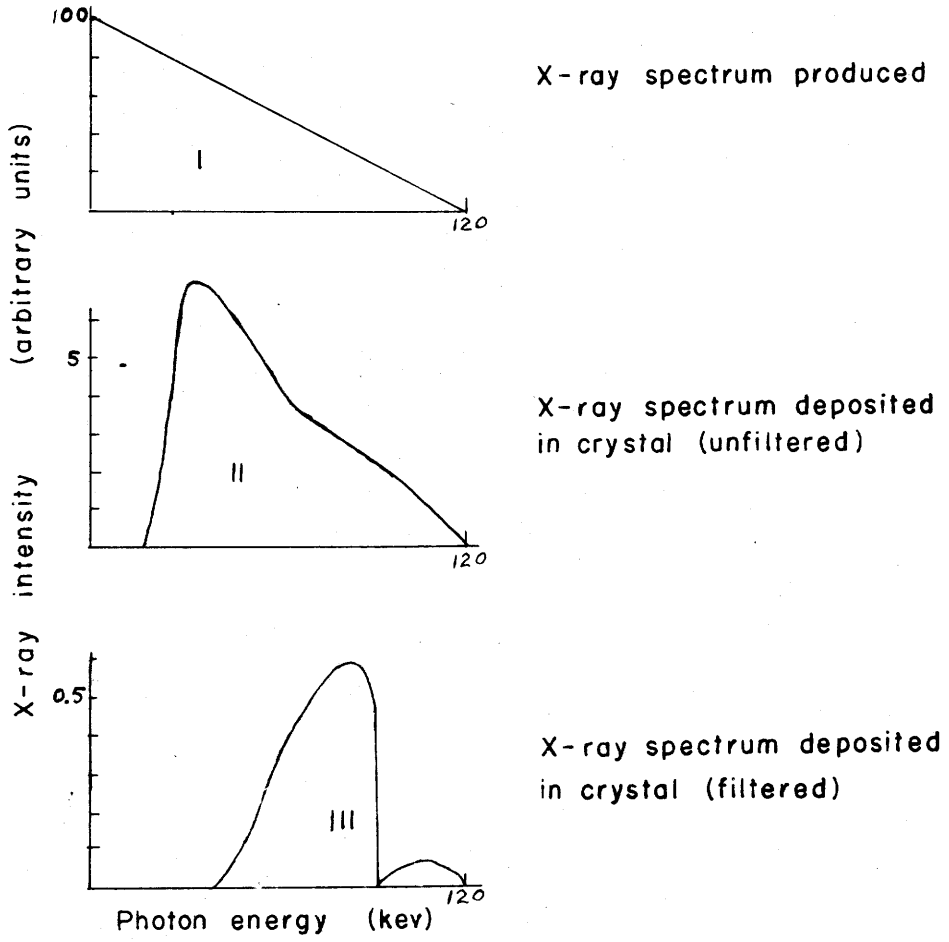

Figure 21. The 120-kev 'A' spectrum as produced, as deposited (unfiltered) in the crystal, and as deposited (filtered) in the crystal.

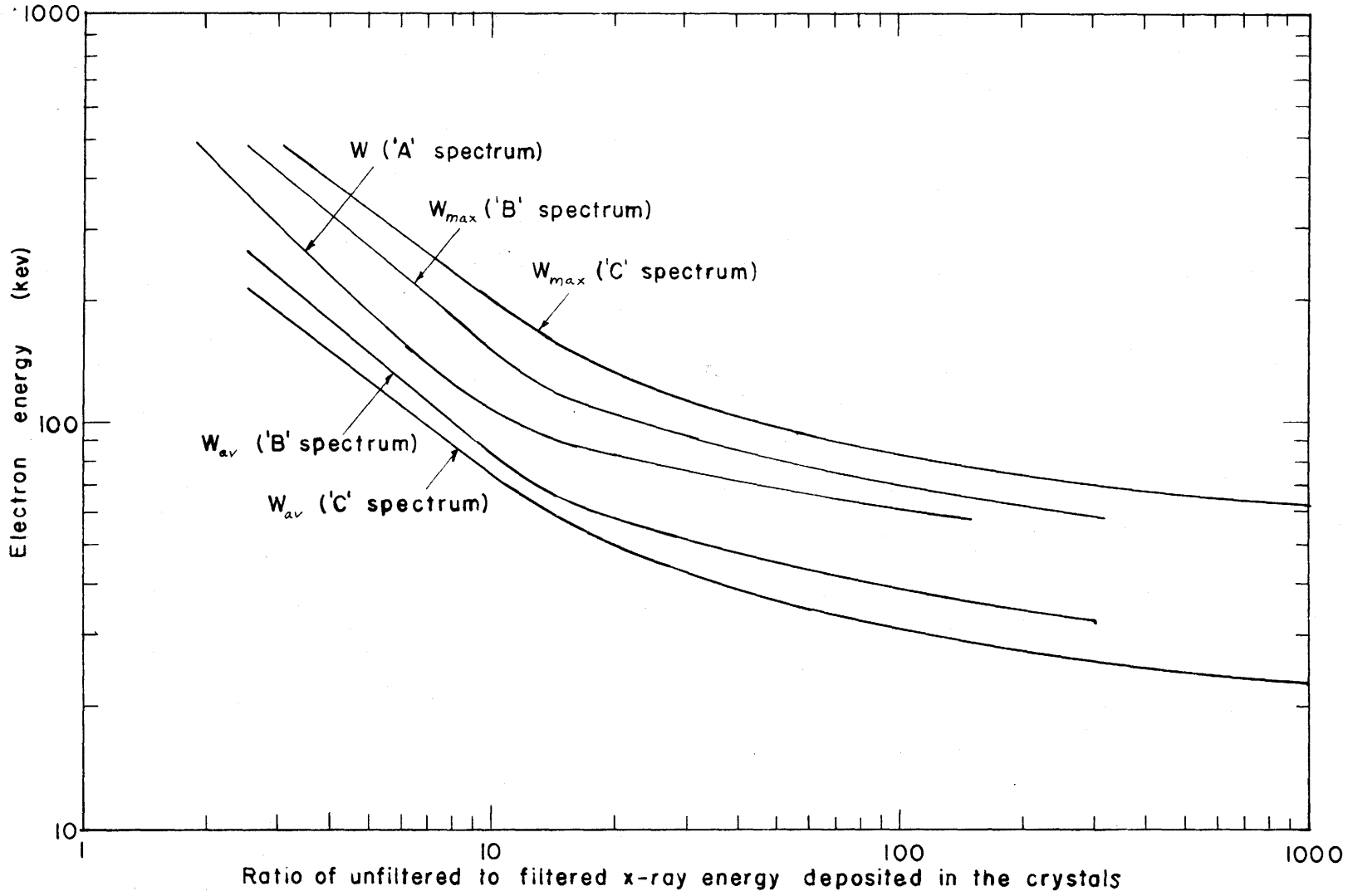

Figure 22. The maximum and average electron energy for the three assumed distributions as a function of the observed ratio of unfiltered to filtered x-ray energy deposited in the crystals.

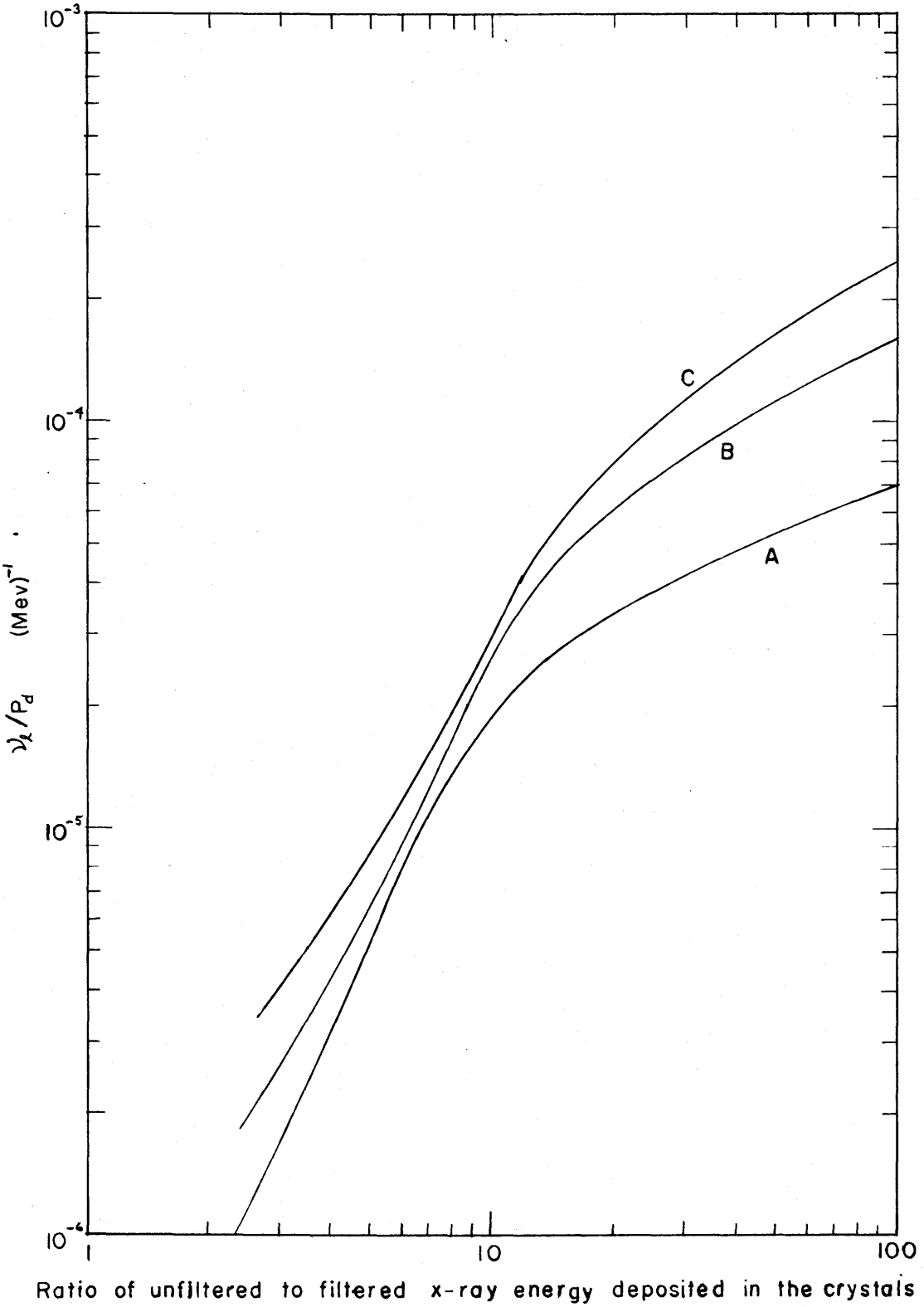

Figure 23. The term ν_ℓ/P_d for the three assumed distributions as a function of the observed ratio of unfiltered to filtered x-ray energy deposited in the crystals.

Using Figure 22, a measurement of the ratio of unfiltered to filtered energy deposited in the crystals yields an indication of the energy of the electrons producing the x rays. The ratio of unfiltered to filtered energy deposited in the crystals, along with an absolute measurement of the unfiltered energy deposited in the crystal can be used with Figure 23 to estimate ν_e representing the number of electrons producing the x rays.

TABLE II

SUMMARY OF X-RAY TRANSMISSION AND ABSORPTION CALCULATIONS

Spectrum type	W_{max} kev	Ratio*	(T H_c) %	W_{av} kev	W_{eff} kev	ν_e/P_{d_1} (Mev)$^{-1}$
A	480	1.97	8.25	480	480	6.70×10^{-7}
B		2.52	7.53	268	294	1.95×10^{-6}
C		3.15	6.95	186	205	4.30×10^{-6}
A	240	3.96	7.15	240	240	3.08×10^{-6}
B		6.04	6.62	134	147	8.88×10^{-6}
C		8.05	6.09	93	103	1.97×10^{-5}
A	120	8.37	5.93	120	120	1.49×10^{-5}
B		14.2	5.27	67	73	4.45×10^{-5}
C		27.1	4.54	46	51	1.05×10^{-4}
A	90	16.0	5.29	90	90	2.97×10^{-5}
B		37.5	4.51	50	55	9.27×10^{-5}
C		81.1	3.75	35	38	2.26×10^{-4}
A	60	137	4.63	60	60	7.63×10^{-5}
B		281	3.56	34	37	2.67×10^{-4}
C		1810	2.63	23	26	7.26×10^{-4}

*The ratio of unfiltered to filtered energy deposited in the crystals.

Lead is a particularly suitable material for the filter in this experiment. The fact that the K edge in the photoelectric effect is located at 88 kev increases the range of photon energies over which there is useful variation in the transmission through the filter. The result is that in the electron energy range of interest, the curves in Figures 22 and 23 are of more constant slope than would be the case, for example, if an absorbing material like copper or aluminum were used.

4.2.6 The calibration of the scintillation detectors.- To obtain quantitative figures for ν_e it is necessary to calibrate the scintillation detectors. This is achieved by using a source of photons of known energy and observing the response of the system.

The signal, as displayed on the oscilloscope resulting from the absorption of a single photon in the crystal, is roughly a triangular pulse with a base of 0.2 μsec. The area of the pulse is a measure of the energy deposited in the crystal. A Co^{60} source (gamma emission at 1.17 and 1.33 Mev) was used to calibrate each detector over a range of anode supply voltages. Two pairs of photomultiplier-crystal units were used. One pair, designated A and B, had the crystal directly in contact with the end of the photomultiplier tube; the other pair, designated A' and B', had the sensitivity reduced by a paper filter placed between the crystal and the photomultiplier tube. The cali-

bration curves are shown in Figure 24.

4.2.7 An estimate of errors.-

(1) The measurement of electron energy.- The determination of electron energy is made through a measurement of the ratio of unfiltered to filtered x-ray energy deposited in the crystal and the use of the curves in Figure 22.

The measurement of this ratio is subject to several errors. The radiation absorbed in the lead filter through the photoelectric effect has a high fluorescent yield and hence some of the energy absorbed photoelectrically will be emitted again. The fluorescent radiation is isotropic and therefore the amount of this radiation reaching the detectors depends on the geometry of the system. With the filter set 25 cm from the detector the fluorescent radiation reaching the detector is approximately 0.1% of the radiation absorbed photoelectrically. The important measured ratios of unfiltered to filtered radiation deposited in the crystals is approximately 10 and therefore the error due to fluorescence is less than 1%. Also affecting the measurement of the ratio is the error in the calibration of the detectors and errors in the measurements made on the oscilloscope trace. The probable error from these sources is estimated to be 10%.

In the calculations leading to the curves of Figure 22 there are also several sources of error. The greatest

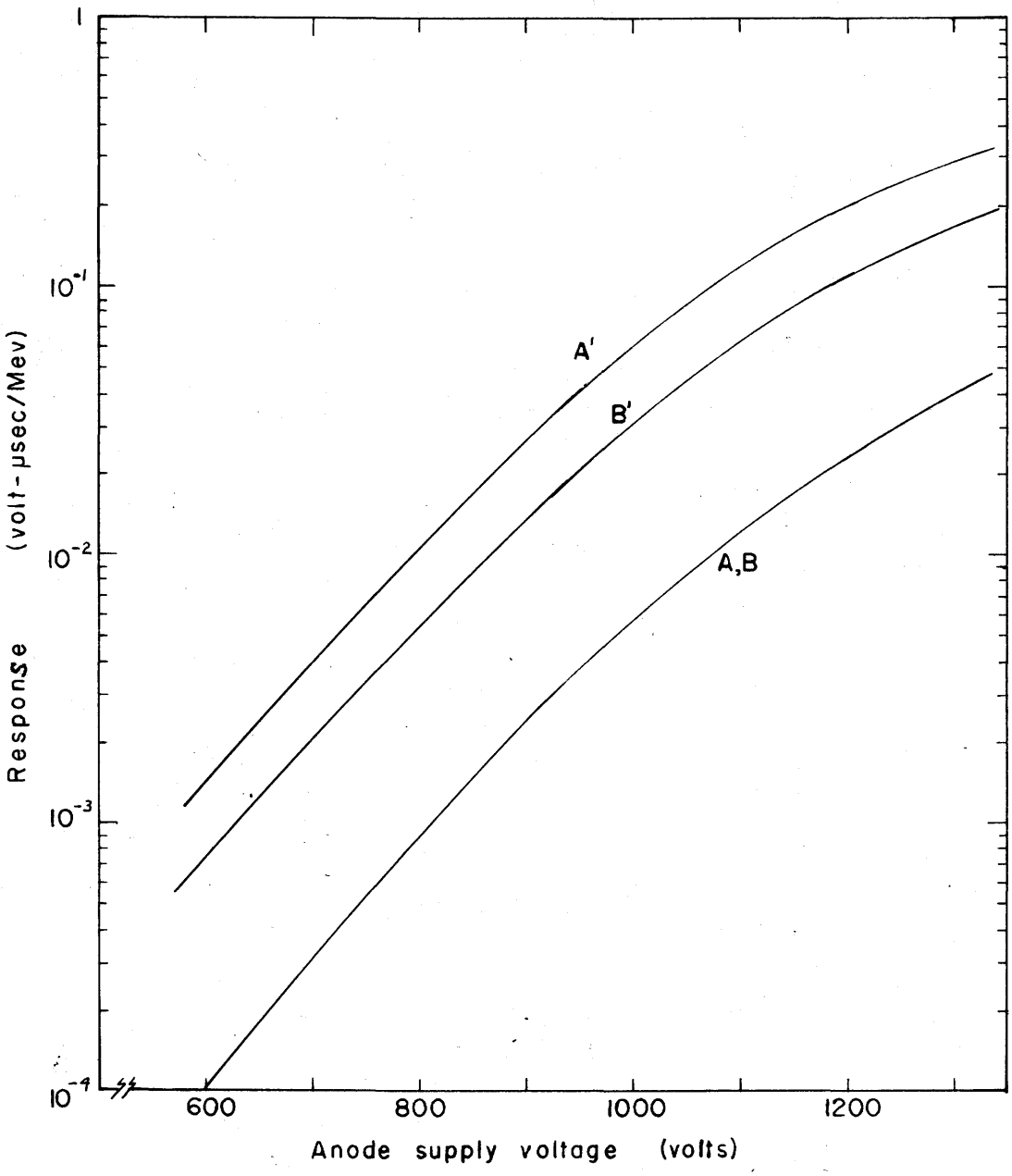

Figure 24. Calibration curves for the scintillation detectors.

of these is believed to be due to the uncertainty in the transmission curves in Figure 19. Because the greatest intensity radiation and the maximum crystal efficiency is at low energies an accurate knowledge of the transmission through the apparatus at low energies is important. Expected errors in the transmission curves should not affect the calculated ratio of unfiltered to filtered energy by more than 10%.

Taking into account the slope of the curves of Figure 22 in the region of interest, the combined effect of the three errors would produce an error of approximately 10% in the value of electron energy assuming the electron energy distribution were known.

(2) The measurement of ν_e. The evaluation of ν_e involves the measurement of the ratio of unfiltered to filtered radiation and the measured magnitude of the unfiltered radiation along with the curves of Figure 23. The uncertainties involved - especially in the calculation of the curves - introduce appreciable errors. Some discussion of the errors has been given as the various factors were considered. A table of the sources of error with the estimated resulting percentage error in the calculation of ν_e is given below.

TABLE III

SOURCES OF ERROR IN THE MEASUREMENT OF ν_ℓ

Source	Percent error
Target efficiency	20
Geometrical factor	30
Atomic number of target	10
Radius of torus	10
Spectral distribution	20
Angular distribution	30
Transmission coefficients	10
Crystal efficiency	10
Calibration error	10
Measurement of trace	10

Combining the components of error through a root-sum-square calculation the probable error in ν_ℓ is 57% if the electron energy distribution is known.

4.2.8 Summary of information obtainable using the scintillation detectors.- (1) This diagnostic technique enables one to determine whether or not the electrons producing the x rays are monoenergetic with the energy of normally accelerated runaway electrons. In case the indication is that the electrons producing the x rays are not normally accelerated electrons there is doubt as to the energy distribution of the electrons.

(2) Even without a knowledge of the electron energy distribution an upper limit on the average energy of the electrons producing the x rays may be determined. The up-

per limit on the average energy of the electrons is obtained by using curve A (corresponding to a monoenergetic beam) of Figure 22.

(3) Even if the electron energy distribution is not known a lower limit on the number of electrons producing the x rays may be obtained. This lower limit is obtained by using curve A (corresponding to a monoenergetic beam) of Figure 23.

CHAPTER 5

RESULTS AND DISCUSSION

5.1 Introduction

In this chapter some data is presented describing the characteristics of the plasma betatron. The diagnostic techniques described in the preceding chapter were used for this purpose.

It is found that the betatron acceleration produces an intense stream of runaway electrons but that disruption of the streaming occurs shortly after the beginning of the acceleration. It is concluded that the disruption of the electron stream is due to an instability.

5.2 Sample results and method of data reduction

For any given set of initial conditions two pulsed operations of the plasma betatron are required if complete information from both diagnostic techniques is to be obtained. Figure 25 shows three representative pairs of (retouched) oscillograms obtained during the course of the experiment. In each case the upper oscillogram shows the signal from the Rogowski coil along with the signal from the scintillation detector monitoring the unfiltered x radiation. The lower oscillograms show the signal from both scintillation detectors - one monitoring the unfiltered x radiation and the other the x radiation coming through a 0.05 - cm thick lead filter. Since an unfiltered x-ray signal is recorded on both oscillograms,

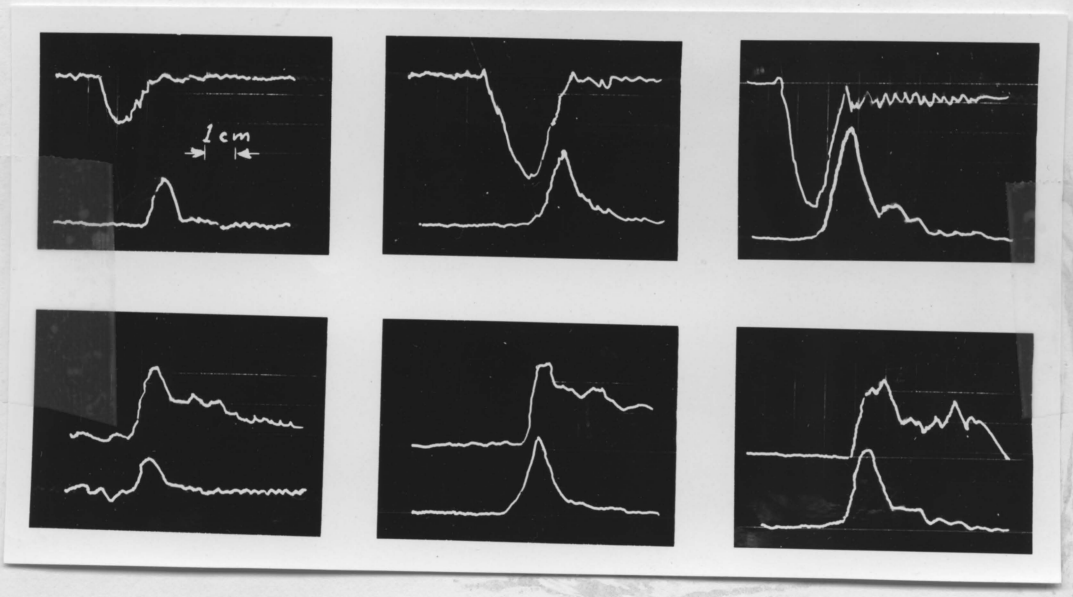

(a) (b) (c)

Accelerating field, 4.4×10^3 volts/m.
Azimuthal magnetic field, 0.1 webers/m^2.
Sweep speed, 0.2 μsec/cm.
All x-ray signals, 0.5 volts/cm.

(a) Upper oscillogram: Upper trace - Rogowski coil (2.0 v/cm)
Lower trace - unfiltered x rays (H.T.=850 v)
Lower oscillogram: Upper trace - filtered x rays (H.T. = 1150 v)
Lower trace - unfiltered x rays (H.T.=800 v)

(b) Upper oscillogram: Upper trace - Rogowski coil (1.0 v/cm)
Lower trace - unfiltered x rays (H.T.= 855 v)
Lower oscillogram: Upper trace - filtered x rays (H.T. =1150 v)
Lower trace - unfiltered x rays (H.T.= 855 v)

(c) Upper oscillogram: Upper trace - Rogowski coil (0.1 v/cm)
Lower trace - unfiltered x rays (H.T.=1190 v)
Lower oscillogram: Upper trace - filtered x rays (H.T.=1330 v)
Lower trace - unfiltered x rays (H.T.=1150 v)

Figure 25. Retouched photograph of representative oscillograms obtained during the plasma betatron experiment.

the consistency of behaviour can be checked.

The trace from the Rogowski coil corresponds to the current flowing in the torus. There is a region near the beginning in which the current rise is approximately linear. The linear part is followed by a region where the current increase is less rapid, a peak is reached and then the current rapidly decreases.

The signal resulting from the detection of the unfiltered x radiation begins somewhat later than the beginning of the Rogowski-coil signal. The signal is characterized by a rapid rise to a peak followed by a less rapid decrease. There are often one or more small peaks following the first peak.

The signal resulting from the detection of the filtered radiation is similar to that for the unfiltered radiation except that the amplitude is smaller and the decrease after the first peak is less rapid. Some x rays are observed over the entire acceleration period.

The analysis of the traces from the scintillation detectors begins with the subdivision of each trace into triangular segments with a base of 0.2 microsecond as indicated in Figure 26. The triangular segment represents the response of the detectors to a single burst of radiation (see Section 4.2.6), hence the first step in effect arbitrarily divides the radiation falling on the

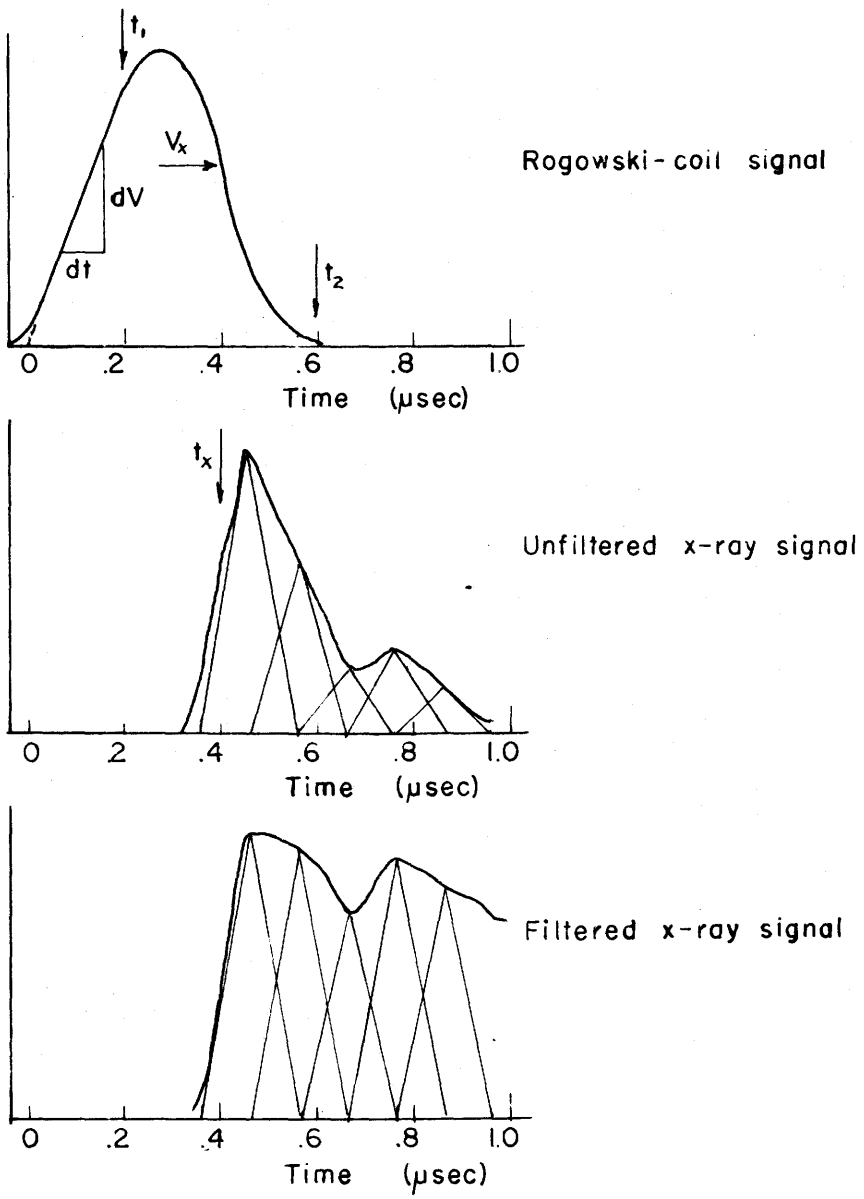

Figure 26. Diagram showing some of the steps involved in analysis of the oscillograms obtained in the plasma betatron experiment.

detectors into separate 'pulses' 0.1 microsecond apart.

Applying the appropriate scaling and calibration factors the amount of radiation energy represented in each pulse may be calculated. The ratio of unfiltered to filtered energy so calculated could be used to determine the energy of the electrons producing the radiation if the type of energy distribution was known. If normal acceleration took place the electrons involved in x ray production would have calculable energy dependent on the accelerating field and the time of appearance of the x rays. It is found, however, that the x rays do not come from normally accelerated electrons; hence the electron energy distribution is not known. Since the electron energy distribution is not known, the A curve of Figure 22 is used in all cases. The value of energy calculated in this way, designated $\overline{W}'$, is an upper limit on the average electron energy whatever the electron energy distribution.

The energy represented in the unfiltered pulses is the energy P_d of equation 4.6. With the value of P_d known, along with the ratio of unfiltered to filtered energy above, a calculation for ν_e could be made using the curves of Figure 23 if the type of electron energy distribution were known. Again since the electron energy distribution is not known the A curve of Figure 23 is used. The value of ν_e calculated in this way represents a lower

limit to the true value of ν_ℓ. This value of ν_ℓ will also represent - within a factor two - the electrons striking the wall of the torus with energies above 40 or 50 kev.

In every case where an analysis of this type was made it was found that by far the majority of electrons striking the walls of the torus are represented in the first two segments of the subdivided oscilloscope trace. The successive segments represent only a few higher energy electrons. In this thesis the ν_ℓ calculated for each segment will be added together and a suitably weighted value of electron energy calculated so that the result from the analysis of a whole trace may be represented by single numbers for ν_ℓ and $\bar{W}'$.

A figure for the beam parameter ν is calculated from the slope of the linear part of the Rogowski-coil trace. As stated in Section 4.1.3, for this calculation it is assumed that the current is composed of runaway electrons only, that is, electrons which are being accelerated freely. If all the electrons are not accelerated freely the calculated value of ν would then be too low. This point is discussed in more detail later.

The oscillograms are also used to establish the times at which certain events occur. They are:

(1) The time t_1 marking the end of the linearly rising portion of the current trace.

(2) The time t_x at which most of the energetic electrons strike the wall of the torus.

(3) The time t_2 indicating the point where the current has decreased to practically zero on the Rogowski-coil trace. The reference point for the measurement of these times is the intersection of the extended linear portion of the Rogowski coil trace with the axis.

Calculations of the energy, W_β, which an electron would have if accelerated without hindrance in the betatron field can also be made. In order to compare the observed electron energy to the appropriate calculated value one must consider the nonzero closing time of the switch in the betatron circuit and the reference point for measuring the time t_x. A simple solution to the problem is given in Appendix D.

For the higher ν values the reduction in the accelerating field due to the beam current must also be taken into account in the calculation of W_β. In this experiment the calculation is complicated somewhat by the fact that the current has normally passed its peak value by the time the x rays are produced. The theoretical energy that an electron would have depends on the instantaneous value of the vector potential A_φ. The contribution to A_φ from the beam current itself of course depends on the instantaneous value of the beam current. The equation 2.29 may be used to find the effective accelerating field

if the value of ν is obtained from the equation (similar to equation 4.4)

$$\frac{\nu}{1 + \lambda\nu} = \frac{1.1 \times 10^{-5}}{E^b} \frac{V_x}{t_x} \qquad 5.1$$

where V_x is the voltage deflection of the Rogowski coil trace at time t_x.

5.3 Experimental results

5.3.1 The effect of changes in beam density.- Adjustment of the duration of the rf pulse resulted in a variation of ν values from approximately 0.002 to 1 as calculated from the Rogowski coil data. Table IV shows the results obtained with a peak accelerating field of 4.4×10^3 volts/m and an azimuthal magnetic field of 0.1 webers/m^2 in argon at 0.3 microns Hg pressure. All observations were made Aug. 3, 1962 except the one at $\nu = 0.0016$ which was made Aug. 6, 1962.

TABLE IV

RESULTS SHOWING EFFECT OF VARIATIONS IN ν
(Peak accelerating field 4.4×10^3 volts/m)

ν	t_1 μsec	t_x μsec	t_2 μsec	$\bar{W}'$ kev	ν_e	W_β kev	ν_e/ν	$\bar{W}'/W_\beta$
0.5	0.08	0.35	0.37	90	0.009	175	0.02	0.51
.14	.12	.34	.38	110	.0009	165	.01	.67
.044	.18	.38	.39	120	.0004	200	.01	.60
.012	.18	.36	.38	120	.0003	185	.03	.65
.0086	.16	.36	.42	120	.0002	185	.02	.65
.0016	.20	.25	.32	<70	>.0001	95	>.06	<.74

Table V shows the results obtained on Aug. 30, 1962 with an accelerating field of 8.8×10^3 volts/m and an azimuthal magnetic field of 0.1 webers/m^2 in argon at 0.2 microns Hg pressure.

TABLE V

RESULTS SHOWING EFFECT OF VARIATIONS IN ν
(Peak accelerating field 8.8×10^3 volts/m)

ν	t_x μsec	$\bar{W}'$ kev	ν_a	W_β kev	ν_a/ν	$\bar{W}'/W_\beta$
1	0.26	105	0.007	340	0.01	0.31
0.061	.26	115	.007	340	.09	.34
.044	.30	115	.003	430	.06	.27
.019	.16	110	.002	150	.09	.73
.007	.16	100	.0005	150	.07	.67

5.3.2 The effect of changes in accelerating field.- Results of measurements taken to determine the effects of variations in the accelerating field are tabulated in Table VI. The azimuthal magnetic field was 0.1 webers/m^2.

TABLE VI

RESULTS SHOWING EFFECT OF VARIATIONS IN ACCELERATING FIELD

Date (1962)	Peak Field ($\times 10^3$ volts/m)	ν	t_1 μsec	t_x μsec	t_2 μsec
Aug 7	.9	0.0016	0.36	0.86	0.80
Aug 7	1.8	.0016	.34	.62	.72
Aug 7	2.6	.0022	.25	.47	.57
Aug 7	3.5	.0022	.23	.40	.46
Aug 6	4.4	.0016	.20	.25	.32
Aug 30	8.8	.007		.16	

5.3.3 The effect of changes in gas pressure.- To determine the extent of the interference by neutral atoms in the acceleration of the electrons, the data in Table VII was obtained on July 25, 1962. The accelerating field was 4.4×10^3 volts/m and the azimuthal magnetic field was 0.1 webers/m^2.

TABLE VII

RESULTS SHOWING EFFECT OF VARIATIONS IN GAS PRESSURE

Pressure (microns Hg)	ν	t_1 usec	t_x usec	t_2 usec
0.10	0.11	0.18	0.36	0.47
.15	.13	.18	.39	.48
.28	.14	.21	.40	.65
.62	.13	.22	.36	1.12

5.3.4 Probe measurements by Olson.- In addition to the data presented above, density measurements by Olson (44) are pertinent to this experiment. Using a double probe technique (45), Olson measured the plasma density in the plasma betatron during the rf pulse. From these measurements an estimate of the total number of electrons in the plasma was made. The corresponding value for the number of electrons in the accelerated beam determined by the Rogowski-coil technique were lower than the value determined from Olson's measurements. The ratio of the two values was found to vary from approximately one half in

the high density (and high rf field) region to approximately one tenth in the low density (and low rf field) region.

5.3.5 Summary of observations.- (1) When the betatron accelerating field is applied to the plasma a transient current is observed corresponding to the production and disruption of an electron stream.

(2) The amplitude of the current depends on the accelerating field and the plasma density.

(3) X radiation is observed at the time of the beam disruption. The energy of the electrons producing the x rays is roughly 100 kev.

(4) While the number of electrons producing the observed x rays varies over a wide range, they represent roughly 1% of the available electrons. It is found that the fraction of electrons involved in x ray production increases considerably with increasing accelerating fields.

(5) It is found that the electrons producing the x rays do not correspond to electrons accelerated freely from the beginning of the acceleration period; the upper limit on the average energy is approximately one quarter to two thirds the 'theoretical' runaway energy.

(6) The current observed during the initial phase of the betatron acceleration does not correspond to all the electrons in the plasma being accelerated freely as runaway electrons.

(7) There is no discernible dependence of the time of beam disruption on the plasma density over the region investigated. The range of plasma densities investigated - as indicated by Olson's measurements - cover more than an order of magnitude, from less than 4×10^{10} cm^{-3} to approximately 3.5×10^{11} cm^{-3}. The range of ν values investigated - as determined by the Rogowski-coil technique - cover more than two orders of magnitude, from 2×10^{-3} to approximately 1.

(8) The time of disruption of the beam depends on the accelerating field. Indications are that the time of disruption varies approximately as the accelerating field to the power minus one half.

(9) The initial phase of the acceleration and the time of appearance of the x rays is not dependent on the initial argon gas pressure - at least for pressures up to 0.62 microns.

5.4 An interpretation of results

The observed disruption of the streaming motion is attributed to a collective effect (instability). Before this is discussed further, two other effects are considered - the effect of imperfections in the apparatus and the interfering effect of neutral gas molecules.

Imperfections in the apparatus are of several types. Recent measurements by Strilchuk (46) indicate the current distribution in the betatron winding may, at the time of

the measurements, have deviated by as much as 5% from the design values. Other perturbations in the accelerating field can be expected to have arisen from magnetic materials near the torus and electrostatic fields from the betatron circuit. The azimuthal magnetic field has two types of inhomogeneity - radial, due to the geometry and azimuthal, due to the separation of the coils used to provide the magnetic field. These perturbations could conceivably cause large-scale movement of both ions and electrons across the azimuthal magnetic field. However it was shown in Chapter 2 that even under the influence of serious perturbations, normal acceleration should still occur - in the absence of instabilities - for at least half a microsecond. The observed disruption of the beam occurs at an earlier time than this. In addition, and of greater significance, if the beam were composed of runaway electrons (as it is expected to be if there are no hindering collective effects), and this beam were forced to the wall by the defects noted above, the intensity of x radiation would be much larger and its quality much harder than is observed. It is concluded therefore that except for the possible role of these perturbations in the excitation of instabilities the perturbations are not a significant factor in the disruption of the beam.

The possibility that neutral particles in some way

impede the acceleration of the electrons was considered. Estimates of the effect of collisions with neutral particles made using the small amount of information available (47) indicated that the effect of these collisions at gas pressures used in this experiment was small. As an experimental check on this conclusion the observations reported in Table VII were made. The data indicate that the neutral particles are not involved with the runaway process or the growth of the instability. The dependence of t_2 on the gas pressure would indicate, however, that neutral particles are involved in the final stages of the disruption of the beam. The apparent persistence of the beam at higher pressure could be due to ionization.

The results of this experiment may be interpreted in at least two ways. Two models are discussed here, each one involving collective effects.

(1) The fractional-stream model.- In this model, it is supposed that with the application of the accelerating field a certain fraction (from about one half to one tenth in this case) of the electrons are decoupled from the ions and are accelerated as runaway electrons while the remainder are trapped, for example, through a density inhomogeneity in the plasma. This mechanism was discussed in Section 2.4.2. At some time after the beginning of the acceleration (typically 0.2 μsec in this experiment) an in-

stability slows down the electrons within the plasma and disrupts the beam. A few of the more energetic electrons strike the walls of the chamber and produce x radiation. The electrons in the runaway electron beam lose approximately 100 kev per electron within the plasma.

In this interpretation the variation in the fraction of electrons which are accelerated could be explained if the temperature of the electrons was lower at the lower plasma densities. Such a temperature variation would indeed be expected to arise from the fact that the rf field is smaller at the low plasma densities.

If the fractional-stream model is substantially correct then the assumption of a normally accelerated stream (initially) - implicit in the technique for measuring ν with the Rogowski coil - is valid.

(2) The whole-stream model.- In this model it is supposed that all the electrons in the plasma are involved in the observed current but that the average streaming velocity is considerably less than that corresponding to normally accelerated runaway electrons. This behaviour must be attributed to an unidentified collective effect operating from the beginning of the acceleration. The collective effect (possibly associated with density inhomogeneities or other imperfections in the apparatus)

could also cause the disruption of the streaming motion. Again a few of the more energetic electrons strike the walls of the chamber and produce x radiation.

In this case the value of ν determined by the Rogowski-coil technique would be too low. There is no evidence to indicate whether the streaming energy, in this interpretation, is given up within the plasma or is transferred to the walls of the chamber. Most of the x radiation which would be produced if the entire streaming energy were transferred to the chamber walls would be so soft that it would be absorbed in the chamber walls.

5.5 Conclusions

While there is much that remains unknown about the processes involved in the plasma betatron, certain conclusions may be made in the light of the experimental results and the preceding discussion.

(1) It is concluded that an intense stream of runaway electrons is produced. Even if the electrons which produce the x rays are the only runaway electrons, they still represent an intense stream since if they were accelerated to near the velocity of light, currents as high as 150 amperes would result. If, however, the fractional-stream model is substantially correct, then the intensity of runaway electrons is much larger.

(2) It is concluded that the disruption of the streaming motion is due to a collective effect (instability)

regardless of which of the proposed models is closest to reality. The collective effect can not, at this point, be identified.

(3) If the fractional-stream model is substantially correct then the energy of the streaming motion (approximately 100 kev per runaway electron) is given up within the plasma. If the whole-stream model is substantially correct the energy of streaming motion (between 1 and 25 kev per electron) may be given up within the plasma.

5.6 Discussion

5.6.1 A comparison of the results with those of the CERN betatron experiments.- The first plasma betatron experiments were conducted at CERN, Geneva, in 1957-58 by Reynolds and Skarsgard (2). Two air-core plasma betatrons - designated Mk I and Mk II - were constructed. Table VIII summarizes some of the quantities describing these two devices along with the plasma betatron - designated US - described in this experiment.

The diagnostic techniques described in this thesis, although basically the same, are more highly developed than those used in the CERN experiments.

In the operation of the CERN Mk I machine, the Rogowski-coil signal showed a large transient current. Associated with the decline of the current was the emission of x rays. Estimates of the energy of the electrons pro-

ducing the x rays were in the 100 to 120 kev range. The possibility was not considered that the electrons producing the x rays were anything but normally-accelerated electrons which prematurely struck the walls of the chamber. The transient current was described as a conduction current (many electrons with a slow drift velocity), rather than a runaway current which encountered an instability.

TABLE VIII

CHARACTERISTIC PARAMETERS OF THE CERN AND U OF S PLASMA BETATRONS

Parameter	Mk I	Mk II	US
Peak accelerating field ($\times 10^3$ volts/m)	.67	1.77	8.8*
Length of accelerating period (μsec)	24	7.8	2.2
Theoretical maximum electron energy (Mev)	2.6	2.0	3.4*
Maximum azimuthal magnetic field (webers/m^2)	.15	.15	.15
Mean orbit diameter (meters)	.52	.52	.38
Chamber bore diameter (meters)	.05	.05	.06

*These figures refer to the maximum values for the experiment reported in this thesis. Design values are 17.7 and 6.75 respectively.

In the operation of the CERN Mk II machine higher accelerating fields were used. Under conditions similar to those used in the Mk I betatron, a similar transient current was observed. In addition to the x rays produced during the decline in the transient current, x rays were

produced over much of the remainder of the acceleration period. For sufficiently low plasma densities (corresponding to $\nu \approx 10^{-4}$), the indications were that a larger proportion (perhaps 100%) of the electrons remain in the betatron until the end of the betatron acceleration. This low density region has not yet been investigated in the experiment described in this thesis.

In summary, the observations made in the CERN experiments and the U of S experiment are consistent. The refinements in the diagnostic techniques in this experiment have, however, produced more precise data on which a new interpretation of the results is based. Most significantly, it has been found that the observed x rays are produced by electrons which have an energy considerably lower than that corresponding to normally accelerated electrons.

5.6.2 A comparison of the results with those of the USSR experiments reported by Stephanovski.- Stephanovski has recently reported (10) some results of an experiment in the USSR which is similar to the one described in this thesis. Two devices were constructed to accelerate electrons in a plasma. One was a betatron - designated OBF-400/80 - and the other - designated OF-400/80 - was built around an identical torus but used induced image currents in adjacent conductors to keep the beam from striking the wall of the chamber. In each case an azi-

muthal magnetic field was provided and plasma formation was accomplished by using a spiraling electron beam (48). Table IX summarizes some of the quantities describing these two devices along with the plasma betatron - designated US - described in this experiment.

TABLE IX

CHARACTERISTIC PARAMETERS OF TWO USSR ACCELERATORS AND THE U OF S PLASMA BETATRON

Parameter	OBF	OF	US
Peak accelerating field ($\times 10^3$ volts/m)	7.0	15	8.8*
Length of accelerating period (μsec)	4.5	2	2.2
Theoretical maximum electron energy (Mev)	5.5	5.2	3.4*
Maximum azimuthal magnetic field (webers/m^2)	.25	.35	.15
Mean orbit diameter (meters)	.40	.40	.38
Chamber bore diameter (meters)	.08	.08	.06
Initial plasma density ($\times 10^{11}$ cm^{-3})	.2-.3	.2-.3	.4-4

*These figures refer to the maximum values for the experiment reported in this thesis. Design values are 17.7 and 6.75 respectively.

Operation of the OBF-400/80 betatron resulted in some electrons reaching the full energy of the machine. These electrons produced a maximum of 1-ampere of current. A transient "conduction" current was observed during the first 0.3 - 0.7 μsec.

In the operation of the OF-400/80 machine, no electrons were observed to reach the maximum energy of the

machine. A transient "conduction" current was observed, however. With azimuthal magnetic fields from 0.25 to 0.35 webers/m^2, x rays were observed along with the current. The energy of the electrons producing the x rays is estimated to be half the energy of normally accelerated electrons. Observations on electromagnetic radiation from the plasma indicated radiation at the electron cyclotron frequency and the electron plasma frequency.

The result that the energy of the electrons producing the x rays is smaller than the corresponding theoretical energy is similar to one of the important results obtained independently in the experiment described in this thesis.

If the oscillogram of the Rogowski-coil signal given by Stephanovski is analysed in a similar manner to that used in this experiment, an interesting result is found. The value of ν calculated in this way is 0.015. However, additional data reported by Stephanovski implies that the initial plasma density corresponds to $\nu = 0.24$. On the basis of an interpretation in terms of the fractional-stream model the indication is, therefore, that only one fifteenth of the electrons are accelerated. The corresponding fraction for the experiment described in this thesis is from one half to one tenth.

This result is in qualitative agreement with the

theory and discussion set down in Section 2.4 where it is suggested that an inhomogeneity in the plasma density may trap large numbers of electrons. In the USSR experiment the plasma was formed by a spiraling beam of electrons rather than an rf field. The plasma formed in this way is likely to be at a lower temperature and there is a probability of an inhomogeneity in the density near the point of electron injection. The wavelength of this inhomogeneity is longer than that associated with the spacing of the coils which produce the azimuthal magnetic field. Because of both the lower plasma temperature and the longer wavelength inhomogeneity, more electrons could be trapped in the USSR experiments.

5.6.3 The experimental results and the two-stream instability.- If all the electrons are accelerated normally, the two-stream instability theory predicts stability for all but the highest ν values encountered in this experiment. However, it has been found that not all electrons are accelerated normally and therefore this ideal two-stream theory does not apply. At least it does not apply for time intervals as long as 0.2 μsec - the duration of the initial phase of the acceleration on which the experimental determination of the nature of the acceleration is based.

It was also shown in Chapter 3 that the presence of a small number of slow electrons would cause the undamped

plasma oscillations to grow much faster and that disruption of the beam could be expected through the two-stream instability for the entire range of ν values investigated. It was suggested also that large amplitude oscillations associated with density inhomogeneities could be amplified and cause disruption of the beam.

Any theory which is to explain the observed disruption of the electron beam must account for the failure of the electrons to gain or maintain large streaming velocities. The two-stream instability theory satisfies this requirement.

The evidence that the time of disruption of the beam is earlier at the higher accelerating fields, is in qualitative agreement with the theoretical investigation of the amplification of plasma oscillations associated with plasma density inhomogeneities. In this case the wave number of the inhomogeneity would be 'in resonance' at an earlier time for a higher accelerating field.

A feature of the evidence which is not explained by the theory is the apparent independence of the instability mechanism on the value of ν. The theory predicts, for example, a rather strong dependence of the time of disruption on the value of ν. It should be noted however that the observed time of disruption of the beam may bear a somewhat indirect relation to the instability mech-

anism. Consequently the apparent discrepancy can not at present be interpreted as a definite disagreement between theory and experiment.

The two-stream instability theory - modified to take account of the presence of a small number of slow electrons - is based on a rather idealized electron velocity distribution. It is not known if a more realistic electron velocity distribution would bring the predictions of the theory into agreement with the observations. A conclusion regarding the identity of the instability in the plasma betatron can not be made at this time.

5.6.4 The instability as a possible plasma heating mechanism.- As was discussed in Section 5.4, the energy of streaming motion - at least 25 kev per electron at the higher ν values - which the electrons lose during disruption of the beam may be given up within the plasma. If so it must appear in some other form(s) - oscillations of ions and electrons, random motion of ions and electrons, etc. Of possible interest for controlled thermonuclear research is the energy which goes into random ion motion. If the collective interaction which takes place in the plasma betatron involves the efficient transfer of energy to the ions, interesting plasma temperatures may result.

Smullin and Getty (49) have conducted an experiment

in which a 1-ampere, 10-kev electron beam was injected into a plasma. The collective interaction between the electron beam and the plasma was found to heat the ions up to a kinetic temperature of a few electron volts. Temperatures about 1000 times higher are needed to produce a significant cross section for thermonuclear fusion reactions. While there are important differences between an externally injected beam-plasma experiment and a runaway electron experiment, the beam disruption reported in this thesis is similar in some respects to that observed by Smullin and Getty. Since, however, the beam currents and electron energies are orders of magnitude higher in the plasma betatron experiment than in the experiments of Smullin and Getty, it is possible that more interesting ion temperatures are also produced. An investigation of ion temperatures in this experiment is being planned.

CHAPTER 6

SUMMARY

(1) Diagnostic techniques.- Several improvements in two diagnostic techniques are described in this thesis. The Rogowski coil has been adapted for the measurement of low-level currents of short duration by winding the coil with resistance wire and enclosing the coil in an electrostatic shield. The observed current leads to estimates for the line density of the accelerated electrons.

The diagnostic technique involving the scintillation detectors has been considerably extended for this work. A pair of scintillation detectors are used. One of them detects the x rays coming directly from the torus while the other detects x rays which have been also passed through a thin sheet of lead. An analysis was made (including the effects of different electron energy distributions) so that quantitative information on the number and energy of the electrons producing the x rays could readily be obtained from one oscillogram. Consideration was given to the effects on the results of the uncertainty in the angular distribution of bremsstrahlung radiation produced in thick targets.

(2) Plasma betatron theory.- It is found that in the absence of collective interactions, moderate accelerating fields applied to a plasma should produce an intense stream of runaway electrons. Two collective effects were considered in this thesis, density inhomogeneities and the two-stream instability. In a practical system where density inhomogeneities may occur, a majority of the electrons may be trapped due to the inhomogeneities and prevented from being accelerated freely. The two-stream instability was

found to be serious under some conditions.

The effect of the azimuthal magnetic field was considered. It is found that because of the azimuthal magnetic field no constriction of the beam can occur. Instead, the pinch forces cause the electron beam to rotate about its axis.

Two disturbing effects were investigated - the self-field of the beam current and defects in the betatron field. In the absence of instabilities it was found that over a wide range of conditions normal acceleration should be possible for at least a half microsecond.

In addition to the two-stream instability, several other possible instability mechanisms were considered briefly. It was found that adequate instability theory does not exist in some cases.

(3) Experimental results.- When the betatron accelerating field is applied to an argon plasma in an azimuthal magnetic field, a transient current is observed corresponding to the production and disruption of an electron stream. Associated with the disruption of the stream is the emission of x rays. Measurements reveal that the upper limit on the average energy of the electrons producing the x rays (representing approximately 1% of all electrons) is from one quarter to two thirds of the "theoretical" runaway energy. It is found that not all the electrons are accelerated freely as runaway electrons.

The time of disruption of the electron stream is found to be independent of the beam density and gas pres-

sure (up to 0.62 microns Hg) but varies approximately as the accelerating field to the power minus one half.

(4) Conclusions.- The observed experimental data are consistent with those of similar experiments previously conducted. The use of refined diagnostic techniques has resulted, however, in more definitive information on the behavior of the plasma betatron over a larger range of conditions than was the case in previous experiments. The major new conclusion arising from the experiment is that the disruption of the beam is due to an unidentified collective interaction.

APPENDIX A

THE EFFECT OF A DEVIATION FROM THE BETATRON CONDITION

The purpose of this Appendix is to estimate the effect of an error in the betatron field. The analysis is carried out in terms of a deviation from the design values of the currents flowing in the betatron winding.

The unbalanced force on an electron in the plane of the equilibrium orbit due to the betatron field is found from equation 2.23.

$$F^b = -e^2 A_\varphi (B^b - A^b/\rho)/m. \qquad A.1$$

In this case the betatron field is provided by a pair of 'inner' and a pair of 'outer' turns. Since the equilibrium orbit is in the plane of symmetry, the contribution to the betatron field from both inner turns may be considered together as may the contribution from the outer turns. The superscript, 1, is adopted for the inner turns and 2 for the outer turns. The magnetic field and vector potential may be written

$$\left.\begin{aligned} B^b &= B^1 + B^2 \qquad A.2 \\ A^b &= A^1 + A^2. \qquad A.3 \end{aligned}\right\}$$

If ϵ' is the fraction of the design current for the inner pair of turns which is diverted from one pair of turns to the other, then

$$\left.\begin{aligned} B^1 &= B^1_o + \epsilon' B^1_o \\ B^2 &= B^2_o - 1.29\,\epsilon' B^2_o \end{aligned}\right\} \qquad A.4$$

where the subscript, o, refers to design values.

The factor 1.29 arises from the fact that the design ratio of current in the inner turns to that in the outer turns is approximately 1.29. A positive ϵ' indicates an increase in the current in the inner turns over the design value. Substituting equation A.4 into equation A.2 one obtains for the magnetic field due to the currents in the betatron winding.

$$B^b = B_o^b + \epsilon'(B_o^1 - 1.29B_o^2). \qquad A.5$$

The magnetic field profiles in the plane of the equilibrium orbit for in inner and outer turns are reproduced from Gore's M. A. Thesis (1,1) in Figure 27(a). From this Figure it is found that for the betatron

$$\left.\begin{aligned} B_o^1 &\approx -0.23B_o^b \\ B_o^2 &\approx +1.23B_o^b \end{aligned}\right\} \qquad A.6$$

in the region of interest. From equations A.6 and A.5

$$B^b = B_o^b(1 - 1.82\epsilon'). \qquad A.7$$

In a similar manner the magnetic vector potential may be written

$$\left.\begin{aligned} A^1 &= A_o^1 + \epsilon' A_o^1 \\ A^2 &= A_o^2 - 1.29\epsilon' A_o^2 . \end{aligned}\right\} \qquad A.8$$

The components of magnetic vector potential may be calculated by a numerical integration using the data in Figure 27(a). The results of such a calculation are shown in Figure 27(b). In the region of interest it is found that

$$\left.\begin{aligned} A_o^1 &\approx (\rho_o/\rho)^{3/2}(A_o^1)_{\rho_o} \\ A_o^2 &\approx (\rho/\rho_o)^{3/2}(A_o^2)_{\rho_o} \end{aligned}\right\} \qquad A.9$$

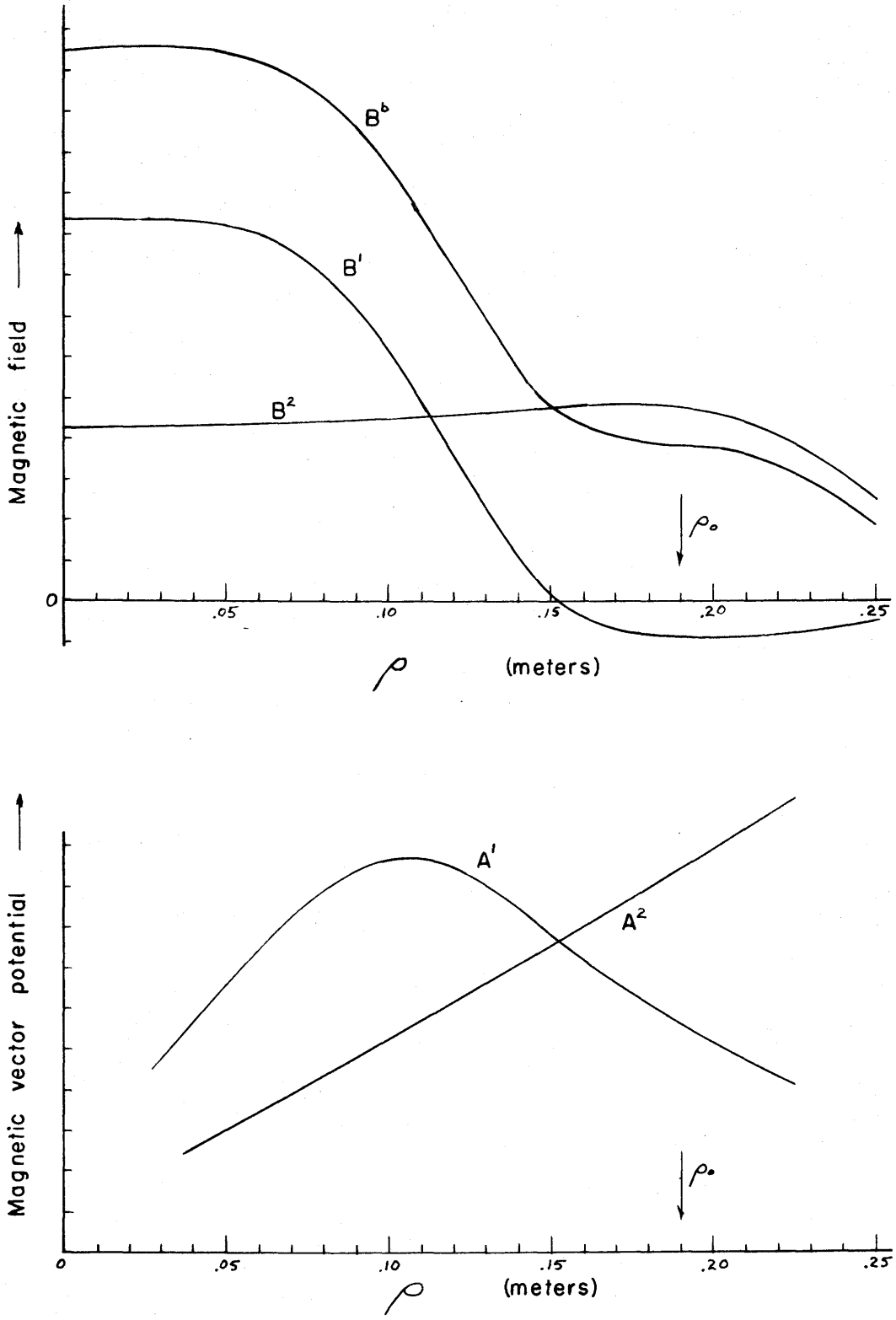

Figure 27. Magnetic field and vector potential profiles for the plasma betatron.

and that

$$\left.\begin{aligned}(A_o^1)_{\rho_o} &= 0.368(A_o^b)_{\rho_o} \\ (A_o^2)_{\rho_o} &= 0.632(A_o^b)_{\rho_o} \quad .\end{aligned}\right\} \qquad \text{A.10}$$

From equations A.3, A.8, A.9, and A.10, it is found that

$$A^b \approx A_o^b + (A_o^b)_{\rho_o} \epsilon' \left[0.368(\rho_o/\rho)^{3/2} - 0.815(\rho/\rho_o)^{3/2}\right]. \qquad \text{A.11}$$

Near the equilibrium orbit, equation A.11 reduces to

$$A^b \approx A_o^b - 0.45\, \epsilon' (A_o^b)_{\rho_o} \quad . \qquad \text{A.12}$$

From equations A.1, A.7, and A.12, the force on an electron is given by

$$F^b \approx -(e^2 A_\varphi/m) \left[(B_o^b - A_o^b/\rho) - \epsilon'(1.82B_o^b - 0.45(A_o^b)_{\rho_o}/\rho)\right] \qquad \text{A.13}$$

The force on an electron due to the betatron field is the force due to the design betatron field plus a radial force due to any error in the current distribution. It is convenient to express the error in the current distribution in terms of ϵ, the error in the ratio of currents in the inner and outer turns.

$$\epsilon \approx 2.3\epsilon' \qquad \text{A.14}$$

From equations A.13, A.14, and 2.29, the net radial force on an electron at the design equilibrium orbit due to an error in the current distribution in the betatron winding is

$$\left.\begin{aligned}F^\epsilon &\approx 0.6\, \epsilon\, e^2 \bar{A}_\varphi\, \bar{A}^b/m\rho \\ &\approx 0.6\, \epsilon\, e^2 A^{b2}/m\rho\,(1 + \lambda\nu)\,.\end{aligned}\right\} \qquad \text{A.15}$$

APPENDIX B

PHOTOELECTRIC AND COMPTON ATTENUATION COEFFICIENTS FOR THE SCINTILLATION CRYSTAL AND PYREX GLASS

The following data on the Nuclear Enterprises NE 102 plastic phosphor was supplied by the manufacturer or was measured.

(1) Dimensions of cylindrical crystal; 5.0 cm long, 3.5 cm in diameter.

(2) Density 1.22 gms/cm^3.

(3) Electron density 3.4×10^{23} cm^{-3}.

(4) Number of atoms per cm barn; H, 0.054; C, 0.048; N, 1.86×10^{-6}; O, 1.8×10^{-6}.

(5) The time delay between deposition of the photon energy and the emission of the fluorescent radiation is in the region of 1 nanosecond.

The carbon component is the dominant component of the crystal so far as the photoelectric effect is concerned. The photoelectric attenuation coefficient, τ, was calculated from published data (43) and is shown in Figure 28.

Using the figure for electron density and published data (42) the Compton attenuation coefficients were calculated and are shown in Figure 28.

The effective atomic number and photoelectric and Compton attenuation coefficients for pyrex glass are required. The figures in the following table were derived from published data (50) on the composition of pyrex glass.

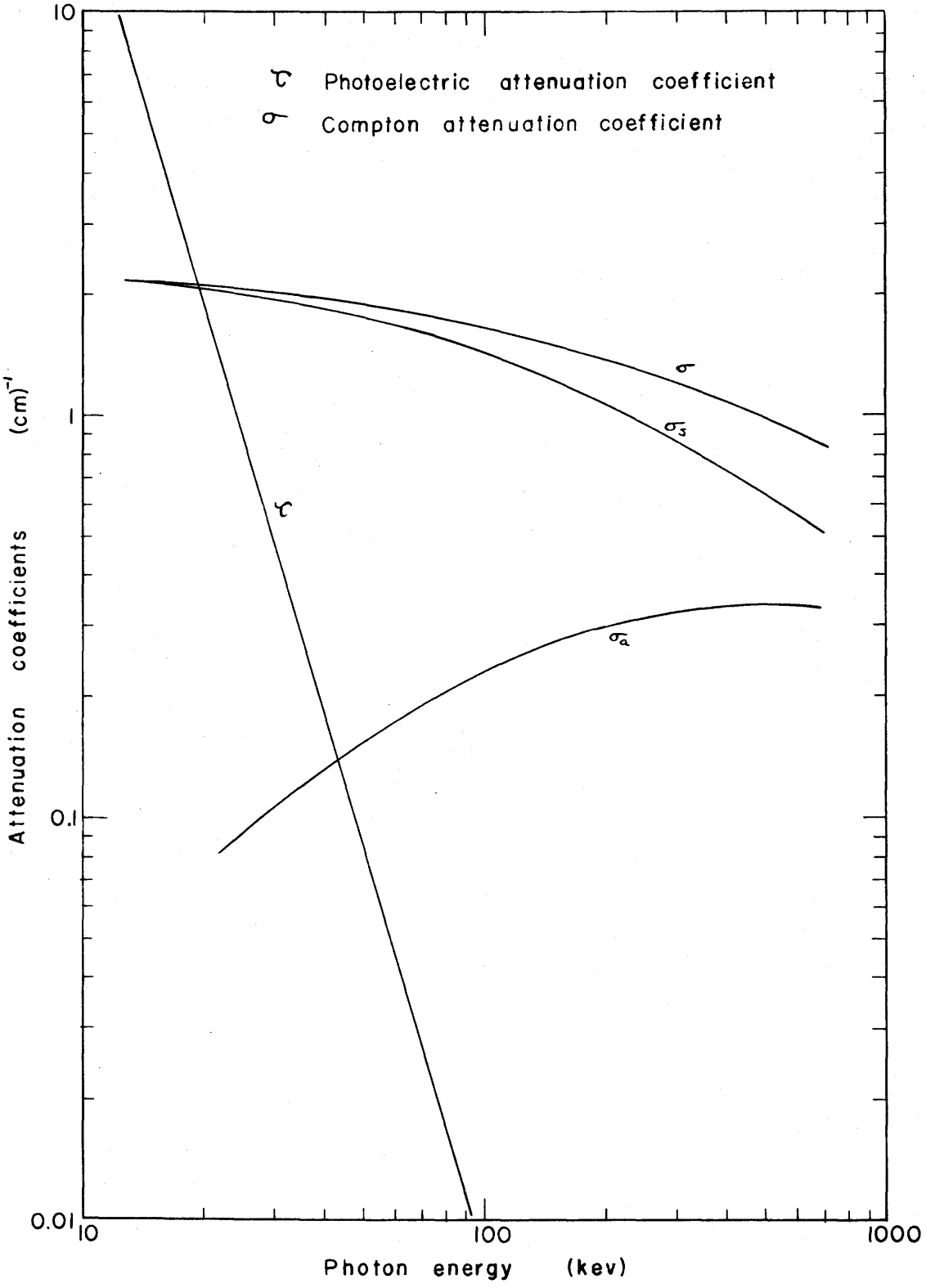

Figure 28. Photoelectric and Compton attenuation coefficients for the NE 102 plastic phosphor as a function of photon energy.

TABLE X

COMPOSITION OF PYREX GLASS

Element	Atomic Number	Atomic Weight	Abundance in Pyrex %	Density gms/cc	Atoms per cc ($\times 10^{21}$)	Electrons per cc ($\times 10^{22}$)
0	8	16.0	53.3	1.24	46.2	37.3
Si	14	28.1	37.8	.876	18.8	26.3
B	5	10.8	3.73	.087	4.85	2.42
Na	11	23.0	3.04	.071	1.86	2.05
Fe	26	55.8	.95	.022	.238	.619
Al	13	27.0	.45	.010	.223	.280
As	33	74.9	.26	.006	.048	.158
Ca	20	40.1	.21	.005	.075	.150
K	19	39.1	.08	.002	.031	.059
			Totals	2.32	72.3	69.3

From the above totals the effective atomic number is taken to be 9.59.

The significant contributions to the photoelectric attenuation coefficients are tabulated below.

TABLE XI

PHOTOELECTRIC ATTENUATION COEFFICIENTS FOR PYREX GLASS

Element	gms/cc	Photon Energy (kev) / τ $(cm)^{-1}$	10	20	40	100
0	1.24		6.82	.719	.072	.0033
Si	.876		29.7	3.64	.402	.0208
Na	.071		1.09	.125	.013	.0006
Fe	.022		3.91	.565	.073	.0045
As	.006		1.33	.202	.027	.0018
			42.8	5.25	.587	.0310

The Compton and photoelectric attenuation coefficients for pyrex glass are shown in Figure 29.

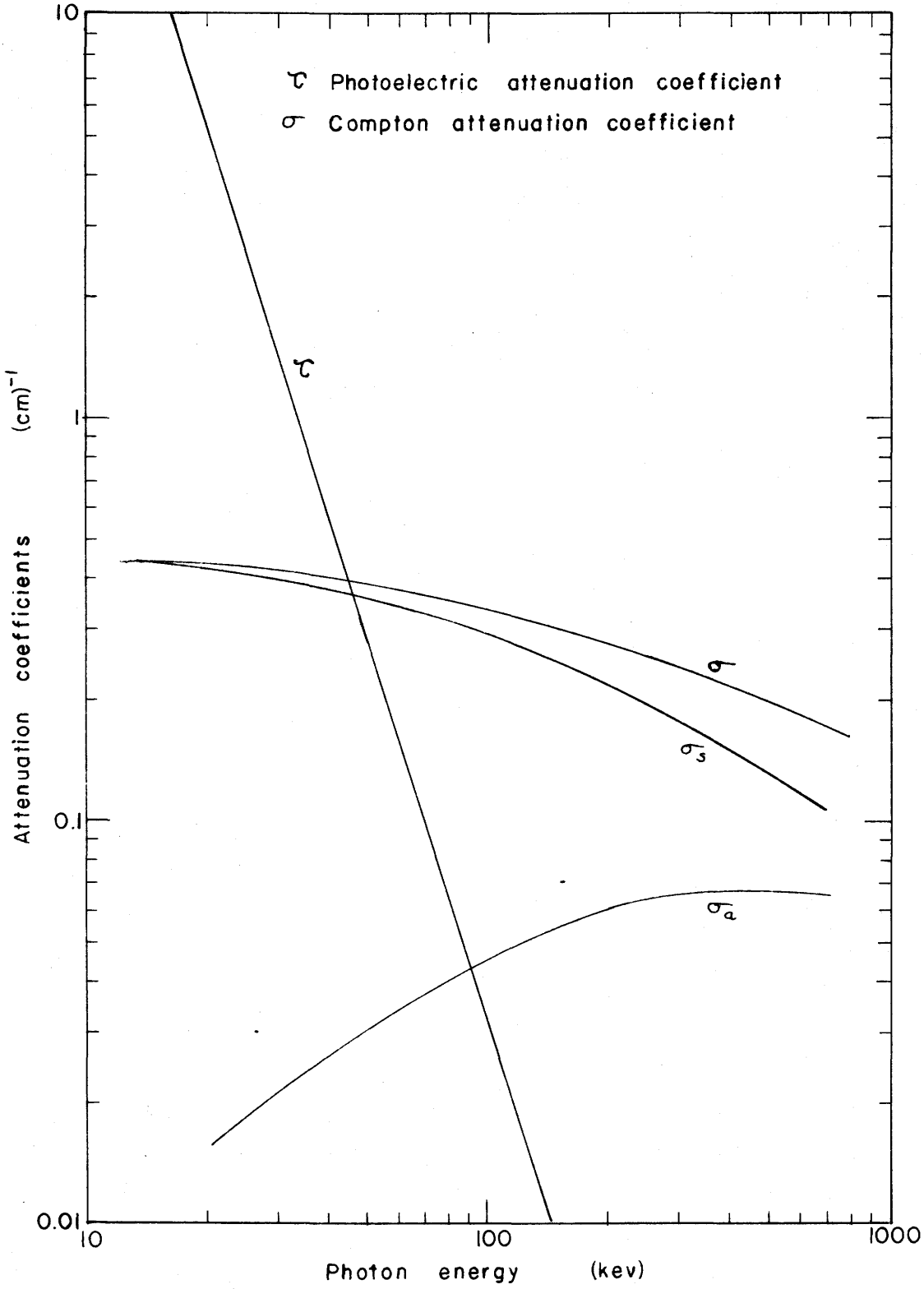

Figure 29. Photoelectric and Compton attenuation coefficients for pyrex glass as a function of photon energy.

APPENDIX C

THE CALCULATION OF EFFECTIVE AND AVERAGE ELECTRON ENERGY CORRESPONDING TO CERTAIN X-RAY SPECTRA

In this appendix calculations are made for the effective and average electron energy corresponding to the B and C x-ray spectra described in Section 4.2.4. Each spectrum is subdivided into five Kramer distributions as shown in Figure 30. Equations 4.23 and 4.24 are then used to calculate W_{eff} and W_{av}. The calculations are tabulated in Table XII. The x-ray energy, P_i, is in arbitrary units.

TABLE XII

TABULATION OF CALCULATIONS ON CERTAIN X-RAY SPECTRA

Spectrum type	Kramer distribution	$\frac{W_i}{W_{max}}$	P_i	$\frac{W_i}{(W_i/W_{max})}$	$\frac{W_i}{(W_i/W_{max})^2}$
B	1	1.00	0.50	0.50	0.50
	2	0.90	0.90	1.00	1.11
	3	0.75	1.13	1.51	2.01
	4	0.52	0.52	1.00	2.00
	5	0.30	0.30	1.00	3.33
	Totals		3.35	5.01	8.95
C	1	0.90	0.45	0.50	0.55
	2	0.70	0.35	0.50	0.72
	3	0.55	0.55	1.00	1.82
	4	0.40	0.40	1.00	2.50
	5	0.25	0.37	1.48	6.00
	Totals		2.12	4.48	11.59

From the above totals the data in Table I is readily obtained.

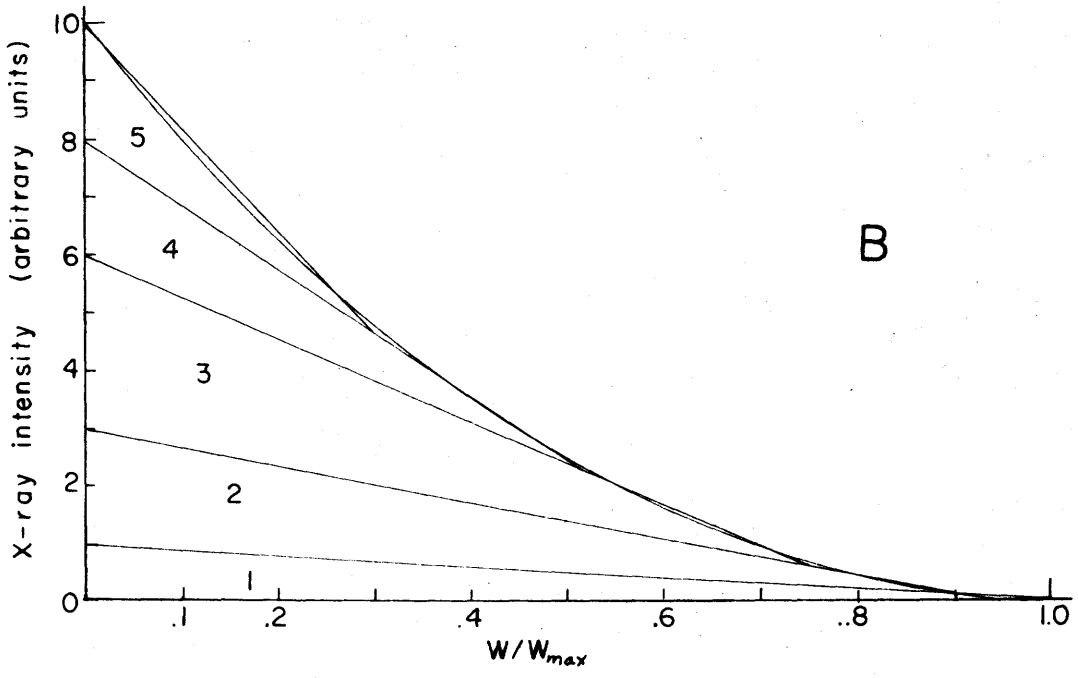

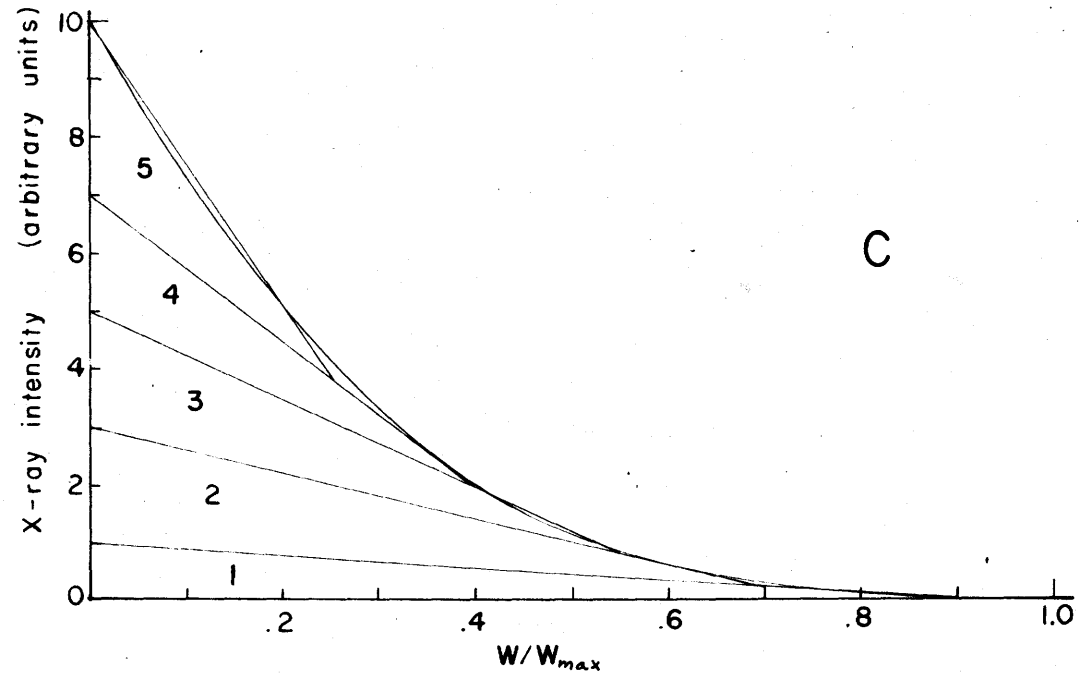

Figure 30. The subdivision of the 'B' and 'C' spectra into five Kramer spectra.

APPENDIX D

THE ACCELERATING FIELD WAVEFORM

The accelerating field in this experiment is produced by a slowly damped oscillating current in the betatron circuit. All observations were made during the first quarter cycle of the oscillating current.

The switches used to close the betatron circuit have a nonzero closing time. Measurements revealed that the closing time varied from less than 0.1 μsec to about 0.2 μsec. The closing time depended on the air pressure in the switches and the degree of contamination of the switching system. It was found, however, that the rise in the accelerating field was approximately linear as illustrated by the solid line in Figure 31 (a). In order to calculate the energy which runaway electrons would have, it is necessary to take into account the switch closing time, t_c.

The linear portion of the Rogowski-coil trace indicates that the average acceleration of the electrons during this time is constant, regardless of whether the fractional-stream or whole-stream model is closest to reality. If it is assumed that the acceleration is proportional to the accelerating field, then the average velocity

$$\bar{v} = K\int_0^t E(t)dt. \qquad \text{D.1}$$

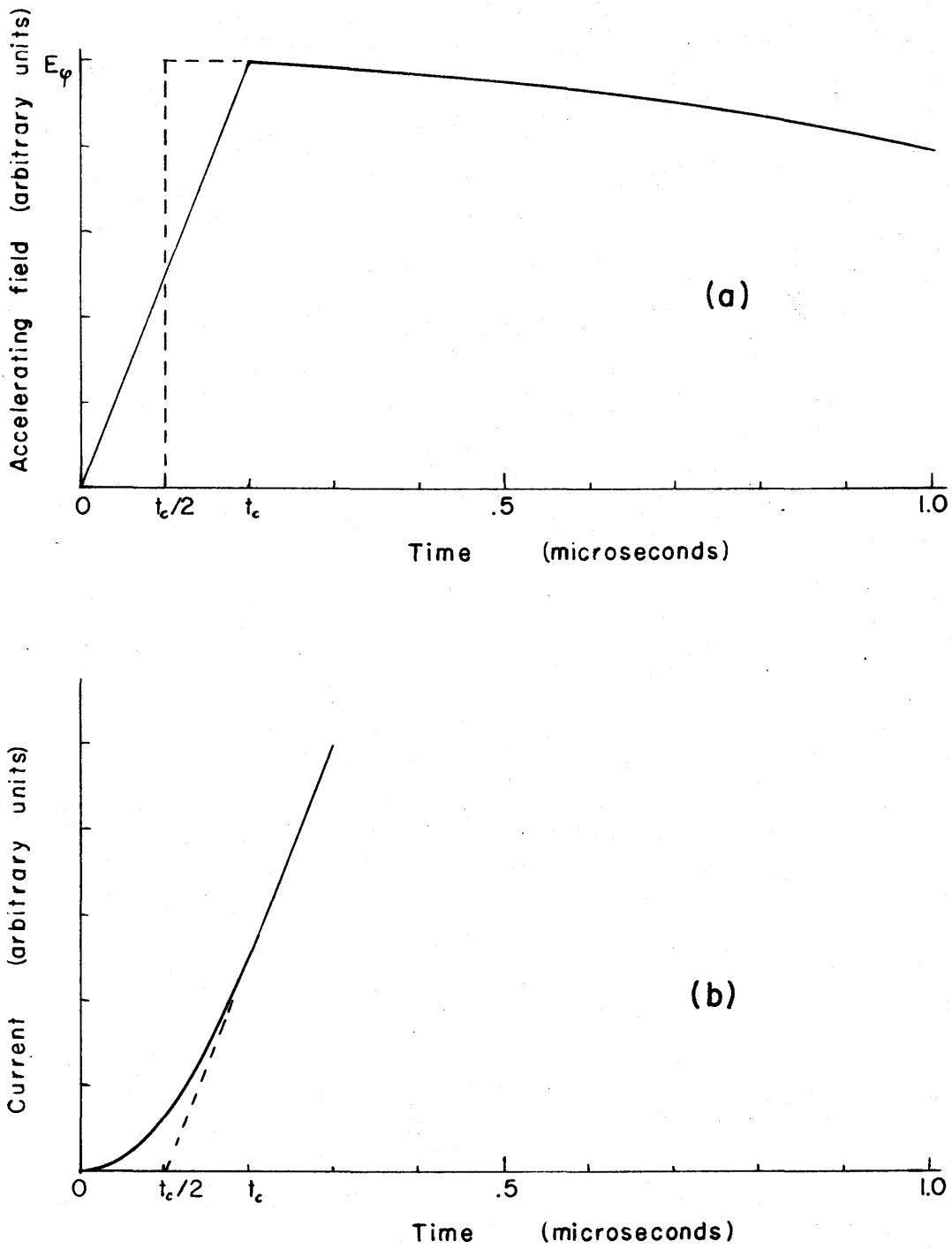

Figure 31. The accelerating field and current waveforms due to the nonzero rise time of the accelerating field.

Assume that E(t) is given by

$$\left.\begin{aligned} E(t) &= E_\varphi t/t_c \qquad 0 \leqslant t \leqslant t_c \\ &= E_\varphi \qquad\qquad\quad t \geqslant t_c \end{aligned}\right\} \qquad \text{D.2}$$

where E_φ is the peak accelerating field. The assumption of a constant accelerating field after time t_c is a good approximation to the actual case for times shortly after t_c. From equations D.1 and D.2

$$\left.\begin{aligned} \bar{v} &= KE_\varphi t^2/2 \qquad 0 \leqslant t \leqslant t_c \\ &= KE_\varphi(t - t_c/2). \qquad t \geqslant t_c \end{aligned}\right\} \qquad \text{D.3}$$

It is evident that for times greater than t_c the velocity is the same as if the accelerating field had been of the form

$$\left.\begin{aligned} E(t) &= 0 \qquad\quad t \leqslant t_c/2 \\ &= E_\varphi . \qquad t \geqslant t_c/2 \end{aligned}\right\} \qquad \text{D.4}$$

The current is proportional to the average velocity and would have the form indicated by the solid line in Figure 31 (b). The dashed line in Figure 31 (b) indicates what the current would be if the accelerating field had the form described by equation D.4 (shown as a dashed line in Figure 31 (a)).

The practice described in Section 5.2 of measuring times from the intersection of the linear portion of the current trace with the axis is now justified so long as the events of interest occur after time t_c. This method is useful because of the variability of the switch closing time and the difficulty of determining with accuracy the beginning of the acceleration.

REFERENCES

1. G. J. Budker, Proceedings of the CERN Symposium on High-Energy Accelerators and Pion Physics, Geneva, 1956, Vol. 1, p. 68.

2. P. Reynolds and H. M. Skarsgard, Betatron Acceleration of Electrons in a Plasma, 1958, CERN report, CERN, 58-19.

3. N. C. Christofilos, Proceedings of the Second United Nations International Conference on the Peaceful Uses of Atomic Energy, Geneva, 1958, Vol. 32 p 279.

4. J. G. Linhart and A. Schoch, Nuclear Instruments and Methods, 4, 332 (1959).

5. G. J. Budker and A. A. Naumov, Proceedings of the CERN Symposium on High-Energy Accelerators and Pion Physics, Geneva, 1956, Vol. 1, p 76.

6. D. Finkelstein, Proceedings of the Second United Nations International Conference on the Peaceful Uses of Atomic Energy, Geneva, 1958, Vol. 32, p 446.

7. D. C. de Packh, Proceedings of the Third International Conference on Ionization Phenomena in Gases, Venice, 1957, p 236.

8. G. Miyamoto et al, Proceedings of the Second United Nations International Conference on the Peaceful Uses of Atomic Energy, Geneva, 1958, Vol. 32, p 308.

9. L. T. Shepherd and H. M. Skarsgard, Phys. Rev. Letters, 10, 121 (1963).

10. A. M. Stephanovski, High Energy Accelerator Papers from USSR Prepared for Presentation at 1961 International Conference. Brookhaven Nationql Laboratory, 1962, p 106.

11. J. V. Gore, M. A. Thesis, University of Saskatchewan, 1961.

12. N. O. O. Eikel and H. M. Skarsgard, Rev. Sci. Instr. 34, 299, (1963).

13. L. T. Shepherd, M. Sc. Thesis, University of Saskatchewan, 1960.

14. L. T. Shepherd, and H. M. Skarsgard, Can. J. Phys. 39. 983, (1961).

15. L. Spitzer, Jr., Physics of Fully Ionized Gases, Interscience Publishers, Inc., New York (1956).

16. S. Chandrasekhar, Plasma Physics, The University of Chicago Press, Chicago (1960).

17. D. J. Rose and M. Clark, Jr., Plasmas and Controlled Fusion, The M.I.T. Press and John Wiley & Sons, Inc., New York (1961).

18. S. Glasstone and R. H. Loveberg, Controlled Thermonuclear Reactions, D. Van Nostrand Co., Inc., Princeton, New Jersey (1960).

19. H. Dreicer, Phys. Rev. 117, 329, 343 (1960).

20. E. R. Harrison, Phil. Mag. 3, 1318 (1958).

21. E. R. Harrison, J. Nuclear Energy C, 4, 7 (1962).

22. J. G. Linhart, The Problem of Runaway Electrons in Plasma, 1957, CERN-PS/JGL 2.

23. G. Schmidt, J. Nuclear Energy C, 3,156 (1961).

24. D. W. Kerst, Phys. Rev. 60, 47, (1941).

25. F. W. Grover, Inductance Calculations, D. Van Nostrand Co., Inc., (1946).

26. D. Finkelstein and P. A. Sturrock, Plasma Physics, Edited by James E. Drummond, McGraw-Hill Book Co., Inc., (1961).

27. Ch. Maisonnier and D. Finkelstein, Beam Intensity Limitation in Neutralized Space Charge Betatrons, 1959, CERN 59-11.

28. C. E. Nielson, et al, Proceedings of the International Conference on High-Energy Accelerators and Instrumentation, CERN, 1959, p 239.

29. I. B. Bernstein and R. M. Kulsrud, Phys. Fluids, 3, 937 (1960).

30. B. B. Kadomtsev and A. V. Nedospasov, J. Nuclear Energy C, 1, 230 (1960).

31. F. C. Hoh, Phys. Fluids, 5, 22 (1962).

32. O. Buneman, Phys. Rev. 115, 503 (1959).

33. H. M. Skarsgard, Can. J. Phys. 41, 450, (1963).

34. S. T. Stephenson, Handbuch der Physik, Vol XXX, X-Rays Spring-Verlag, Berlin, 1957.

35. H. W. Koch and J. W. Motz, Rev. Mod. Phys. 31, 920, (1959).

36. A. H. Compton and S. K. Allison, X-Rays in Theory and Experiment, D. Van Nostrand Co., Inc. (1935).

37. H. A. Kramers, Phil, Mag. 46, 836 (1928).

38. H. Kulenkampff and L. Schmidt, Ann. der Phys. 43. 494 (1943).

39. National Bureau of Standards Handbook No. 85(to be published).

40. D. V. Cormack, Trans. IX Int. Congress Radiology, p 1400, (1960).

41. H. Kulenkampff, Handbuch der Physik, Band XXIII, Quanten, Julius Springer, Berlin (1926).

42. K. Siegbahn, Beta- and Gamma-Ray Spectroscopy, North-Holland Publishing Co., Amsterdam (1955).

43. G. W. Grodstein, X-Ray Attenuation Coefficients from 10 key to 100 Mev, National Bureau of Standards Circular 583, (1957).

44. O. D. Olson, M. Sc. Thesis, University of Saskatchewan, 1962.

45. O. D. Olson and H. M. Skarsgard, Can. J. Phys. 41, 391 (1963).

46. A. R. Strilchuk, Private communication.

47. H. S. W. Massey and E. H. S. Burhop Electronic and Ionic Impact Phenomena, Clarendon Press, Oxford (1952).

48. J. G. Linehart and L.Th. M. Ornstein, Production of Plasma in a Toroidal Vessel by means of a Spiral Electron Beam, (1959) CERN 59-2.

49. L. D. Smullin and W. D. Getty, Phys. Rev. Letters, 9, 3 (1962).

50. F. C. Frary, C. S. Taylor, J. D. Edwards, Laboratory Glass Blowing, McGraw-Hill Book Co., Inc., New York (1928).